NAVAL POSTGRADUATE SCHOOL

MONTEREY, CALIFORNIA

THESIS

AN INVESTIGATION OF THE PERFORMANCE OF A RIBBON AND SMALL PLANAR MAGNETIC TRANSDUCER, MADE FOR USE IN AIR, AS AN UNDERWATER ACOUSTIC VELOCITY SENSOR

by

YoungWoo Kwon
Javier Honorato

September 2016

Co-Advisor:	Daphne Kapolka
Co-Advisor:	Steven R. Baker

Approved for public release. Distribution is unlimited.

THIS PAGE INTENTIONALLY LEFT BLANK

REPORT DOCUMENTATION PAGE		*Form Approved OMB No. 0704–0188*

Public reporting burden for this collection of information is estimated to average 1 hour per response, including the time for reviewing instruction, searching existing data sources, gathering and maintaining the data needed, and completing and reviewing the collection of information. Send comments regarding this burden estimate or any other aspect of this collection of information, including suggestions for reducing this burden, to Washington headquarters Services, Directorate for Information Operations and Reports, 1215 Jefferson Davis Highway, Suite 1204, Arlington, VA 22202-4302, and to the Office of Management and Budget, Paperwork Reduction Project (0704-0188) Washington, DC 20503.

1. AGENCY USE ONLY *(Leave blank)*	2. REPORT DATE September 2016	3. REPORT TYPE AND DATES COVERED Master's thesis	
4. TITLE AND SUBTITLE AN INVESTIGATION OF THE PERFORMANCE OF A RIBBON AND SMALL PLANAR MAGNETIC TRANSDUCER, MADE FOR USE IN AIR, AS AN UNDERWATER ACOUSTIC VELOCITY SENSOR		5. FUNDING NUMBERS	
6. AUTHOR(S) YoungWoo Kwon and Javier Honorato			
7. PERFORMING ORGANIZATION NAME(S) AND ADDRESS(ES) Naval Postgraduate School Monterey, CA 93943-5000		8. PERFORMING ORGANIZATION REPORT NUMBER	
9. SPONSORING /MONITORING AGENCY NAME(S) AND ADDRESS(ES) N/A		10. SPONSORING / MONITORING AGENCY REPORT NUMBER	
11. SUPPLEMENTARY NOTES The views expressed in this thesis are those of the author and do not reflect the official policy or position of the Department of Defense or the U.S. Government. IRB Protocol number ____N/A____.			
12a. DISTRIBUTION / AVAILABILITY STATEMENT Approved for public release. Distribution is unlimited.		12b. DISTRIBUTION CODE	

13. ABSTRACT (maximum 200 words)

The use of vector sensors in sonar receiving array applications is an area of active investigation by the U.S. Navy. A vector sensor combines the outputs of a monopolar (pressure) sensor co-located with one or more orthogonal dipolar (velocity or, more commonly, pressure-gradient) sensors to achieve a modest (5–6 dB) amount of directivity at a single point. The directivity of an array formed using such sensors is also modestly improved by the same amount. More importantly, though, the azimuthal angle ambiguity that occurs in the beam pattern of a line array of point pressure sensors is removed by employing vector sensors instead. This thesis describes an investigation into the underwater use of a pressure-gradient transducer technology that has been employed in airborne acoustic applications for many years (mostly as a source), but, to our knowledge, has heretofore never been employed under water. The devices examined include planar-magnetic and true ribbon transducers. The planar-magnetic transducer is very closely related to what was developed first (i.e., the true magnetic ribbon transducer). The same as an ordinary magnetic loudspeaker or microphone, both the planar-magnetic and true ribbon transducers employ a mutually orthogonal electrical conductor, magnetic field, and axis of motion of a diaphragm. We present the results of measurements made both in air and water of the transmitting and receiving responses of a planar-magnetic and a true ribbon transducer. We also present a procedure for the free-field reciprocity calibration of a pressure-gradient transducer.

14. SUBJECT TERMS vector sensor, monopolar, dipolar, pressure transducer, pressure gradient transducers, planar magnetic, magnetic ribbon, free-field.			15. NUMBER OF PAGES 161
			16. PRICE CODE
17. SECURITY CLASSIFICATION OF REPORT Unclassified	18. SECURITY CLASSIFICATION OF THIS PAGE Unclassified	19. SECURITY CLASSIFICATION OF ABSTRACT Unclassified	20. LIMITATION OF ABSTRACT UU

THIS PAGE INTENTIONALLY LEFT BLANK

AN INVESTIGATION OF THE PERFORMANCE OF A RIBBON AND SMALL PLANAR MAGNETIC TRANSDUCER, MADE FOR USE IN AIR, AS AN UNDERWATER ACOUSTIC VELOCITY SENSOR

YoungWoo Kwon
Lieutenant Commander, Korean Navy
B.S., Korean Naval Academy, 2004

Javier Honorato
Lieutenant Commander, Chilean Navy
B.S., Chilean Naval Polytechnic Academy, 2002

Submitted in partial fulfillment of the
requirements for the degree of

MASTER OF SCIENCE IN ENGINEERING ACOUSTICS

from the

**NAVAL POSTGRADUATE SCHOOL
September 2016**

Approved by: Daphne Kapolka
Co-Advisor

Steven R. Baker
Co-Advisor

Daphne Kapolka
Chair, Engineering Acoustic Department Committee

iii

THIS PAGE INTENTIONALLY LEFT BLANK

ABSTRACT

The use of vector sensors in sonar receiving array applications is an area of active investigation by the U.S. Navy. A vector sensor combines the outputs of a monopolar (pressure) sensor co-located with one or more orthogonal dipolar (velocity or, more commonly, pressure-gradient) sensors to achieve a modest (5–6 dB) amount of directivity at a single point. The directivity of an array formed using such sensors is also modestly improved by the same amount. More importantly, though, the azimuthal angle ambiguity that occurs in the beam pattern of a line array of point pressure sensors is removed by employing vector sensors instead. This thesis describes an investigation into the underwater use of a pressure-gradient transducer technology that has been employed in airborne acoustic applications for many years (mostly as a source), but, to our knowledge, has heretofore never been employed under water. The devices examined include planar-magnetic and true ribbon transducers. The planar-magnetic transducer is very closely related to what was developed first (i.e., the true magnetic ribbon transducer). The same as an ordinary magnetic loudspeaker or microphone, both the planar-magnetic and true ribbon transducers employ a mutually orthogonal electrical conductor, magnetic field, and axis of motion of a diaphragm. We present the results of measurements made both in air and water of the transmitting and receiving responses of a planar-magnetic and a true ribbon transducer. We also present a procedure for the free-field reciprocity calibration of a pressure-gradient transducer.

THIS PAGE INTENTIONALLY LEFT BLANK

TABLE OF CONTENTS

LIST OF FIGURES

xi

THIS PAGE INTENTIONALLY LEFT BLANK

LIST OF TABLES

ACKNOWLEDGMENTS

THIS PAGE INTENTIONALLY LEFT BLANK

I. INTRODUCTION

A. VECTOR SENSORS AND ARRAYS

The use of vector sensors in sonar receiving array applications is a current area of investigation by the U.S. Navy [1]. A vector sensor combines the outputs of a monopolar (pressure) sensor co-located with one or more orthogonal dipolar (velocity or, more commonly, pressure-gradient) sensors to achieve a modest (5–6dB) amount of directivity at a single point.

An acoustic velocity usually cannot be obtained directly, and thus the pressure gradient sensors are used to get an acoustic velocity indirectly. Pressure gradient sensors can be analyzed using Euler's equation, which relates acoustic velocity (actually acceleration) to the acoustic pressure gradient as

$$\rho_0 \frac{\partial \vec{u}}{\partial t} = -\vec{\nabla} p \; . \tag{1.1}$$

1. Vector Sensors and the Measurement of Acoustic Intensity at a Point

Conventionally, the acoustic intensity is the time-average of the instantaneous intensity of a sound wave, and it can be expressed as

$$I = \frac{1}{T} \int_0^T p\boldsymbol{u} \; dt \; . \tag{1.2}$$

Since vector sensors measure both acoustic pressure and particle velocity of sound at a point, they can be used to obtain the acoustic intensity at a field point.

2. Cardioid-type Beam Patterns Formed using Vector Sensors

The pressure sensor of a vector sensor has an omnidirectional (monopolar) response. The velocity sensor is usually a pressure-gradient sensor, which has a dipolar pressure response.

In the vector sensor, the monopole and the dipole beam patterns are combined to create a new beam pattern, which has a directional characteristic. The relative amount of

1

monopolar and dipolar contribution is a variable. For equal amounts of each, the result is a so-called "cardioid" beam pattern, which takes this name from its heart shape. The cardioid beam pattern has exactly one null direction, and it has a directivity D of 3 and a directivity index DI of 4.8dB. As Figure 1 shows, this cardioid beam has a much higher detecting preference in its maximum response direction while rejecting sound from the opposite side.
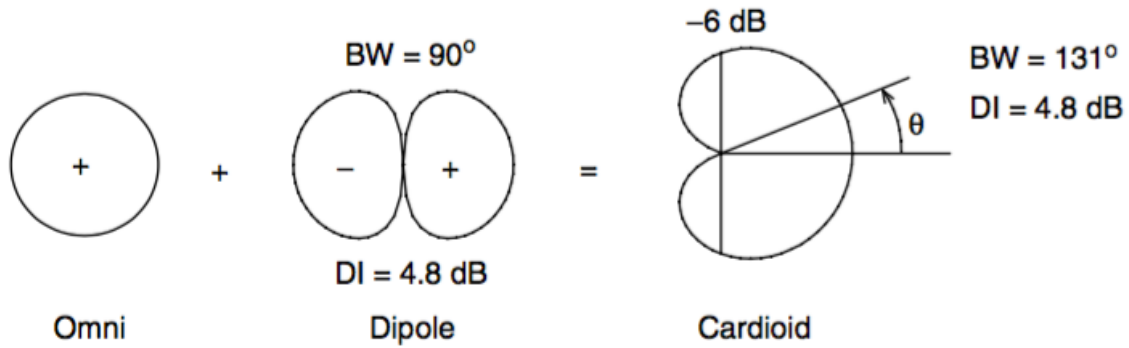
Figure 1.   Synthesis of a Cardioid Beam Pattern in dB Scale. Source [2].

3.   Beam Pattern of Array of Steerable Cardioid versus Monopole Sensors

As we know, a target fire-control solution requires detection, localization, and identification, and vector sensors improve the bearing estimate with the same number of array elements. Multiple vector sensors compared to an array of hydrophones can be made as a steerable array in order to improve their sound localization ability. For example, because they are steerable in both polar and azimuthal angles, the azimuthal angle ambiguity that occurs in the beam pattern of a line array of point pressure sensors is removed by employing vector sensors instead.

Figure 2 shows a seven-element line array that has seven cardioid elements. All the elements are steered to 120 degrees from the polar axis (defined in Figure 3) and 30 degrees out of the page in azimuthal angle. In this case, the polar angle dependence of the far-field directional factor magnitude $|H|$ is shown for each element in the plane that includes the polar axis and the maximum response axis.

2
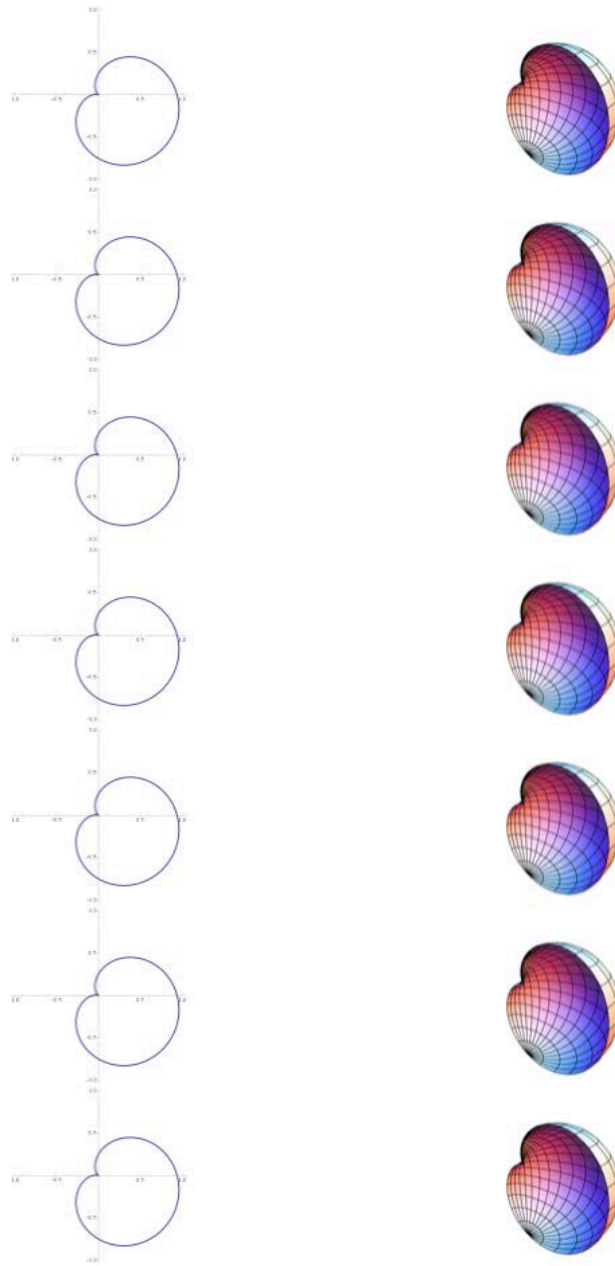
Figure 2.   Line Array of Seven Cardioid Elements All Steered to 120 Degrees from the Polar Axis and 30 Degrees out of the Page in Azimuth Angle.

3
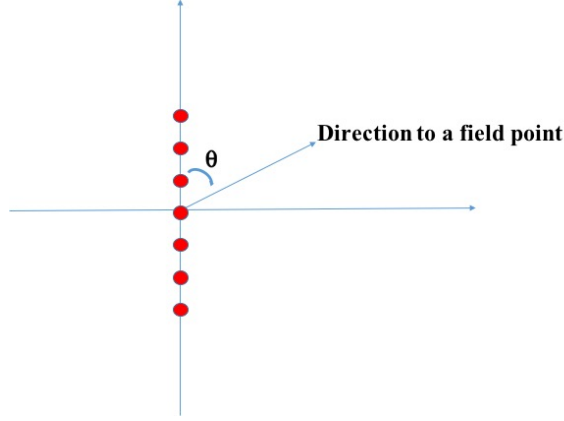
Figure 3.   Seven-Element Line Array and Polar Angle of θ.

The directional factor of a line array of steered cardioids can be obtained using the Product Theorem, as follows.

In spherical coordinates, the directional factor of an unsteered point line array of N elements with a separation distance of d and of a single wideband cardioid element can be expressed as

$$H_{point\ line\ array}(\theta) = \frac{1}{N} \frac{\sin\left[\left(\frac{N}{2}\right)kd\cos\theta\right]}{\sin\left[\left(\frac{1}{2}\right)kd\cos\theta\right]} \text{, and} \tag{1.3}$$

$$H_{wideband\ cardioid}(\theta) = \frac{1+\cos\theta}{2} = \cos^2\left(\frac{\theta}{2}\right). \tag{1.4}$$

If θ and ϕ are the usual spherical polar and azimuthal angles and θ_0 and ϕ_0 are their steered values, the steered point line array of N elements with a separation distance of d is shown as

$$H_{steered\ point\ line\ array}(\theta_0;\theta) = \frac{1}{N} \frac{\sin\left[\left(\frac{N}{2}\right)kd\left(\cos\theta-\cos\theta_0\right)\right]}{\sin\left[\left(\frac{1}{2}\right)kd\left(\cos\theta-\cos\theta_0\right)\right]} \tag{1.5}$$

4

In addition, the steered directional factor for a single wideband cardioid element $H_{single\,cardioid}(\theta_0,\phi_0;\theta,\phi)$ can be expressed in terms of the usual spherical coordinate by the Addition Theorem [3]. By the Product Theorem [3], the directional factor for a linear array of identical, equally spaced, steered vector sensor is realized as

$$H_{cardioid\,line\,array}(\theta_0,\phi_0;\theta,\phi)=H_{single\,cardioid}(\theta_0,\phi_0;\theta,\phi)H_{point\,line\,array}(\theta_0,\theta) \qquad (1.6)$$

Figure 4 shows a 3-D surface plot of the magnitudes directional factor of a seven-point line array and seven-element steered cardioid line array. The element spacing is $\lambda/2$.
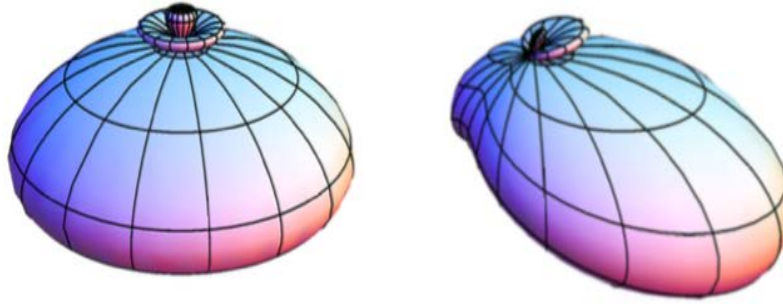
Left Plot is |H| for Seven Point Elements Steered to a polar angle of 120 Degrees and Right Plot |H| is Seven Cardioid Elements Steered to a polar angle of 120 Degrees.

Figure 4.   Full 3-D Plots Directional Factor |H| for Elements Arrays Steered to 120 Degrees from Polar Axis.

Figure 5 shows the directional factor for a line array of seven point elements steered 120 degrees from the polar axis. The azimuthal ambiguity is apparent because of the cylindrical symmetry.
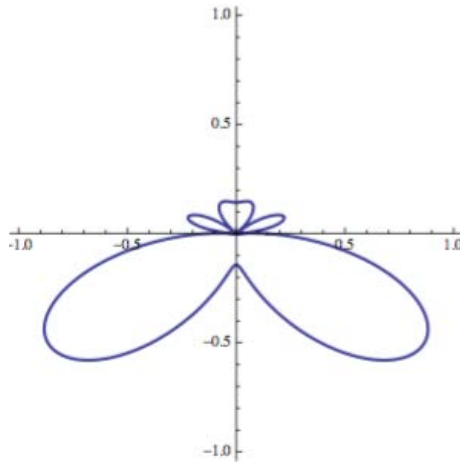
This pattern is in the vertical plane that includes the polar axis and the steered axis.

Figure 5.　Polar Angle Dependence of Directional Factor |H| for a Line Array of Seven Point Elements Steered to 120 Degrees from the Polar Axis.

The steered cardioid line array makes a beam pattern that is steered 120 degrees without ambiguity like Figure 6. This beam pattern is in the vertical plane that includes the polar axis and the steered axis.
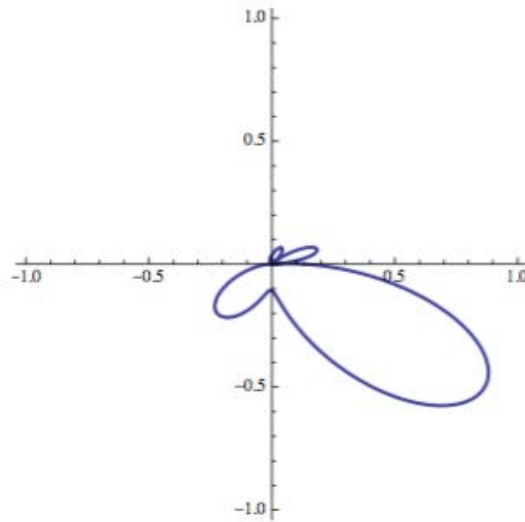
This pattern is in the vertical plane that includes the polar axis and the steered axis.

Figure 6.　Polar Angle Dependence of Directional Factor |H| for a Line Array of Seven Cardioid Elements Steered to 120 Degrees from the Polar Axis.

6

4. Practical Realization of an Acoustic Particle Velocity Sensor

There are a couple of devices to measure the particle velocity directly (hot-wire and laser anemometers) and indirectly (true ribbon and planar-magnetic transducer).

a. Direct Velocity Measurement

This part introduces two of the most common sensor technologies to measure particle velocity directly: hot-wire and laser anemometers. A hot-wire is one of the thermal anemometers. It has an exposed hot wire in order to measure the change in wire temperature. Once heat loss can be measured, it can be converted into a fluid velocity. The hot-wire response is non-linear, which makes the calibration hard to apply. The Microflown sensor, which has two closely spaced heated wires, is one example of a hot-wire sensor [4] (Figure 7).

The temperature around the wires in the figure is changed by a particle velocity flow, and it changes the temperature of those wires.

Figure 7.   Microflown Sensor. Source [4].

Laser Doppler anemometry is a type of laser Doppler velocimetry. It uses the Doppler shift in a laser beam to measure particle velocity at one point (Figure 8). It has very high accuracy and high spatial resolution due to its small measurement volume but is not practical for sonar array applications due to its complexity and cost [4].
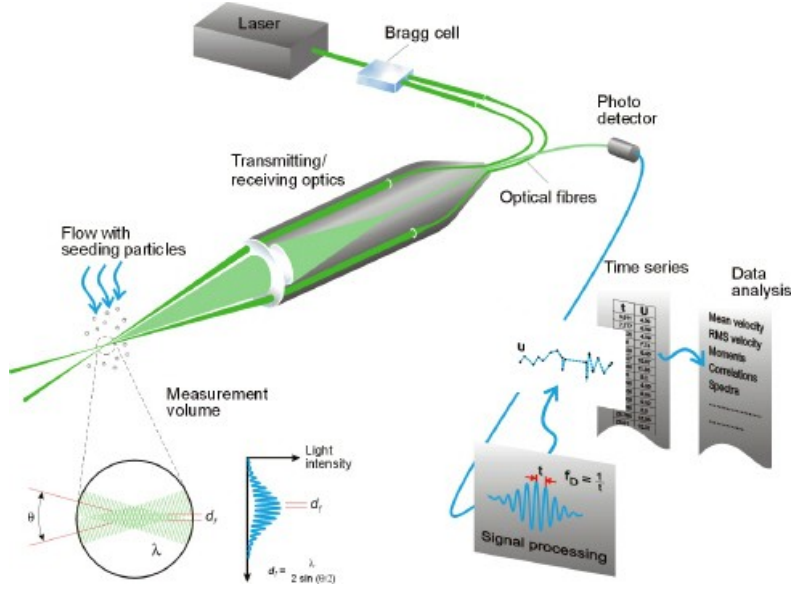
Figure 8.   Laser Doppler Anemometer (LDA) System Source [5].

b.   *Indirect Velocity Measurement (Velocity Estimation from Pressure Gradient)*

According to class notes [6], it is possible to measure the particle velocity directly through the aforementioned devices, but many devices take the particle velocity from a measurement of the pressure gradient through Euler's Equation (1.1). The acceleration of a fluid particle depends on the pressure gradient. The acoustical acceleration of a monofrequency sound wave is given by

$$\tilde{a} = -\frac{1}{\rho_0}\nabla\tilde{p} = j\omega\tilde{u} \; . \tag{1.7}$$

We can rearrange this equation in terms of $\tilde{u}$ to get

$$\tilde{u} = -\frac{1}{j\omega\rho_0}\nabla\tilde{p} \; . \tag{1.8}$$

The previous equation signifies that the particle velocity estimation is possible by measuring the pressure gradient, and most underwater acoustic particle velocity sensors use this technique.

8

As an example for a spherical wave, the particle velocity is radial and for radius r equals

$$\tilde{u} = \frac{\tilde{p}}{\rho_0 c}\left(1 + \frac{1}{jkr}\right).$$ (1.9)

Equation (1.9) is a specific example of Euler's Equation (1.1), which is relevant to far-field transducer calibration. It shows that the particle velocity is not in phase with the pressure, and the specific acoustic impedance of z is not equal to $\rho_0 c$. Thus, the impedance of z can be expressed as

$$z = \rho_0 c \cdot \cos\theta e^{j\theta}$$ (1.10)

where θ is the phase difference between pressure and particle velocity. Figure 9 shows the relationship between θ and kr at a distance r from the source of a spherical wave of wave number k.
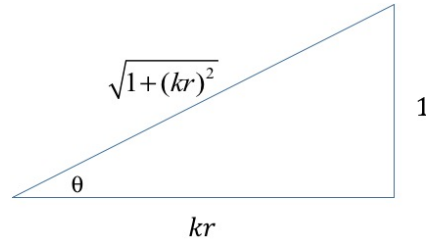
Figure 9.   The Relationship between θ and kr.

The impedance of z can be rewritten in terms of the acoustic pressure and the particle velocity as

$$z = \frac{\tilde{p}}{\tilde{u}} = \rho_0 c \cdot \cos\theta.$$ (1.11)

For large values of kr, θ approaches zero, and the wavefront approaches a plane wave. So, rewriting the impedance in terms of an outgoing plane wave yields

$$z = \frac{\tilde{p}}{\tilde{u}} = \rho_0 c .$$ (1.12)

9

From this equation, we can estimate the magnitude of the particle velocity. For example, for a *100dB re 1μPa* plane wave in water, the magnitude of the particle velocity is

$$\tilde{u} = \frac{\tilde{p}}{\rho_0 c} = \frac{10^{100/20} \mu Pa}{1.54 x 10^{12} \mu Pa * s/m} = 0.065 \mu m/s \ . \tag{1.13}$$

Figure 10 shows a typical design used to measure the pressure gradient and thus to estimate the particle velocity in water. This device has neutral buoyancy, and the mass of outer case is m_c. Due to the pressure gradient across the case, there will be an acceleration. If the case velocity of v_c is different with the water velocity of v_w, it means that there are additional forces on the case. Inside the case, there is an inertial proof mass of m_p which is connected with a spring with a constant of k and damping of R. If the velocity of m_p moves with the velocity of v_p, there will be a difference between the v_c and v_p. This difference can be used to estimate the water velocity [6].
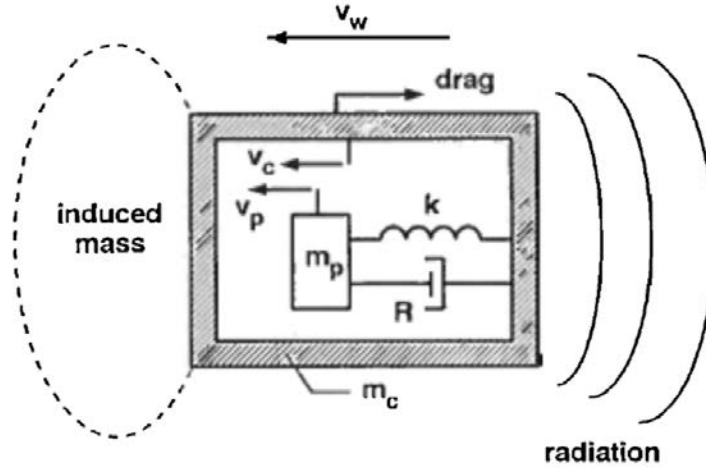
Figure 10.   Schematic Cross Section of a Rigid-Shell Velocity Sensor Submerged in Water Source [6].

There are other technologies to measure the pressure gradient, and one of those is the magnetic-ribbon-type pressure-gradient sensor. This type of device is typically used

in air rather than in water. This type of transducer is examined in more detail in the following section.

5. Magnetic Ribbon-Type Transducers

Magnetic ribbon-type transducers are part of a common family of pressure gradient transducers that have long been used in air. These transducers are also commonly classified as either "true magnetic ribbon" or "quasi-ribbon" transducers. The quasi-ribbon transducer is also known as the planar magnetic transducer. Ribbon-type transducers may be either sources or receivers.

a. *True Ribbon Transducer*

Figures 11 and 12 show examples of true ribbon transducers; Figure 11 shows a source (a "tweeter,") and Figure 12 shows a microphone element. The basic construction is composed of a very lightweight corrugated metal foil "ribbon" suspended between two parallel bar magnets of opposite polarity. Similar to an ordinary magnetic loudspeaker (Figure 13) or microphone, both the true ribbon and planar magnetic transducers employ a mutually orthogonal electrical conductor, magnetic field, and axis of motion of a diaphragm.

In the true ribbon transducer, the foil ribbon is both the conductor and the diaphragm. The ribbon is corrugated, giving it a small amount of stiffness. Its tension keeps the ribbon centered between the magnetic poles, but is otherwise not important because ribbon transducers always operate above their mass-spring resonance frequency.

Electrically, as a source, current flows along the axis of the conductor, and in the presence of the transverse magnetic field, results in a force and motion normal to the ribbon surface. As a receiver, the motion of the foil normal to its surface induces a voltage in the axial direction of the foil. The output voltage is proportional to the velocity of the ribbon. This is very convenient for its use as a velocity sensor.

Acoustically, as a source, a ribbon transducer is like an open-back (unbaffled) loudspeaker; as a receiver, it senses the pressure gradient. As either a source or receiver, it has a dipole beam pattern at low frequencies (long wavelength compared to width).

11

Especially for use in air, a low mass diaphragm (ribbon) is important and is usually made of aluminum, as thin as 1.8 microns for a microphone element.
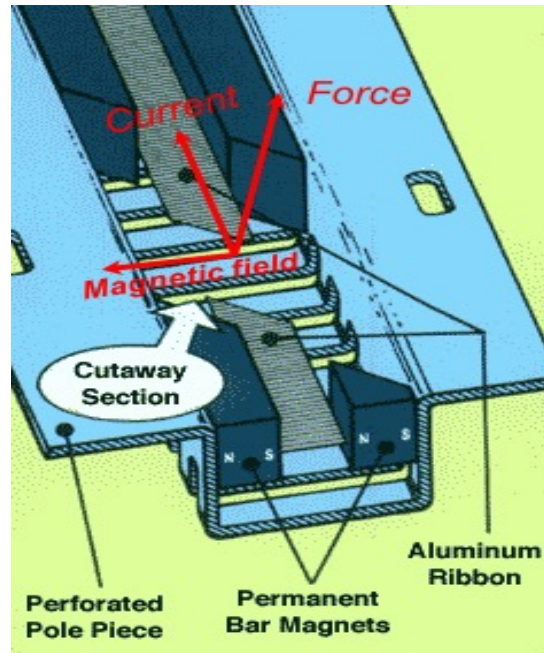
Figure 11.   True Ribbon Tweeter. Source [7].
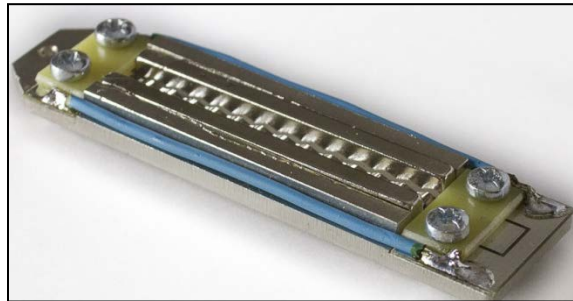
Figure 12.   True Ribbon Microphone. Source [8].
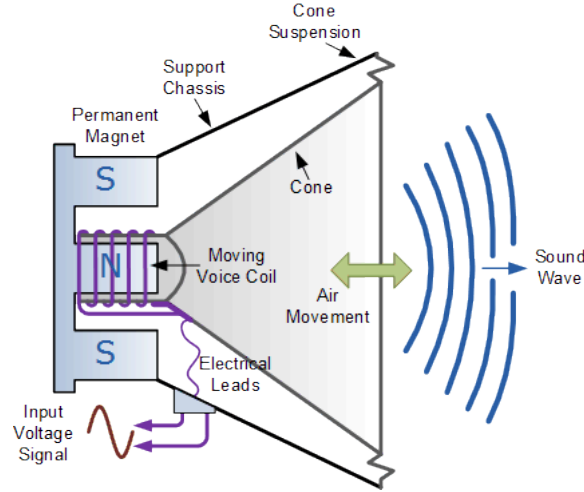
Figure 13.　Moving Coil Transducer. Source [9].

b.　Quasi-Ribbon (Planar-Magnetic Transducer)

The quasi-ribbon transducer, also known as the planar-magnetic transducer, is a variation of the true ribbon transducer. Figure 14 shows an example of such a transducer, identical to the one used in this thesis except for its size.

While the true ribbon transducer has a corrugated aluminum foil for its electrode and diaphragm, the quasi-ribbon transducer employs a stretched thin plastic (usually mylar) diaphragm mounted to a frame to which is bonded a serpentine foil conductor. Parallel rows of bar magnets are positioned on one or both sides of the stretched diaphragm. The serpentine foil conductor and rows of magnets are arranged so that the current flow is between the rows of magnets. The magnetic poles alternate between adjacent rows, as shown in Figure 14, to make the magnetic field direction as much in the plane of the diaphragm as possible at the locations of the conductors. Employing rows of magnets on both sides of the diaphragm produces a "push-pull" design. It is more expensive, but improves the linearity of the transducer's operation (its magnetic induction). As for the true ribbon transducer, the diaphragm tension is small and is not otherwise important as it also operates above its mass-spring resonance frequency.

Compared to the true-ribbon transducer, the planar-magnetic transducer offers several advantages. By its construction, the planar-magnetic transducer offers essentially

unlimited diaphragm area, which is a great advantage for use as a loudspeaker. It is also much more rugged, and its serpentine conductor is designed so it has much greater length in the magnetic field than is possible with a ribbon foil. This design results in a much greater voltage output when used as a receiver than a true ribbon transducer would have, and it does not require an output step-up transformer. (Though there is no comparison to be made to the true ribbon transducer, the serpentine conductor of the planar-magnetic transducer also results in its electrical impedance, which is almost completely resistive, i.e., it has very small inductance).

One disadvantage of the planar-magnetic transducer is that the mass of its diaphragm and serpentine conductor is much greater than the mass of the true ribbon transducer's foil; a lighter diaphragm is more responsive to either a magnetic or acoustic force. Therefore, planar-magnetic transducers are not used in place of true ribbon transducers as microphones, where their higher-mass diaphragms would limit their sensitivity. In addition, as speakers, the higher-mass diaphragms of planar-magnetic transducers can be compensated for by applying higher current drive, which is easy to do.
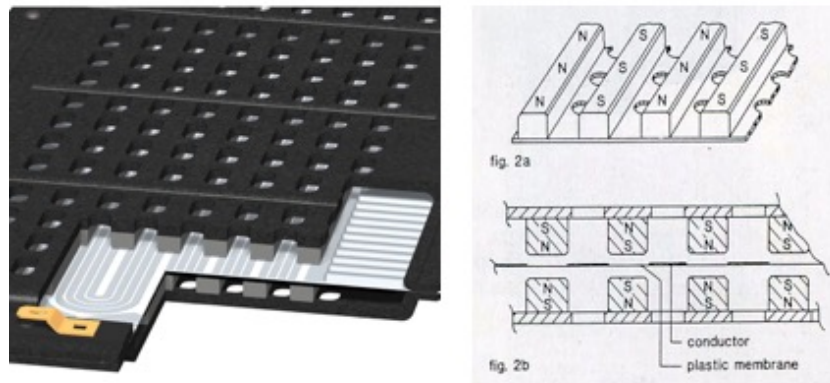
This is a cutaway drawing of a larger version of the B-G NEO3W transducers, made by the same company, so the construction is the same as the NEO3W, which has a "push-pull" magnet design.

Figure 14.   Planar Magnetic Source. [10].

14

B. MAGNETIC RIBBON-TYPE PRESSURE-GRADIENT TRANSDUCERS AS UNDERWATER VELOCITY SENSORS

Magnetic ribbon-type and planar-magnetic pressure-gradient velocity sensors exist in air, but to our knowledge, have not heretofore been adapted for underwater use. For this reason, this thesis describes an investigation into the underwater use of magnetic ribbon-type transducer technology as pressure-gradient sensors.

C. OUTLINE OF REMAINDER OF THESIS

Since this thesis investigates the possibility of adapting magnetic ribbon-type transducers from air to underwater use, it will involve measuring beam patterns and calibrating in air. After reconfiguring for underwater use, the beam pattern and calibration are repeated in an underwater tank.

Chapter II describes the calibration theory for acoustic pressure-gradient transducers. In this chapter, we deal with transducer sensitivities and calibration procedures other than reciprocity. In addition, we review the free-field reciprocity calibration of a pressure transducer and present the free-field reciprocity calibration of a pressure gradient/velocity transducer.

Chapters III and IV describe the experimental sensors' test results and analysis. Chapter III presents the results and analysis for the in-air tests, and Chapter IV presents the corresponding measurements in water.

Chapter V provides a summary of this thesis and makes recommendations for future work.

THIS PAGE INTENTIONALLY LEFT BLANK

II.   THEORY: CALIBRATION OF ACOUSTIC PRESSURE-GRADIENT TRANSDUCERS

A.   TRANSDUCERS SENSITIVITIES

In this section, we describe the basic about the sensitivities. These include free-field wave quantities, free-field, far-field propagation limit and the acoustic sensitivities.

1.   Free-Field Wave Quantities, Free-field Transducer Calibration

Placing a sensor (transducer) in a wave field of any kind may disturb the field. As a rule, one would like to know the value of a wave field quantity at a point or points in space that would exist in the absence of a sensor being placed there to measure it. This is certainly the case in navy sonar applications. The value of such a wave field quantity is its "free-field" value (as opposed to the "actual," potentially disturbed, value). By the appropriate procedure, a sensor may be calibrated to yield a free-field wave quantity from its signal output. This procedure is referred to as performing a "free-field calibration" of a sensor.

2.   Free-field, Far-Field ("Spherical Wave") Propagation Limit

In almost all sonar applications, the source or target and receiver are expected to be well separated from one another where "far-field" propagation conditions apply. As applied here, the term far-field propagation conditions refers to the absence of wave interference on a small scale with range, in a given direction, such as can occur in the vicinity of a spatially extended source. (Note, for such interference to occur, a source's spatial extent must be comparable to or greater than a wavelength, which is certainly common in sonar applications.) The commonly quoted condition on the range for such far-field propagation conditions to apply is

$$r \gg \frac{\left(\frac{L}{2}\right)^2}{\lambda}, \tag{2.1}$$

where L is a length characterizing the greatest lateral extent of a source, and λ is the acoustic wavelength.

It is a property of the linear wave equation for the propagation of sound in an unbounded, stationary, homogeneous and isotropic fluid that the free-field (i.e., absent of scattering from any objects or obstacles) acoustic pressure radiated from any bounded, time harmonic source asymptotically with increasing range can be cast in phasor form, in spherical polar coordinates [11], as

$$\tilde{p}^{ff}(r,\theta,\phi,t) \equiv \lim_{r\to\infty} \tilde{p}(r,\theta,\phi,t) = \frac{\tilde{P}^{ff}_{axis}(1m)}{r(m)} \tilde{H}(\theta,\phi)e^{j[\omega t - k(r-1m)]}, \qquad (2.2)$$

where $\tilde{P}^{ff}_{axis}(1m) \equiv \lim_{r\to\infty} r\,\tilde{p}(r,\theta_{axis},\phi_{axis},0)e^{+jk(r-1m)}$ is the on axis far-field pressure, referred to a range of 1 meter (units of Pa-m; and, as written above, properly includes its phase), r (m) is the range in meters, k is the acoustic wavenumber, and $\tilde{H}(\theta,\phi)$ is the far-field directional factor. $\tilde{H}(\theta,\phi)$ is conventionally normalized to 1 on the acoustic axis, i.e., such that $\tilde{H}(\theta_{axis},\phi_{axis}) = 1 + j0$. The acoustic axis is generally chosen as the most convenient direction of maximum response magnitude with regard to the symmetry of the source (note that there may be more than one direction of equal, maximum response magnitude). We refer to this as the free-field, far-field acoustic pressure. In the context of transducer calibration, this propagation limit is also referred to as the "spherical wave" propagation limit.

3.   Acoustic Transducer Transmitting and Receiving Sensitivities; Free-Field Sensitivities

The transmitting and receiving properties of acoustic transducers are specified by their transmitting and receiving "sensitivities." An acoustic transducer sensitivity is a dimensioned transfer function between the electrical and the acoustical worlds. It is always the ratio of an output quantity to an input quantity, electrical to acoustical or vice-versa. Unless otherwise stated, it assumes linear response, so that the sensitivity is independent of signal strength. It is a time-harmonic concept (as is impedance, for

18

example); it may be complex-valued (a phasor), or it may be frequency and/or propagation-direction dependent.

Note, throughout this thesis, we use a tilde ("~") over a symbol to signify a phasor quantity; we signify a phasor quantity's magnitude by its phasor symbol absent the tilde.

a.   Pressure Transducers

Figure 15 is helpful to understand the various possible definitions of acoustic transducer sensitivity. It depicts an acoustic transducer (T), which might be either a projector or a receiver.
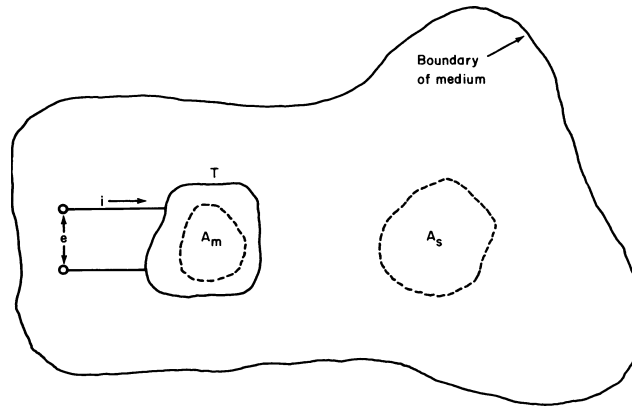
As stated in [12], "transducer T of an arbitrary shape in a medium with an arbitrary boundary; "A_s" is the area over which the transmitted pressure is measured, "A_m" is the area over which the received pressure is measured ,*e* is the voltage and *i* is current." [12].

Figure 15.   Understanding Acoustic Sensitivity Source. [12].

The transmitting sensitivity of an acoustic projector might be denoted, for example, by the letter *"S"* (for "speaker strength"). For a projector, the signal input is either a driving voltage or a driving current; the signal output is most commonly considered to be the acoustic pressure at a field point or an average over field points, but it might also be considered to be an acoustic pressure gradient or an acoustic velocity. Referring to Figure 15, for example,

$$\tilde{S}_e = \frac{avg\ free\text{-}field\ or\ actual\ \tilde{p}\ on\ A_s}{source\ driving\ voltage\ \tilde{e}},$$ (2.3)

19

or

$$\tilde{S}_i = \frac{avg\ free\text{-}field\ or\ actual\ \tilde{p}\ on\ A_s}{source\ driving\ current\ \tilde{i}}, \qquad (2.4)$$

might represent a projector's pressure transmitting voltage $(\tilde{S}_e)$ or current $(\tilde{S}_i)$ sensitivity. The acoustic pressure appearing in the sensitivity may be either the free-field pressure or the actual pressure; it may be either the value at a point (i.e., $\lim A_s \longrightarrow 0$) or averaged over area A_s. Which of these choices is taken must be specified. In sonar applications, it would also be common to take the pressure to be the free-field, far-field acoustic pressure in a specified direction, referred back to a range of 1 meter, i.e., $\tilde{P}_{axis}^{ff}(1m)\tilde{H}(\theta,\phi)$ as defined in the previous section.

The receiving sensitivity of an acoustic sensor is most commonly denoted *"M"* (for "microphone sensitivity"). The signal input is an incident acoustic field quantity, and the output is most commonly specified as either an open circuit voltage or a short circuit current. For example,

$$\tilde{M}_o = \frac{receiver\ open\text{-}ckt\ voltage\ \tilde{e}_o}{avg\ free\ field\ or\ actual\ \tilde{p}\ on\ A_m}, \qquad (2.5)$$

or

$$\tilde{M}_s = \frac{receiver\ short\text{-}ckt\ current\ \tilde{i}_s}{avg\ free\ field\ or\ actual\ \tilde{p}\ on\ A_m}, \qquad (2.6)$$

might represent a sensor's pressure receiving open-circuit voltage $(\tilde{M}_o)$ or short circuit current $(\tilde{M}_s)$ sensitivity. Just as for transmitting sensitivity, whether the acoustic pressure is free-field or actual, and whether it is the value at a point or averaged over an area (A_m in Figure 15), must be specified. Note, for a free-field calibration, the point or area over which the free-field incident field quantity is defined may not lie within the fluid at all when the transducer is present; by definition it is the acoustic field quantity in the absence of the transducer.

20

b. *Pressure-gradient (Velocity) Transducers*

In the case of acoustic pressure-gradient (velocity) transducers, the general situation is much more complicated than for acoustic pressure transducers, as the former are inherently vector-field devices. We restrict ourselves to transducers, which possess only a single mechanical degree of freedom, that is, which can only produce acoustic velocity or force (pressure-gradient) at a point of application in a single particular direction and which can only respond to acoustic pressure gradient or velocity along that same direction (the "the sense axis").

To further distinguish pressure and pressure-gradient transducers, we consider only pressure-gradient transducers comprised of bodies that can only translate and not rotate, and that are not capable of dilatation, i.e., have zero net volume velocity. As sources, in the long wavelength limit, their radiation is strictly dipolar; it has no monopolar component. As receivers, in the long wavelength limit, they do not respond to acoustic pressure directly, only to its gradient. Transducers employing rigid bodies or flat planar pistons constrained in their motion, or stretched planar flexible diaphragms, such as those used in the present research project, are examples of the type of pressure gradient transducer being considered here.

In considering the calibration of pressure-gradient transducers, we consider only the case of "point" transducers, that is, the case that the transmitted or received field is taken to be produced or sensed at a single point for the purposes of calibration. As a source, then, we might consider a pressure-gradient transducer to produce a certain pressure gradient or velocity at a point in space in response to a certain electrical input. Alternatively, as a receiver, we might consider a pressure-gradient transducer to produce a certain electrical output in response to a certain pressure-gradient or velocity at a point in space. Its transmitting current sensitivity, for example, might be expressed as

$$\tilde{S}_i = \frac{free\text{-}field\ \nabla\tilde{p}\ or\ \tilde{u}\ at\ a\ field\ point}{source\ driving\ current\ \tilde{i}}, \tag{2.7}$$

or its receiving open-circuit voltage sensitivity might be expressed as

$$\tilde{M}_o = \frac{receiver\ open\text{-}ckt\ voltage\ \tilde{e}_o}{component\ along\ sense\ axis\ of\ free\text{-}field\ \nabla\tilde{p}\ or\ \tilde{u}\ at\ a\ point}. \qquad (2.8)$$

B.   CALIBRATION PROCEDURES OTHER THAN RECIPROCITY

Using either a previously-calibrated source or receiver, the calibration of another source or receiver may be accomplished by substituting it for either the previously-calibrated source or receiver, as appropriate, and measuring the relative response (acoustic or electric) of the two. The ratio of their sensitivities equals the ratio of their responses in this substitution procedure. This procedure is known as a *comparison calibration.*

A primary calibration, that is, one that is not obtained by comparison, may be obtained by several procedures, some more practical (or even possible) than others. Direct excitation of a sensor by independently calculable means may be possible. For example, pistonphones and electrostatic actuators are common devices for the primary calibration of microphones in air, at least at low frequencies [13]. The standard primary calibration procedure the employs a true wave field exploits the Principle of Acoustic Reciprocity [14] and is termed a *reciprocity calibration*.

Reciprocity calibration is commonly performed as a primary calibration procedure for pressure transducers, not so for pressure-gradient transducers, though a reciprocity calibration procedure for pressure gradient transducer can be developed. For a so-called "free-field" calibration, however, it is not necessary to develop a separate procedure for the calibration of pressure and pressure-gradient transducers, as acoustic pressure and its gradient are both non-zero and related to one another by Euler's Equation (Chapter I, Section A. 4.b).

$$\rho_0 \frac{\partial \vec{u}}{\partial t} = -\vec{\nabla}p \qquad (2.9)$$

C.   REVIEW OF FREE-FIELD PRESSURE RECIPROCITY CALIBRATION OF PRESSURE TRANSDUCERS

It is important to note that although transducer sensitivities and calibration procedures can consider phase, as a rule it is uncommon to be provided the phase

response of an acoustic transducer. Phase response of acoustic transducers is of obvious importance in array applications. Nevertheless, the incorporation of phase in a reciprocity calibration procedure is considered a specialty-within-a-specialty at this time. Accordingly, in what follows, all electrical and acoustical quantities that could be taken to be phasors are taken to be their magnitudes.

It is overwhelmingly the case that a free-field reciprocity calibration procedure would be performed to calibrate an acoustic receiver (a microphone or hydrophone) rather than a source; sources are overwhelmingly calibrated with the aid of previously-calibrated receivers. Reversible transducers (those that can act as either source or receiver) need not be calibrated separately as sources and receivers, as their free-field transmitting and receiving sensitivities are related in a known fashion—their receiving sensitivity can be calibrated, and their transmitting sensitivity calculated from that. Accordingly, the context of the following discussions of the free-field reciprocity calibration of acoustic transducers is the calibration of a receiver (sensor).

The usual free-field, far-field reciprocity calibration procedure is often called a "spherical-wave" reciprocity calibration (procedure), because far-field propagation conditions, as described earlier ($p \sim 1/r$ with range), are assumed to apply in the intended operational situations of the transducer being calibrated, and so they are also obeyed in the calibration procedure. The procedure is also sometimes referred to as a three-transducer reciprocity calibration procedure, because it employs three transducers: one a dedicated projector, one a dedicated receiver (that we are presuming is to be calibrated), and one a reversible transducer that is used as both a source and a receiver.

Three far-field transmission measurements are made using these three transducers, and are depicted in Figure 16.

1.   Procedure

In the calibration procedure, first, two reference points, separated by a distance d, are established. The line-of-sight between these two points establishes the radial direction for the far-field propagation conditions assumed in the calibration. These points also serve as either the reference free-field reception point for the sound transmitted from a

source, or the reference free-field reception point for the sound received by a receiver. In the former case, the reference point is located some distance away from the source; in the latter case, the reference point is located "at" the receiver.
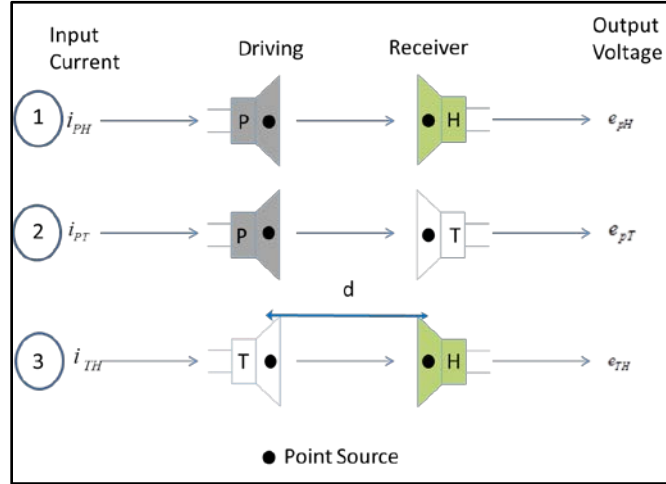
Figure 16.   Diagram of the Three Measurements for Reciprocity Calibration.
Adapted from [12].

The three transducers need not be small compared to the acoustic wavelength λ; they need not be omnidirectional; all that is required is that they be in the far field of one another ($d \gg$ (lateral extent)$^2/\lambda$). If this requirement is obeyed for all three transducers, then the lateral extent of any transducer acting as a receiver in the calibration procedure will be small compared to the lateral extent of any lobe in the directional response of any transducer acting as a source. In any case, it is customary to arrange the three transducers so that their maximum response axes are all aligned along the line of sight between the two reference points, and to perform any calibration of relative directional response as a separate procedure. Then the radiation incident upon any transducer acting as a receiver will be very similar to that of a point source a distance d away.

In measurement 1, a dedicated source P (for "projector") is driven by current i_{PH} and open-circuit voltage e_{PH} is recorded from the dedicated receiver H (for "hydrophone"). In measurement 2, the same source P is driven by current i_{PT} and open-circuit voltage e_{PT} is recorded from the reversible transducer (T). From these

24

measurements is established the receiving sensitivity of the dedicated receiver relative to that of the reversible transducer:

$$\frac{M_{OH}}{M_{OT}} = \frac{e_{PH}/i_{PH}}{e_{PT}/i_{PT}} = \frac{e_{PH}i_{PT}}{e_{PT}i_{PH}},$$

(2.10)

where M_{OH} is the Free-Field Voltage Sensitivity (FFVS) of the hydrophone and M_{OT} is the Free-Field Voltage Sensitivity of the reciprocal transducer.

In measurement 3, the reversible transducer T is now driven as a source by current i_{TH} and open-circuit voltage e_{TH} is recorded from the dedicated receiver H. If P_H is the free-field sound pressure produced by the reversible transducer at the hydrophone, and S_{IT} is the transmitting current response of the reversible transducer, we have

$$\frac{e_{TH}}{i_{TH}} = \frac{e_{TH}}{P_H}\frac{P_H}{i_{TH}} = M_{OH}S_{IT}.$$

(2.11)

Now, it is a property of all reversible transducers that

$$\frac{M_O}{S_I} = J \text{ (magnitudes)},$$

(2.12)

where J is a constant, called the "reciprocity parameter." This result is often called the Electroacoustic Reciprocity Theorem [12]. It is a consequence of properties of a reversible transducer and of the Reciprocal Property of the Acoustic Field. J depends upon the type of propagation conditions and the definitions of the sensitivities employed in the calibration procedure. For the free-field, far-field propagation conditions in the present calibration procedure, J is the so-called "spherical-wave reciprocity parameter" [12]:

$$J_s = \frac{2d}{\rho_0 f} \text{ (magnitude)}.$$

(2.13)

It can further be shown that J_s is the inverse of the acoustic transfer (or "mutual') acoustic impedance magnitude Z_s (ratio of free-field pressure p^{ff} to volume velocity U)

25

for the propagation of spherical waves from a vanishingly small pulsating sphere at one point to a field point a distance d away:

$$J_s = \frac{1}{Z_s}; \; Z_s = \frac{p_{rcvr}^{ff}}{U_{src}} = \frac{\rho_0 c}{2d}. \tag{2.14}$$

Then, we have for the free-field, far-field receiving sensitivity,

from Equations (2.11) and (2.12)

$$\frac{e_{TH}}{i_{TH}} = M_{OH} \frac{M_{OT}}{J_s}. \tag{2.15}$$

Rearranging, we end up with

$$\frac{1}{M_{OT}} = \frac{i_{TH}}{e_{TH}} \frac{M_{OH}}{J_s}. \tag{2.16}$$

From Equation (2.10)

$$\frac{e_{PH} i_{PT}}{e_{PT} i_{PH}} = M_{OH} \frac{i_{TH}}{e_{TH}} \frac{M_{OH}}{J_s}. \tag{2.17}$$

solving for M_{OH},

$$M_{OH} = \left[\frac{e_{PH} i_{PT} e_{TH}}{i_{PH} e_{PT} i_{TH}} J_s \right]^{1/2} \tag{2.18}$$

This is true as long as each transducer is in the far field from the other. Furthermore, the advantage of this method is that it is not necessary to measure the acoustic pressure, only the voltage, current, and distance between driving and receiver reference points.

We can now ask, is there a free-field, far-field reciprocity procedure for the calibration of pressure-gradient or velocity sensors? The answer is that it appears there are none in the literature. Professor Steven R. Baker of the Naval Postgraduate School has derived one. However, it turns out that for free-field, far-field (i.e., spherical-wave) propagation conditions, because both the acoustic pressure and pressure gradient are everywhere non-zero and are related to each other in a known way (for a spherically-diverging wave field) by Euler's Equation, it is not necessary to have a separate

spherical-wave calibration procedure specific to pressure-gradient sensors. This is the essence of a recommendation by Bobber for the calibration of pressure-gradient receivers, presented in the next section. It is to be remembered, however, that Bobber's recommendation is only valid for a free-field, far-field calibration; it is not a valid procedure for the reciprocity calibration of pressure-gradient sensors, in general.

D.   FREE-FIELD RECIPROCITY CALIBRATION OF PRESSURE GRADIENT/ VELOCITY TRANSDUCERS

We describe the theory about acoustic pressure-gradient, and then recommend for calibration a velocity receiver.

1.   Far-Field Acoustic Pressure Gradient, Velocity

As was stated earlier, the far-field (phasor) acoustic pressure radiated from any bounded, time-harmonic source can be cast, in spherical polar coordinates, as

$$\tilde{p}^{ff}(r,\theta,\phi,t) \equiv \lim_{r\to\infty} \tilde{p}(r,\theta,\phi,t) = \frac{\tilde{P}^{ff}_{axis}(1m)}{r(m)} \tilde{H}(\theta,\phi) e^{j[\omega t - k(r-1m)]}. \tag{2.19}$$

The acoustic velocity is found from the acoustic pressure gradient according to Euler's Equation:

$$\vec{\tilde{u}} = \frac{-1}{j\omega\rho_0} \vec{\nabla} \tilde{p}. \tag{2.20}$$

Then, substituting the above expression for $\tilde{p}^{ff}(r,\theta,\phi,t)$, the far-field acoustic velocity is

$$\vec{\tilde{u}}^{ff}(r,\theta,\phi,t) = \frac{-\tilde{P}^{ff}_{axis}(1m)}{j\omega\rho_0} \vec{\nabla}\left[\frac{\tilde{H}(\theta,\phi)}{r(m)} e^{-jk(r-1m)} \right] e^{j\omega t}. \tag{2.21}$$

In spherical component form,

$$\left\{ \tilde{u}^{ff}_r, \tilde{u}^{ff}_\theta, \tilde{u}^{ff}_\phi \right\} = \frac{\tilde{P}^{ff}_{axis}(1m)}{\rho_0 c} \frac{e^{j[\omega t - jk(r-1m)]}}{r(m)}$$
$$\left\{ \left(1 + \frac{1}{jkr}\right) \tilde{H}(\theta,\phi), \frac{1}{(-jkr)} \frac{\partial \tilde{H}(\theta,\phi)}{\partial\theta}, \frac{1}{(-jkr\sin\theta)} \frac{\partial \tilde{H}(\theta,\phi)}{\partial\phi} \right\} \tag{2.22}$$

27

Note, on the axis of any lobe in the beam pattern, $\dfrac{\partial \tilde{H}(\theta,\phi)}{\partial \theta} = \dfrac{\partial \tilde{H}(\theta,\phi)}{\partial \phi} = 0$,

$\tilde{u}_\theta^{ff} = \tilde{u}_\phi^{ff} = 0$, and there is only a radial component of acoustic velocity, which is related to the pressure by the specific acoustic impedance of an outgoing "pure" spherical wave:

$$\left\{ \tilde{u}_r^{ff}, \tilde{u}_\theta^{ff}, \tilde{u}_\phi^{ff} \right\} = \frac{\tilde{P}_{axis}^{ff}(1m)}{\rho_0 c} \frac{e^{j[\omega t - jk(r-1m)]}}{r(m)} \left\{ \left(1 + \frac{1}{jkr} \right) \tilde{H}(\theta,\phi), 0, 0 \right\} = \left\{ \frac{\tilde{p}^{ff}(r,\theta,\phi,t)}{\tilde{z}_{sph}}, 0, 0 \right\}, \quad (2.23)$$

where

$$\tilde{z}_{sph} = \frac{\rho_0 c}{\left(1 + \dfrac{1}{jkr} \right)} = \rho_0 c \left(\frac{jkr}{1+jkr} \right). \qquad (2.24)$$

Furthermore, in the limit $kr \gg 1$,

$$\lim_{kr \to \infty} \tilde{u}_r^{ff} = \lim_{kr \to \infty} \frac{\tilde{p}^{ff}(r,\theta,\phi,t)}{\tilde{z}_{sph}} = \frac{\tilde{p}^{ff}(r,\theta,\phi,t)}{\rho_0 c}. \qquad (2.25)$$

This defines, then, the plane-wave limit, i.e., $\lim r \gg r_{far\text{-}field} = $ (max lateral extent)^2/2 and $\lim kr \gg 1$.

2.   Bobber's Recommendation for Calibrating a Pressure-Gradient (Velocity) Receiver—a Hybrid Approach

As a simple procedure, Bobber [12] recommends obtaining the free-field received axial velocity sensitivity for a pressure-gradient transducer by a "hybrid" procedure. This hybrid procedure begins by performing a free-field, far-field (spherical wave) received pressure calibration with the velocity-sensitive axis oriented along the radial direction, then obtaining the velocity sensitivity by applying the proportionality factor relating radial velocity to pressure for far-field propagation conditions, e.g.,

$$\textit{Free - field axial velocity sensitivity in } \frac{volts}{\frac{m}{s}} =$$

28

$$Free\text{-}field\ pressure\ sensitivity\ in\ \frac{volts}{Pa} \times \left[\frac{free\text{-}field,\ far\text{-}field\ acoustic\ pressure}{free\text{-}field,\ far\text{-}field\ radial\ acoustic\ velocity} \right] =$$

$$Free\text{-}field\ pressure\ sensitivity \times \frac{\rho_0 c}{\left(1 + \dfrac{1}{jkr}\right)} =$$

$$Free\text{-}field\ pressure\ sensitivity \times \frac{jkr}{(1 + jkr)} \rho_0 c. \qquad (2.26)$$

Bobber [12] also points out that the previously given kr-dependent factor results in a magnitude difference in the free-field velocity sensitivity of less than 0.5 dB (~ 5%) for ranges r greater than about $1/2\ \lambda$ (1/2 wavelength). For practical sonar applications, then, the approximation that the free-field received axial velocity sensitivity of a pressure gradient (velocity) sensor equals $\rho_0 c$ times its free-field received pressure sensitivity is very well justified.

For all our experiments, the source-to-receiver distance d was 2 meters. For our in-air measurements, the smallest value of kd (f=300 Hz) was 11.0; the maximum kd-dependent correction to the velocity sensitivity would be 0.036 dB. For our in-water measurements, the smallest value of kd (f=1 KHz) was 8.4; the maximum kd-dependent correction to the velocity sensitivity would be 0.06 dB. In all cases, the kd-dependent correction was considered negligible and was not applied.

29

THIS PAGE INTENTIONALLY LEFT BLANK

III. IN-AIR MEASUREMENTS

A. PRESSURE-GRADIENT TRANSDUCERS USED IN THIS THESIS

In this research, we use two sort of pressure gradient transducers or velocity transducer, and they will be explained.

1. True Ribbon Transducer

The true ribbon transducer used in our thesis is the model RE-254, shown in Figure 17, which is manufactured by Audio Components DIY in Latvia.

The RE-254 employs an aluminum foil, 2.5 microns thick. It is designed for use as a microphone element. Because of its size and fragility, it was not tested as a speaker.

Figure 17.   True Ribbon Transducer. Source [8].

The ribbon has an electrical resistance of about 0.26 ohms. It is normally used with a 35-to-1 step-up transformer; however, we did not use it.

2. Planar-Magnetic Transducer

The planar-magnetic transducer used in this thesis, shown in Figure 18, was manufactured by the Bohlender-Graebener Company. It is designed as a high frequency speaker. The model used in the present thesis is the NEO 3W, whose dimensions are shown in Figure 19 and Table 1. It employs a push-pull magnet design (see Figure 14). We have no information about the thickness or mass of the diaphragm. It comes with a plastic cover bonded to the back, but we removed this. Two NEO 3W transducers were bought and tested, and we assigned them serial numbers 1 and 2.

The NEO 3W has a push-pull magnet design.

Figure 18.   Planar-Magnetic Transducer. Source [15].
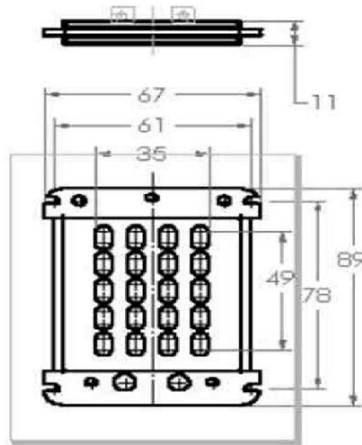
Dimensions are in mm.

Figure 19.   Dimensions of Planar-Magnetic Transducer. Source [16].

Table 1.   Specifications of Planar-Magnetic Transducer. Source [17].

Specifications	
Power Handling	20 Watts RMS; 50 Watts Max
Impedance	4 ohms
Freq. Range	2000-20,000 Hz
SPL	93 dB 2.83V/1m
Dimensions	3-1/2"L 2–5/8" W ½" D

B.   MEASUREMENT OF THE COMPLEX IMPEDANCE OF THE PLANAR-MAGNETIC TRANSDUCER

Table 2 lists the electronic equipment used to measure the complex electrical impedance of the NEO 3W transducers. A diagram of the measurement setup is shown in Figure 20.

Table 2.   Complex Impedance Apparatus

Equipment	Brand
02 Planar Magnetic	NEO 3W
Network Analyzer	Agilent E5061B 5Hz –3 GHz
Impedance Analyzer	16047E Test Fixture

Procedure:

In order to measure the complex impedance, it is necessary to set up the Agilent E5061B, with a frequency range of 300 Hz to 4800 Hz, and time sweep of 120 seconds.

Figure 20.   Block Diagram to Measure the Complex Impedance.

The impedance magnitude for planar-magnetic transducers 1 and 2 is shown in Figure 21. The resistance and reactance of planar-magnetic transducers 1 and 2 are shown in Figures 22 and 23, respectively.
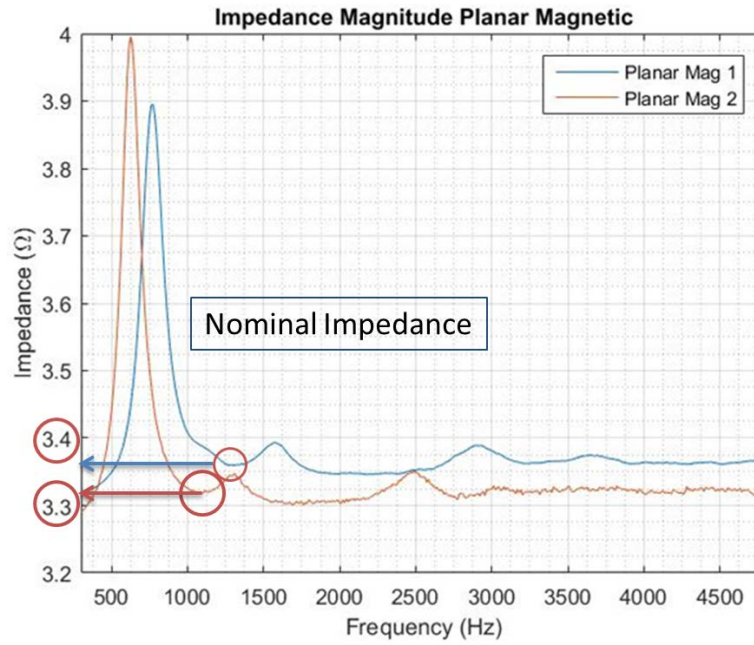
Figure 21.   Impedance Magnitude of Planar-Magnetic 1 and 2.
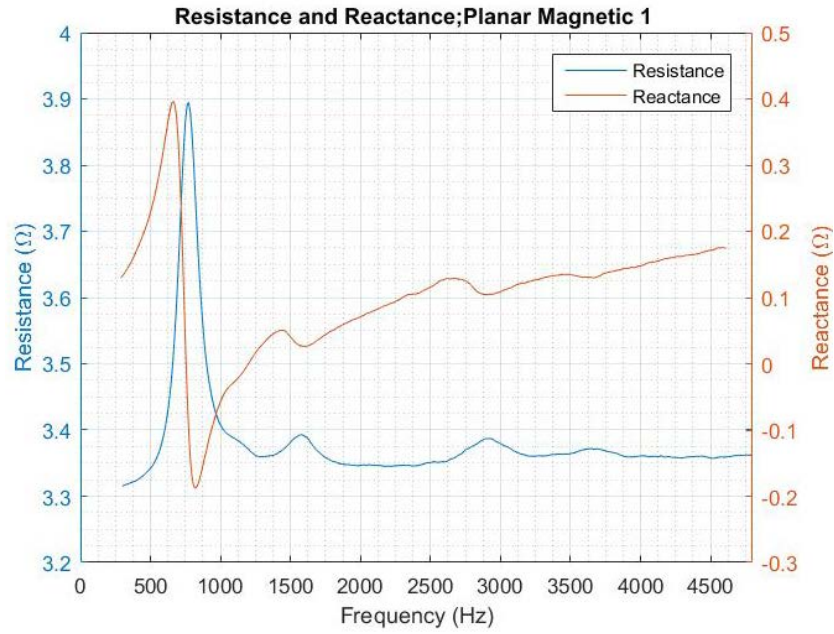
Figure 22.　Resistance and Reactance of Planar-Magnetic 1.
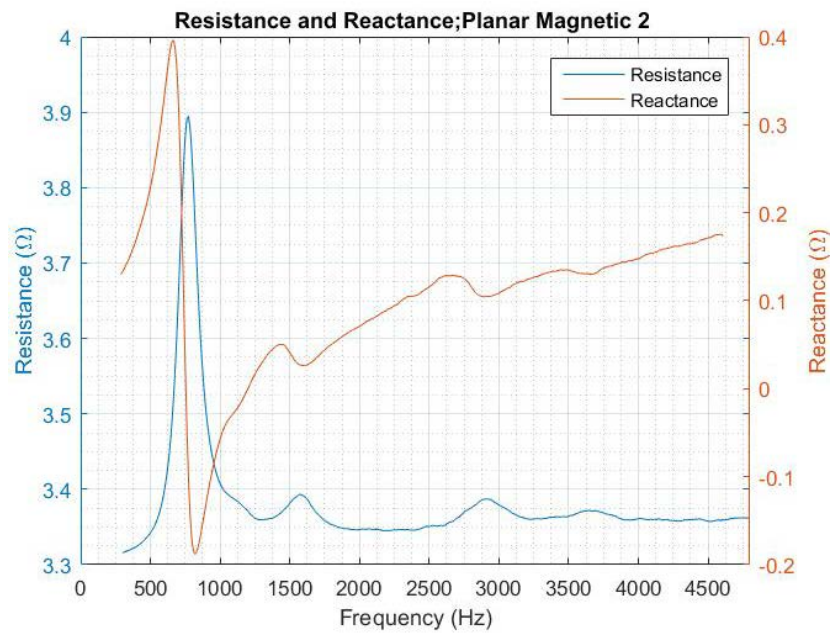
Figure 23.　Resistance and Reactance of Planar-Magnetic 2.

Figure 21 shows the strong feature of the peak for both planar-magnetic transducers that is the typical signature of the mechanical resonance. The resonance of planar-magnetic transducer 1 is between 770 Hz and 780 Hz, and in the case of planar magnetic transducer 2 is between 620 Hz and 630 Hz. In addition, there is evidence of other mechanical resonances at frequencies of roughly 1500 Hz and 2900 Hz.

The first minimum above the resonance (see red circles in Figure 21) shows the nominal impedance to be between 3.3 and 3.4 ohms in comparison to the manufacturer's value for the NEO 3W of 4 ohms according to Table 1.

Figures 22 and 23 show the resistance versus reactance part of both planar magnetic transducers. Both graphs show the resistance is greater than the reactance. In fact, the reactance has a value of 0.2 ohms roughly in comparison to the resistance between 3.3 ohms and 3.4 ohms. We notice the resistance is almost 20 times greater than the reactance showing that we have a very resistive load in the operating frequency. This is a direct consequence of the serpentine pattern of the foil conductor as opposed to the coil design of a typical loudspeaker.

C.   GENERAL DESCRIPTION OF ACOUSTIC MEASUREMENTS IN AIR

Now we describe the anechoic chamber, the general set-up for each experiment, the auxiliary transducers used in measurements in air and the calculation of far-field.

1.   Anechoic Chamber

The Naval Postgraduate School Physics Department anechoic chamber is shown in Figure 24. It provides an echo-free region in which basic acoustic research may be conducted on sound sources, receivers, and scatterers, without interference from wall reflections or external noises.

The following legend is copied from a picture outside the anechoic chamber depicting it:

> Isolation: Noise transmission from outside is minimized by a floating room within a room construction. The outer 12" concrete walled room is separated from the inner room of concrete block sides and floor by a 2"

blanket of Fiberglass or cork. The Fiberglass wedges are attached to the walls, ceiling and floor of the inner room.

Absorption: Reflection of sounds from the side walls is minimized by the Fiberglass wedges, which are designed to trap and absorb sounds incident upon them. These 40" wedges absorb approximately 99% of the energy of incident sounds of frequency greater than 100 cycles per second [18].
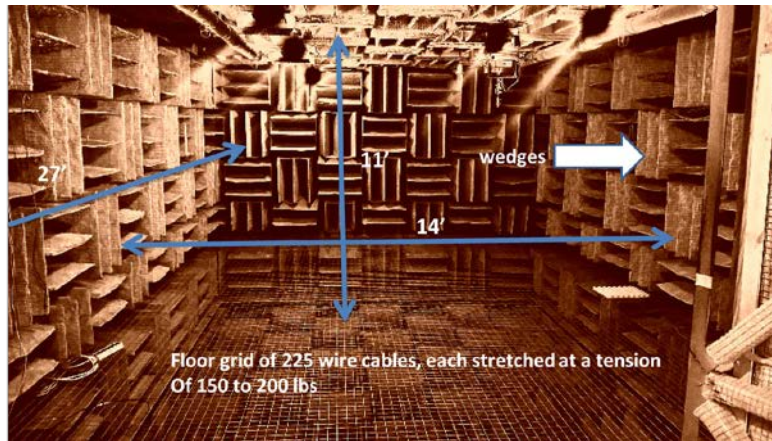
Figure 24.   NPS Physics Department Anechoic Chamber.

2.   General Setup

All measurements conducted in the anechoic chamber, such as beam patterns, comparison calibrations and reciprocity calibrations, were set up with 2 meters' separation between sources and receivers, as is shown in Figures 25 and 26. Furthermore, the drivers and receivers were vertically located at the approximate center of the anechoic chamber. One transducer was affixed to a rotator; the other could not be rotated.
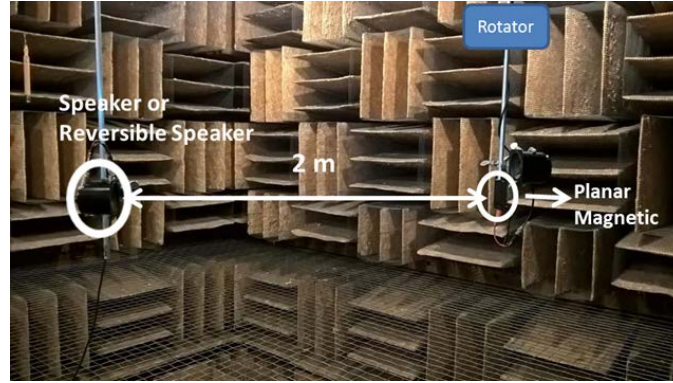
Figure 25.   Speaker or Reversible and Planar Magnetic (PM 1 or PM 2).
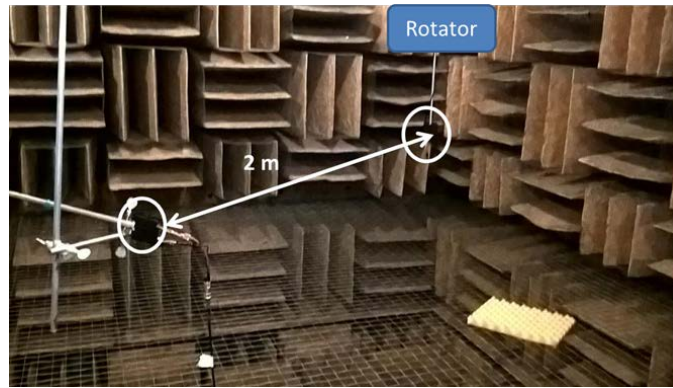
Figure 26.   Planar Magnetic 1 and Planar Magnetic 2 (PM 1 or PM 2).

It is noteworthy that all experiments performed in the anechoic chamber were accomplished in the following range of frequencies from 300 Hz to 4800 Hz, whose wavelengths compared to transducer width are shown in Table 3.

Table 3.   Wavelength Compared to Width of Planar Magnetic Transducer

Frequency (Hz)	$\lambda = \dfrac{c}{f} = \dfrac{343\,m/s}{f}$	Width planar magnetic	$\dfrac{\lambda}{Transducer\ \text{width}}$
300	1.14 m	0.067 m	17.0
1200	0.28 m	0.067 m	4.12
2100	0.16 m	0.067 m	2.39
3000	0.11 m	0.067 m	1.64
3900	0.09 m	0.067 m	1.34
4800	0.07 m	0.067 m	1.04

All acoustic wavelengths are greater than the width of the planar magnetic transducer;
the same is true for the true ribbon transducer.

3. Auxiliary Transducers Employed

Besides the true ribbon and planar-magnetic transducers, other acoustic transducers used are a laboratory standard-quality condenser microphone and two small loudspeakers. (One is used as source, and the other is used as a reversible transducer in the reciprocity calibration.)

a. GRAS Condenser Microphone

The GRAS 40 AF free-field microphone serial number 31881 (Figure 27) is used as a receiver in the thesis. It has the following specifications shown in Table 4, and more details are provided in Appendix D.

Table 4.   Specifications of GRAS Condenser Microphone Type 40 AF

SPECIFICATIONS	
Frequency Range (+/- 1 dB)	5Hz-10 KHz
Resonance Frequency	14 KHz
Sensitivity	45 mV/Pa or -26.88 dB re 1V/Pa

Figure 27.   GRAS 40 AF Free-Field Microphone and Its Dimensions. Source [19].

b.   Optimus Speaker

The Optimus speaker model XTS 35 (Figure 28) is used as a source in the thesis. It has the specifications shown in Table 5.

Table 5.   Specifications of OPTIMUS Speaker XTS 35. Source [20].

SPECIFICATIONS	
Frequency Response	140Hz-20KHz
Power Handling	15 Watts (RMS)
Max Power	30 Watts
Impedance	8Ω
Diameter	3"

Figure 28.   Optimus Speaker Model XTS 35.

c.   Radio Shack Speaker

A Radio Shack speaker mid-range tweeter is used as the reversible transducer for reciprocity calibration in air in this thesis. It is shown in Figure 29, and we can notice that the speaker is closed back and has the following specifications presented in Table 6.

Table 6.   Specifications of Radio Shack Speaker Mid-Range Tweeter. Source [20].

SPECIFICATIONS	
Frequency Response	700Hz-20KHz
Power Handling	30 Watts (Max)
Efficiency	89 dB $SPL/1W/1m$
Impedance	8Ω
Diameter	3"

In the research, this speaker is used as a reversible transducer. Numbers 2 and 3 show this type of speaker is closed back.

Figure 29.   Radio Shack Mid-Range Tweeter Speaker.

d.   *Turntable System Type 9640*

The turntable system type 9640 is made up of turntable type 5960 and its controller, as shown in Figure 30. It rotates a test object for the measurement of its directional response [21] and is used in this thesis to determine the beam pattern in air. More details are available in Appendix D.

Figure 30.   Turntable System Type 9640. Source [21].

4.   Far-field Propagation Conditions

To verify that all experiments are conducted in far-field conditions, the usual formula for the far-field transition range is calculated from

$$r = \frac{\left(\dfrac{L}{2}\right)^2}{\lambda},$$ (3.1)

where L is a representative lateral transducer dimension and λ is the acoustic wavelength. The Radio Shack and Optimus speakers have the same diameter (see Tables 5 and 6), and this is the greatest lateral dimension of all the transducers used. Therefore, this dimension is used for a "worst case" calculation of far-field range. Table 7 shows the variables and the different values, and Table 8 shows the range to the far-field.

Table 7.   Variables and Values Used to Calculate the Range to Far-Field

Variables	Values
L	Diameter= 3" roughly 7.62 cms
c	343 m/s
f	From 300 Hz to 4800 Hz

Table 8.   Range to Far-Field

Frequency (Hz)	$r = \dfrac{\left(\dfrac{L}{2}\right)^2}{\lambda}$
300	1.3 mm
2100	8.9 mm
3000	12.7 mm
3900	16.5 mm
4800	20.3 mm

The results show that all measurements are in the far-field.

D.   IN-AIR BEAM PATTERNS

Experiments were conducted to measure the receiving and transmitting beam patterns of the planar-magnetic transducers and the receive beam pattern of the true ribbon transducers. These beam patterns are used to verify the shape and behaviors of the lobes at different frequencies.

1.   Experimental Procedure

All beam pattern experiments are conducted with a 2-meter separation between source and receiver. Receiving and transmitting beam patterns are measured for the planar-magnetic transducer(s); only receiving beam patterns are measured for the true ribbon transducer, due to its poor performance as a radiator at the frequencies of interest to us.

For the receiving beam pattern, the planar-magnetic or the true ribbon transducer is affixed to the rotator as a receiver, and the loudspeaker is affixed to the non-rotating hanging rod. The angular orientation of the rotator is then set to its midpoint (180.0 degrees in its display), and the designated "front" face of the receiving transducer is manually "pointed" toward the loudspeaker. This ensures that the beam pattern data are collected with the "front" lobe spanning the central portion of the data set.

43

For the transmitting beam pattern, the planar-magnetic transducer is affixed to the rotator as a source, and the microphone is affixed to the non-rotating hanging rod as a receiver. Again, the planar-magnetic transducer is mounted to the rotator so that the beam pattern data are collected with the front lobe spanning the central portion.

The rotator can revolve in both directions, clockwise (CW) or counter-clockwise (CCW) with constant rate, but we use only one direction in order to minimize the experimental error. The rotator makes slightly more than one complete rotation, because it takes a little time for the rotator to come into steady rotation when it starts to rotate again. The few degrees of extra rotation in addition to a full 360-degree rotation guarantees that a full rotation occurs at constant speed.

Each beam pattern measurement is conducted at constant frequency, and this is manually selected by using the function generator. We use six frequencies from 300Hz to 4800Hz in increments of 900Hz.

The time base of the oscilloscope can show 10,000 samples and adjust the time scale. For the planar-magnetic transducer, we use a 200-second time span with 50 samples per second. For the true ribbon transducer, we use a 400-second time span with 25 samples per second. Both time spans depend on the rotation rate and are enough for full 360-degree rotation.

In order to get data from the experiments, first, the rotator should be stopped and then the oscilloscope would be manually triggered to show the magnitude of the received signal. After few seconds with the oscilloscope running, the rotator is started. It is automatically stopped at the full 360-degree rotation. Once the rotation is completed, the oscilloscope is stopped to get the magnitude data.

2. Data Analysis Procedure

All the beam pattern data analyses in air are conducted by MATLAB (code in Appendix E) using raw data from the experiment in accordance with same procedure. The experiments' raw data has two types of values; one is the 360-degree revolution time data, and the other is the magnitude data corresponding to the specific time. In the beam

pattern experiments for the planar-magnetic transducer, we use 120 seconds of the revolution time, which means the rotation rate is 3 degrees per second. The data sampling rate is 50 samples per second, or 50 samples/3degrees. And, for the true ribbon transducer, we use 360 seconds revolution time, which means rotation rate is 1 degree per second and it guarantees higher resolution than the planar-magnetic transducer's beam pattern analysis. The data sampling rate is 25 samples per second, and 25 samples/degree.

For the data analysis, we assume that the rotation rate selected on the rotator is correct. Then, an analysis is done for each beam pattern data set to estimate the location of the acoustic axis, and correct the raw angular position data to set the angle of this axis to zero.

To estimate zero degrees, first, we perform a 257-point average of the raw magnitude data. For example, Figure 31 shows both unprocessed and 257-point smoothed magnitude data for the planar-magnetic transducer, at a frequency of 2100Hz.
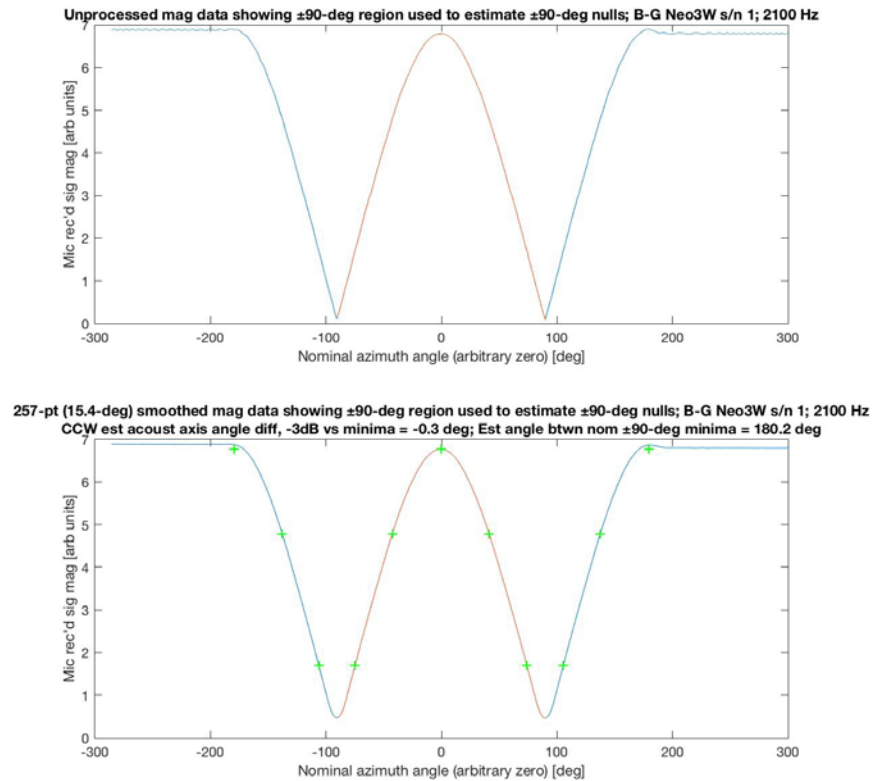
Figure 31.   Unprocessed Magnitude Data and 257-Point-Smoothed Magnitude Data.

45

From 257-point-smoothed magnitude data, we determine the maximum magnitude of the central (front) lobe and find the -3 dB and the -12 dB points in the smoothed data.

One estimate for the zero-degree direction is the midpoint of the -3 dB points. The -12 dB points are used to estimate the locations of the minima (ideally nulls). A second estimate for the zero-degree direction is the midpoint of the -12 dB points. The magnitude difference in the two zero-degree estimates is less than 2.1 degrees (Table 10) in all cases. We examine polar plots of the directional responses for all our data sets and judge that the plots using zero degrees as estimated using the -12 dB points are more likely to be correct.

Once we estimate the zero-degree direction, we adjust the raw rotation angle data with respect to the estimated zero-degree direction. Then, we average the raw data over approximately 1 degree (17 points for the planar-magnetic data, 25 points for the true ribbon data) to produce a data record that is centered at the estimated acoustic axis (see Figure 32, for example), and these data are used for polar plots.
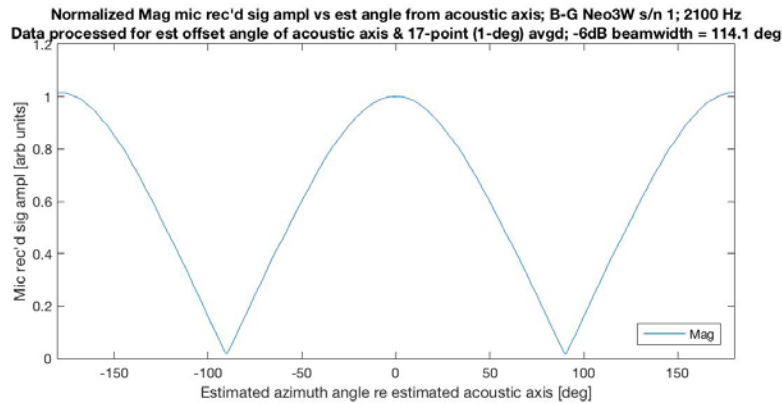
Figure 32. Clipped Magnitude Data from -180 Degrees to +180 Degrees Using Adjusted Acoustic Angle.

3. Planar-Magnetic Transducer Beam Patterns in Air

The electronic equipment listed in Table 9 and Figure 33 shows the experimental setup for measurement beam patterns in the anechoic chamber.

Table 9.　　Beam Pattern Apparatus (Planar Magnetic Transducer)

Equipment	Brand
Planar Magnetic	NEO 3W
Microphone	40 AF free-fields
Speaker	Optimus (Source)
Power Amplifier	Hp 476A
Power Module	GRAS power Module Type 12 AA (20 dB)
Turntable Controller	Type 5997 Bruel & Kjaer
Lock in Amplifier	Stanford Research Model SR530
Oscilloscope	Tektronic DPO2014
Function Generator	Agilent 33220 A

The function generator is set to output a sinusoidal signal to the power amplifier, which then transmits the signal to the source to radiate sound. The received signal passes through the lock-in amplifier; thereby it is filtered by a very narrow band-pass filter to be displayed by the oscilloscope and recorded as data points. We took 10,000 points for this experiment at 50 sample points per second. Of these, 6,000 points were kept corresponding to 120 seconds for the full 360-degree rotation (3 degrees per second).
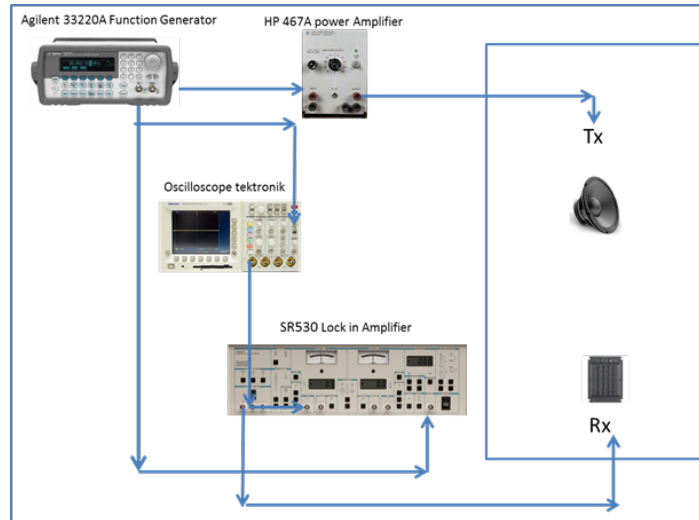
Figure 33.　　Block Diagram for the Planar-Magnetic Beam Pattern Measurement in Air.

a. Receiving Beam Pattern Analysis

Figure 34 and Figure 35 show the receiving beam pattern of the planar-magnetic transducer 1. Each figure includes the six selected frequencies' beam pattern plus an ideal cardioid beam pattern. Basically, both figures have the same information, but Figure 34 depicts the magnitude on a linear scale while Figure 35 represents the conventional 40 dB range.
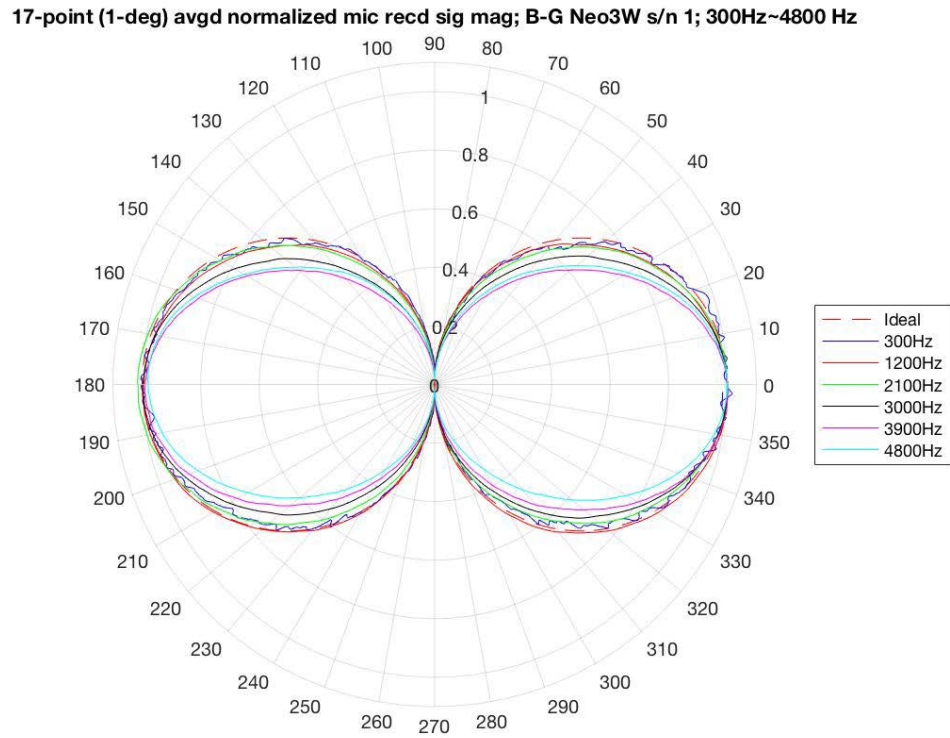
Figure 34.   Receiving Beam Pattern of Planar-Magnetic Transducer in Linear Scale.
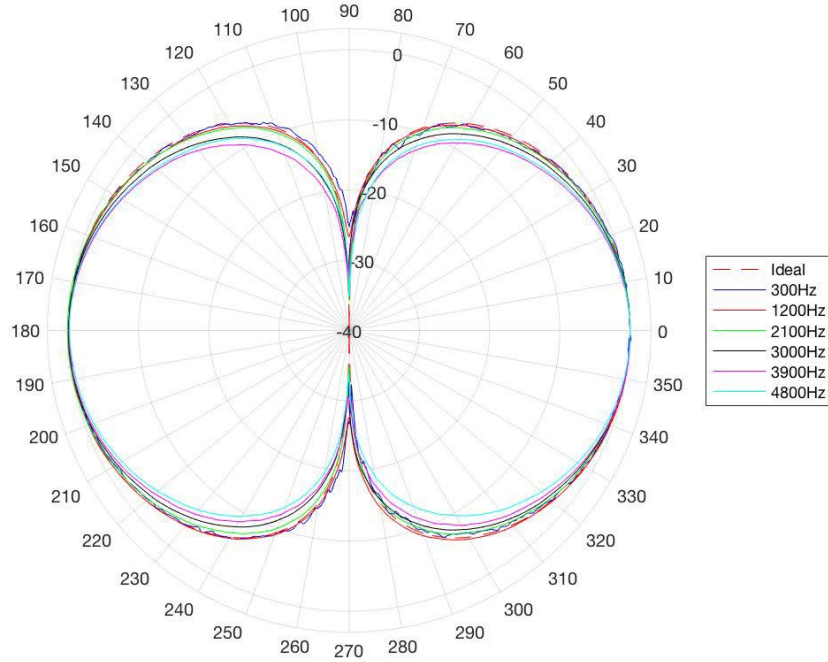
Figure 35.   Receiving Beam Pattern of Planar-Magnetic Transducer in dB Scale.

At all six selected frequencies, the planar-magnetic transducer beam pattern corresponds well with an ideal dipole beam pattern.

An ideal cardioid beam pattern has 120 degrees beam width at the -6 dB points. Since -6 dB corresponds to 0.5 on a linear scale, we find the angle between these points on the linear scale. Table 10 shows the receiving -6 dB beam width of the planar-magnetic transducer. According to the measured beam width, we find that the higher frequency has a narrower beam width and higher directivity.

Table 10.   Beam Width (-6dB) and Angular Offset Differences of the Planar-Magnetic Transducer

Freq. (Hz)	Receiving BW (Deg)	Transmit BW (Deg)	Angular offset difference(Deg), -3dB estimate vs -12dB estimate		$\dfrac{\lambda}{Trans.\text{width}}$
			Receiving	Transmitting	
300	117	121	0.0	-0.4	17.0
1200	120	118	-1.7	-1.3	4.12
2100	114	115	-0.3	-0.5	2.39
3000	109	110	-1.0	1.4	1.64
3900	101	105	-2.1	1.4	1.34
4800	98	99	0.4	1.1	1.04

Beam width (-6 dB) of ideal cardioid is 120 degrees, and the planar-magnetic width is 0.067m. Angular offset difference between acoustic axis as estimated using the -3 dB points versus the – 6 dB points.

b.   *Transmitting Beam Pattern Analysis*

Figure 36 and Figure 37 show the transmitting beam pattern of the planar-magnetic transducer 1. Each figure includes the six selected frequencies' beam pattern plus an ideal cardioid beam pattern. Basically, both figures have the same information, but again Figure 36 depicts the magnitude in linear scale while Figure 37 represents the conventional 40 dB range.
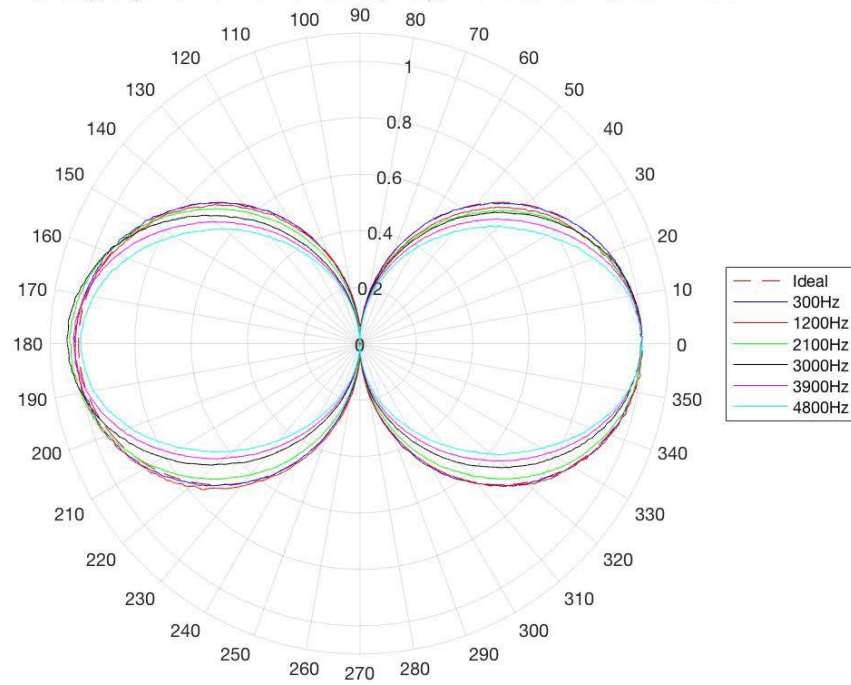
Figure 36.   Transmitting Beam Pattern of Planar-Magnetic Transducer in Linear Scale.
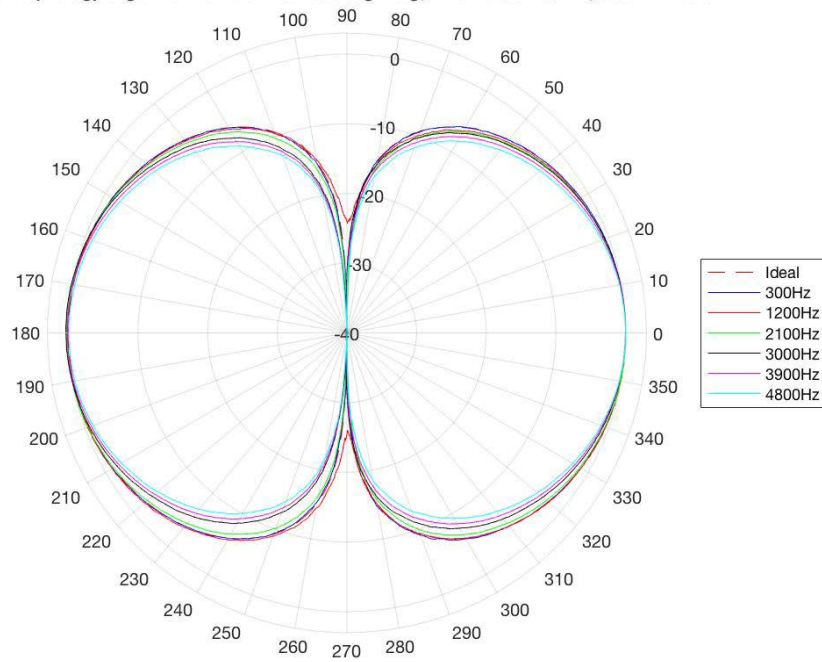
Figure 37.   Transmitting Beam Pattern of Planar-Magnetic Transducer in dB Scale.

The transmitting beam patterns of the planar-magnetic transducer are also similar to an ideal dipole beam pattern. Table 10 shows the transmitting -6 dB beam widths of the planar-magnetic transducer. According to the measured transmitting beam widths, the higher frequency has a narrower beam width and higher directivity. Also, the -6 dB transmitting beam widths are nearly the same as the – 6 dB receiving beam widths, as expected.

4.   True Ribbon Transducer Beam Patterns in Air

The electronic equipment is listed in Table 11, and Figure 38 shows the experimental setup for measuring the beam pattern of the true ribbon transducer in the anechoic chamber.

Table 11.   Beam Patterns Apparatus (True Ribbon Transducer)

Equipment	Brand
Ribbon Transducer	Model RE-254
Speaker	Optimus
Power Amplifier	Hp 476A
Power Module	GRAS power Module Type 12 AA (0dB)
Lock in Amplifier	Stanford Research Model SR530
Turntable Controller	Type 5997 Bruel & Kjaer
Oscilloscope	Tektronic DPO2014
Function Generator	Agilent 33220 A
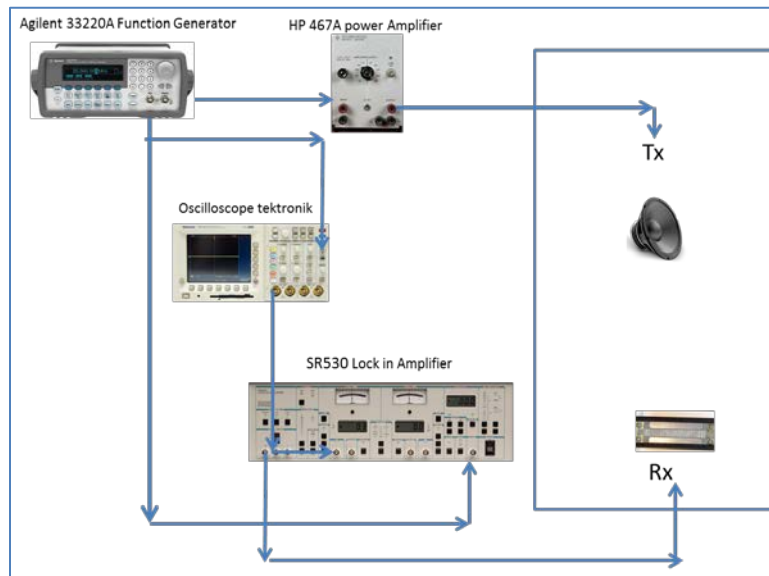
Figure 38.   Block Diagram for the True Ribbon Beam Pattern Measurement in Air.

The setup for measurement of the true ribbon transducer's beam pattern is almost same as the planar-magnetic transducer experiment. The only difference is the receiver, where the true ribbon replaces the planar-magnetic transducer.

We take 10,000 data points for this experiment at 25 sample points per second. Rotating at a constant rate of 360 seconds for a full 360-degree rotation (1 degree per second), this gives a higher angular resolution than the planar-magnetic beam patterns.

a. Receiving Beam Pattern Analysis

Figure 39 and Figure 40 show the receiving beam pattern of the true ribbon transducer. Each figure includes the six selected frequencies' beam pattern plus an ideal cardioid beam pattern. Again, Figure 39 has a linear scale while Figure 40 has a dB scale.

For the planar-magnetic beam pattern analysis, we use 17-point (1-degree) averaged magnitudes, but for the true ribbon beam pattern, we use 25-point (1-degree) averaged magnitudes.

Table 12 shows the wavelengths of frequencies we use in this experiment and the width of true ribbon. All frequencies' wavelengths are greater than the width of the true ribbon, so that we expect the true ribbon would have dipole beam patterns at all frequencies.

Table 12.   Wavelength Compared to Width of True Ribbon Transducer

Frequency (Hz)	$\lambda = \dfrac{c}{f} = \dfrac{343\,m/s}{f}$	Width true ribbon
300	1.14 m	0.022 m
1200	0.28 m	0.022 m
2100	0.16 m	0.022 m
3000	0.11 m	0.022 m
3900	0.09 m	0.022 m
4800	0.07 m	0.022 m
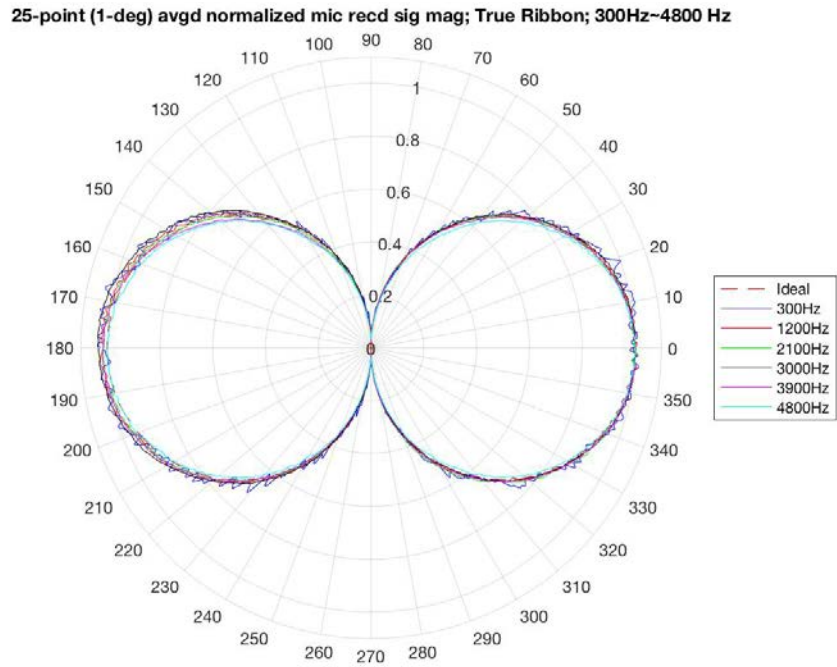
Figure 39.   Receiving Beam Pattern of the True Ribbon Transducer in Linear Scale,
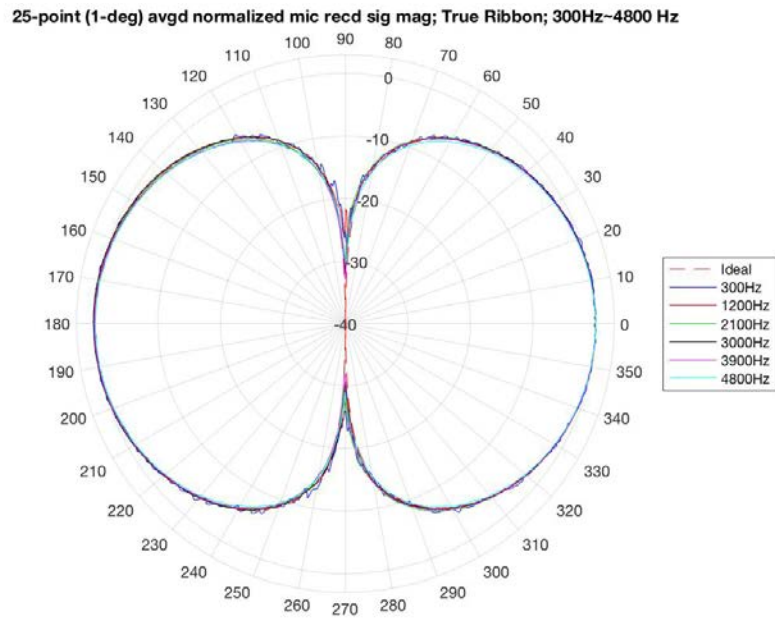
Figure 40.   Receiving Beam Pattern of the True Ribbon Transducer in dB Scale.

At the frequency of 300 Hz, we could observe more noise than at other frequencies because the true ribbon transducer receives a weaker signal at low frequency.

54

However, the true ribbon transducer has good dipole beam patterns over all frequencies, and the -6 dB beam widths are very close to the ideal cardioid one (Table 13).

Table 13.   Receiving Beam Width (-6dB) and Angular Offset Difference of the True Ribbon Transducer

Freq. (Hz)	Receiving BW (Deg)	Angular offset difference(Deg), -3dB estimate vs -12dB estimate (Receiving Beam Pattern)	$\dfrac{\lambda}{Trans.\text{width}}$
300	123	- 0.3	51.8
1200	122	- 0.3	12.7
2100	122	- 0.7	7.27
3000	121	0.0	5.00
3900	121	- 0.7	4.09
4800	117	- 0.5	3.18

Beam width (-6 dB) of ideal cardioid is 120 degrees and the true ribbon width is 0.022m. Angular offset difference between acoustic axis as estimated using the -3 dB points versus the – 6 dB points.

E.   IN-AIR, ON-AXIS COMPARISON CALIBRATIONS

Comparison calibration is a method to obtain the transmitting or receiving sensitivity of an unknown transducer by comparison with a calibrated microphone. The transmitting sensitivity of an unknown transducer is obtained directly using the calibrated microphone as a receiver. The receiving sensitivity of an unknown transducer is obtained from the ratio of two received voltage measurements, one from the unknown transducer and one from the calibrated microphone.

1.   Planar-Magnetic Transducer Transmitting Sensitivity

The electronic equipment is listed in Table 14, and the setup for the transmission voltage response experiment in the anechoic chamber is shown in the block diagram in Figure 41. The separation between source and receiver is 2 meters.

Table 14.   Comparison Calibration Apparatus (Planar Magnetic Transducer)

Equipment	Brand
Planar Magnetic	NEO 3
Microphone	GRAS 40 AF free-field microphone
Power Amplifier	Hp 476A
Power Module	GRAS power Module Type 12 AA (20dB)
Speaker	Optimus
Signal Analyzer	Stanford Research Model SR785
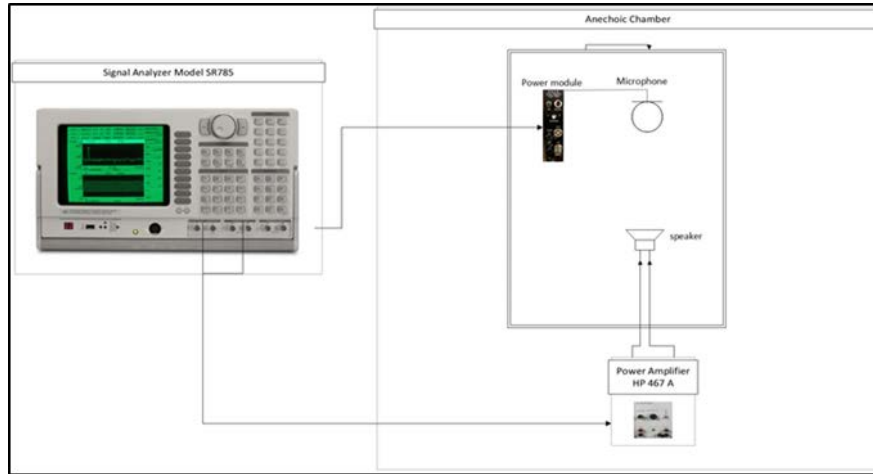
Figure 41.   Block Diagram for Transmission Voltage Response.

To measure the Transmitting Voltage Response (TVR), we use the configuration as shown in Figure 42.

Figure 42.   Configuration for the Transmitting Voltage Response.

The Stanford research model SR 785 signal analyzer is set up in the range of frequencies from 240 Hz to 3800 Hz with constant voltage.

Steps are presented for calculating the Transmitting Voltage Response (TVR). It is the acoustic pressure level as a function of input voltage, and its unit is Pa/V at a range of 1 meter.

The data obtained from the SR785 signal analyzer are frequencies in the "x" axis, and voltage gain=(microphone system output voltage)/(drive voltage to speaker) in the "y" axis. In this case, the output gain magnitude, is amplified by the factor of 10, from a GRAS power module type 12AA. Therefore, for this calculation, the raw magnitude data must be divided by a factor of 10, before we can apply the microphone sensitivity to obtain the TVR.

The gain in the power module is set to 20 dB, and the calculation to obtain a gain of 10 is shown below:

$$20 dB = 20 \log_{10}(GAIN),$$
(3.2)

$$10^1 = GAIN$$
(3.3)

The sensitivity of the GRAS 40 AF free-field microphone is 45.3 mV/Pa.

The distance is 2 meters between the driver and receiver, but the TVR is referenced to a range of 1 meter. Therefore, to adjust the range, a factor of

$$20 \log_{10}(2m)$$
(3.4)

must be added. There also is the factor $20 \log_{10}(20 \times 10^{-6})$, which must be subtracted to make the reference pressure $20 \mu Pa$. Finally, the calculation of the Transmitting Voltage Response is:

$$TVR = 20 log_{10}(\text{raw SR785 data}) - 20 log_{10}(10) - \ldots$$
$$20 log_{10}(45.3 mV / Pa) - 20 log_{10}(20 \cdot 10^{(-6)}) + \ldots$$
$$20 log_{10}(2m) \ dBre \frac{20 \mu Pa}{V} @1m$$
(3.5)

The final result can be seen the graph in the Figure 43.
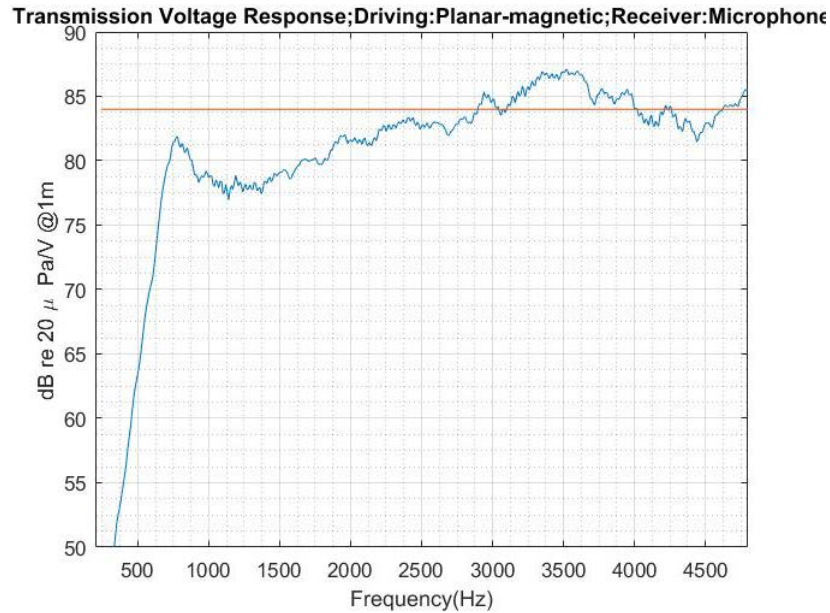
Figure 43.   Transmission Voltage Response of the Planar-Magnetic Transducer.

The manufacturer data about the transmitting voltage response of the planar-magnetic was done in a baffle of 9"x22," with a driving voltage of 2.83 V/1 m, in a frequency range of 2 KHz to 20 KHz, and gives an average value of 93 dB. The manufacturer Transmission Voltage Response (TVR) referenced to 1V is 9dB. When this is subtracted from the manufacturer sensitivity of 93 dB, it yields 84 dB. The 84 dB is shown in the red line of the Figure 43. We expect our TransmissionVoltage Response (TVR) is smaller (blue curve in Figure 43) because our transducer is not mounted in a baffle, so the difference we observe between our estimated Transmission Voltage Response and the manufacturer's is probably reasonable.

2.   Planar-Magnetic Transducer and True Ribbon Transducer Receiving Sensitivities

In this point is to obtain the sensitivity of the true ribbon and planar-magnetic transducers

a.   *Planar-Magnetic Transducer*

The experiment consists of two measurements or configurations as is shown in Figure 44. The measurement basically consists of mounting independently the microphone and planar-magnetic transducer as a receiver in the far-field. After that, the Optimus loudspeaker (LS) is used as a source for both configurations. The signal analyzer data collected is the output voltage of the planar-magnetic transducer (PM), divided by Optimus loudspeaker (LS). Similar to the previous measurements, the results are divided by the gain setting of the power supply/preamplifier factor of 10 and multiplied by the microphone sensitivity (45.3 mV/Pa), as shown in Equation (3.6). In this manner, it is possible to obtain the free-field open circuit voltage sensitivity.

Configuration	Driving	Receiver	Measurement
1			Voltage
2			Voltage
Configuration	Driving	Receiver	Measurement
1			Voltage
2			Voltage

Figure 44.   Configuration for Comparison Calibration of Planar-Magnetic and True Ribbon Transducers.

$$Free-Field\ Voltage\ sensitivity = \frac{\left(PM_{out}\Big/LS_{in}\right)}{\left(\dfrac{MIC_{out}}{10}\Big/LS_{in}\right)} \cdot 45.3\frac{mV}{Pa}$$

(3.6)

The Equation (3.7) shows the calculation of the free-field voltage sensitivity in dB

$$20\log_{10}\left(\frac{PM_{out}}{LS_{in}}\right) - 20\log_{10}\left(\frac{\dfrac{Mic_{out}}{10}}{LS_{in}}\right) + 20\log_{10}\left(45.3\times10^{-3}\right) \tag{3.7}$$

Figure 45 shows plots of the first two terms in Equation (3.7), where the blue curve represents the raw voltage frequency response of the planar-magnetic transducer in dB and the red curve represents the raw voltage frequency response of the microphone in dB. Figure 46 shows the results calculated by Equation (3.7) represented by the blue curve.
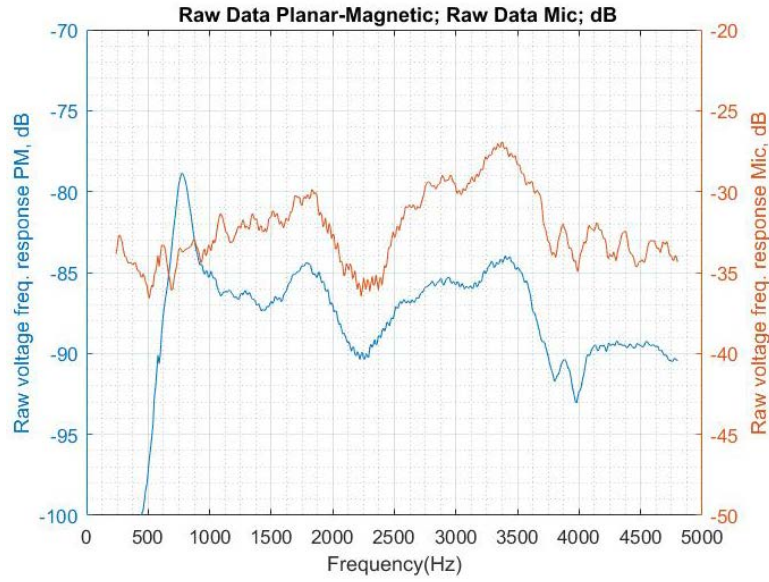
Figure 45.　Raw Data Planar-Magnetic and Raw Data Microphone.
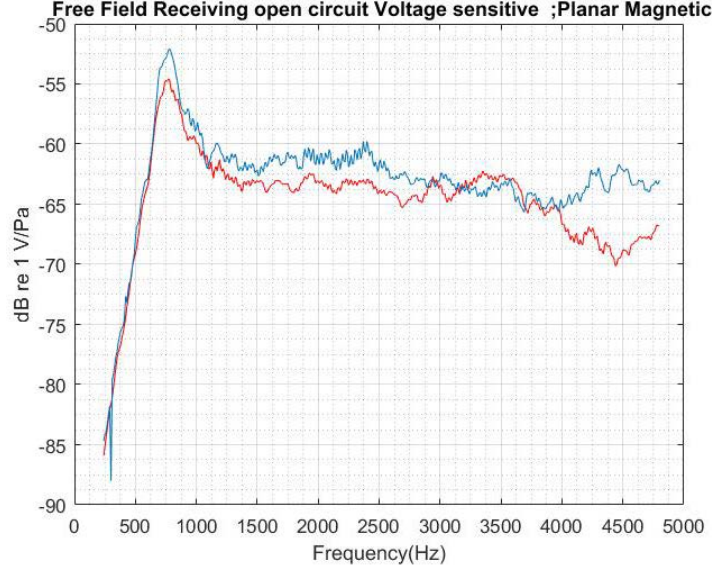
Figure 46.   Comparison Calibration of the Planar-Magnetic Transducer Using Two
Methods of Calculation.

Since the planar-magnetic transducer is reversible, that is, it can act as either a
source or receiver, its transmitting and receiving sensitivities are not independent, and so
another estimate of its receiving sensitivity should be obtainable from the results for its
Transmission Voltage Response, shown in Figure 43.

For a reversible transducer, its open-circuit receiving sensitivity M_o and its
current transmitting sensitivity S_i are related by

$$\frac{M_o}{S_i} = J = \frac{2d}{\rho_0 f},$$ (3.8)

where M_o = open-ckt receiving voltage sensitivity in V/Pa; S_i = current transmitting
sensitivity in Pa/amp @ 1 m. We do not have the current transmitting sensitivity. We
have the voltage transmitting sensitivity S_v. However, these are related by

$$S_i = S_v \cdot Z,$$ (3.9)

where Z is the transducer's electrical impedance. The electrical impedance of the planar-
magnetic transducer is nearly a constant 3.5 ohms. Using this value for Z and also setting

61

d=1 m, the reference range for S_v and S_i, we have the independent estimate of M_o from S_v

$$M_o = \frac{2d}{\rho_0 f} S_i = \frac{2d}{\rho_0 f}(3.5\Omega) \cdot S_v \ . \tag{3.10}$$

The result is plotted as the red curve in Figure 46. The agreement between the two curves is satisfactory up to about 4 KHz. The difference above 4 KHz is probably due to acoustical conditions during the performance of the experiments, i.e., scattering from the nearby objects.

b.   True Ribbon Transducer

Using a comparison calibration, we now use the true ribbon as a receiver. Table 15 shows the electronic equipment used, and Figure 47 shows the diagram of the experiment.

Table 15.   Comparison Calibration Apparatus (True Ribbon Transducer)

| Equipment	Brand
Ribbon Microphone	Model RE-254
Microphone	40 AF free-fields
Power Amplifier	Hp 476A
Power Module	GRAS power Module Type 12 AA (20dB)
1 Speaker	Optimus
Signal Analyzer	Stanford Research Model SR785

The distance between driver and receiver is 2m.
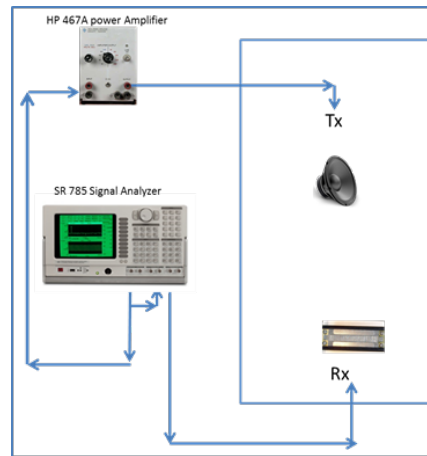
Figure 47.   Block Diagram for Receiving Voltage of the True Ribbon Transducer as a Receiver.

62

As depicted in Figure 44, two types of measurements are conducted using the same procedure as for the planar-magnetic transducer. The only difference here is that the microphone system gain setting of its power supply/preamplifier, is 1 not 10 (see the graph in Figure 48). The free-field open circuit sensitivity is calculated as in Equation (3.7), only taking a microphone gain of 1, as shown in the Figure 49.
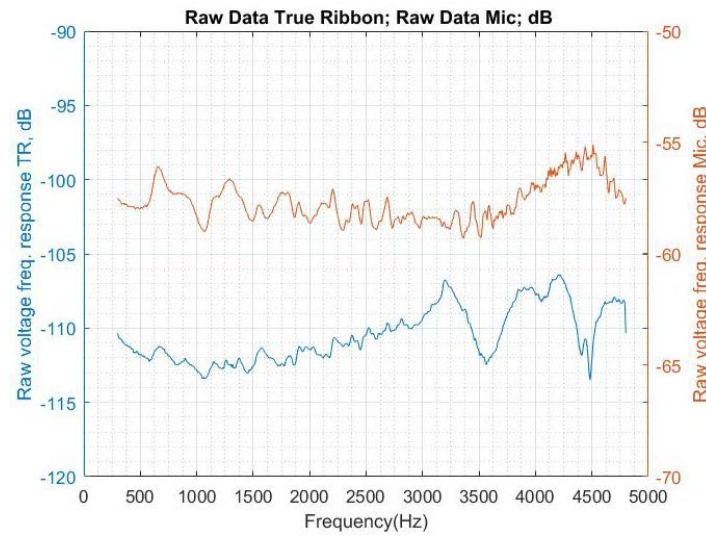
Figure 48.   Raw Data True Ribbon and Raw Data Microphone.
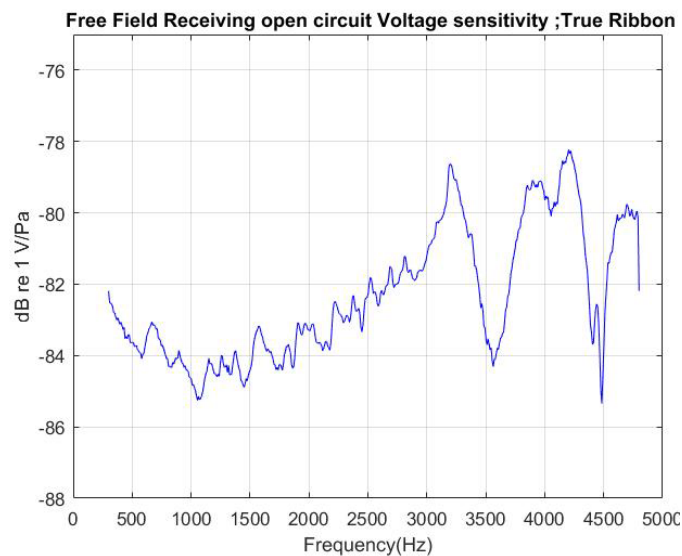
True ribbon transducer and microphone independently measured

Figure 49.   Comparison Calibration of the True Ribbon Transducer.

Figure 49 shows many irregularities, especially at frequencies above 3000 Hz. The cause of these is unknown. It is possible that the sound field at the receiver location is not the same for the true ribbon transducer and the microphone, because we took independent acoustic measurements, first for the microphone and then for the true ribbon transducer. So, we decide to take another measurement this time with the true ribbon transducer and microphone mounted together on the same rod, as is shown in Figure 51. In this case, we could record directly the ratio of their receiving voltages at the same time. The result is shown in Figure 50.

The results are better, but there are still irregularities, including an unexpected "bump" above 3.5 kHz.
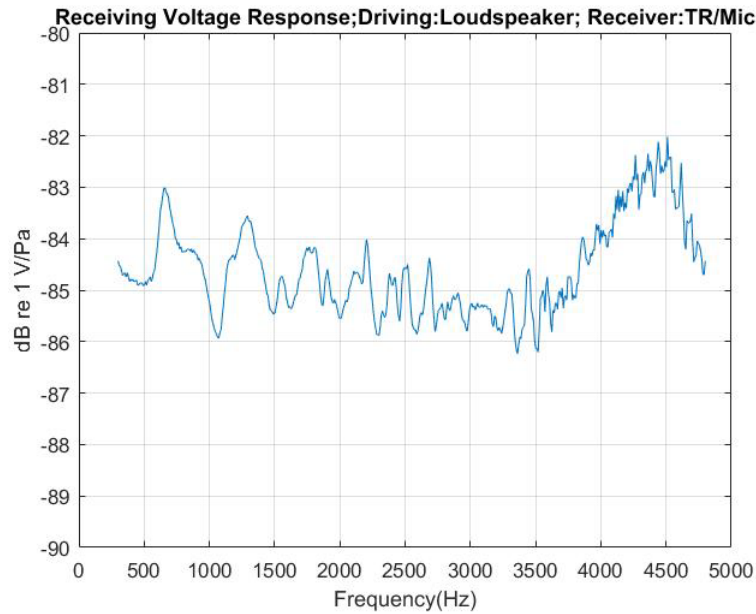
True ribbon transducer and microphone simultaneously measured.

Figure 50. Comparison Calibration of True Ribbon.

Figure 51.   True Ribbon Transducer and Microphone Attached on the Same Bar.

F.   IN-AIR, ON-AXIS RECIPROCITY CALIBRATIONS

A three-transducer spherical wave reciprocity calibration procedure is carried out for both planar-magnetic transducers (see Chapter II, Section C). One Radio Shack mid-range speaker is used as the dedicated source, a second is used as the reversible transducer; and each planar-magnetic transducer is (sequentially) used as the dedicated receiver. The main idea is to obtain a calibration of the receiving sensitivities.

The following experiment is conducted in the anechoic chamber at a temperature of 23°C. Two different measurements are carried out (voltages and currents), and three configurations for both planar-magnetic transducers are used as shown in Figure 52.

Configuration	Driving	Receiver		Measurement
1			PM1, PM2	Voltage
2	Reversible		PM1, PM2	Current
3			Reversible	Voltage

Figure 52.   Configurations for the Reciprocity Calibration of Planar-Magnetic Transducers 1and 2 (PM1and PM2).

The electronic equipment used for the reciprocity calibration is listed in Table 16, and the block diagrams are shown in Figures 53 and 54.

65

Table 16.   Reciprocity Calibration Apparatus (Planar-Magnetic Transducer)

Equipment	Brand
2 Planar Magnetic	NEO 3W (used Driving and Receiver)
Power Amplifier	Hp 476A
Resistor	Standard Precision 1% resistor (1 Ohms)
Oscilloscope	TEKTRONIK TDS 3014
Voltmeter	Agilent 34410 A
2 Speaker	Radio Shack mid-range (1 Transmitter other as reversible)
Signal Analyzer	Stanford Research Model SR785
Low Noise Pre Amplifier	SRS SR 560
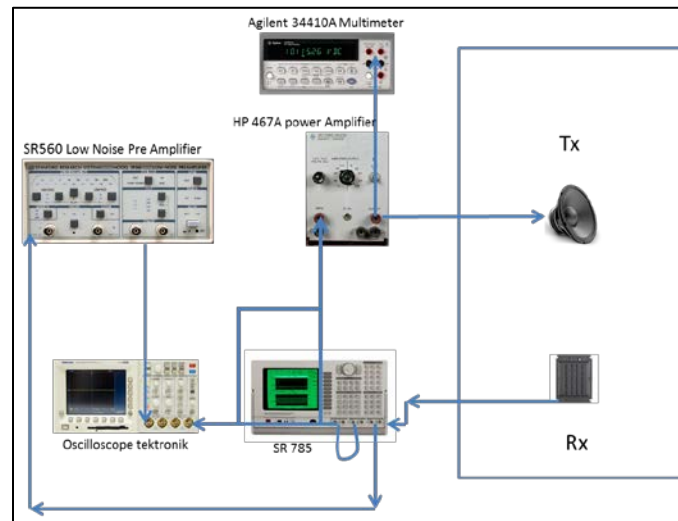
Figure 53.   Block Diagram for Voltage Measurements.
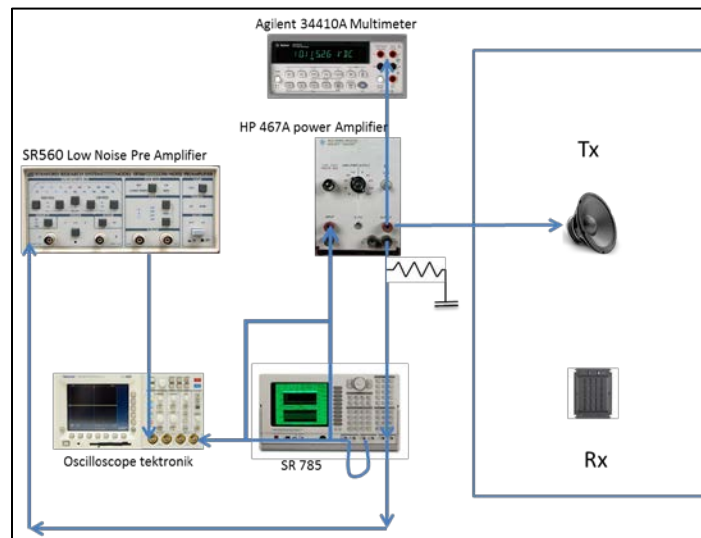
Figure 54.   Block Diagram for Current Measurements.

1. Reciprocity Calibration of Both Planar-Magnetic Transducers

Using one Radio Shack speaker as a sound source or transmitter, and the same brand speaker as a reversible transducer, we make the required measurements to determine the free-field reciprocity calibration of the receiving sensitivity of the unknown transducer, which in this case is planar-magnetic transducer 1 or planar-magnetic transducer 2.

According to *The Stanford Research SR785 Channel Dynamic Manual* [22], we set up a start frequency of 300Hz and a sweep stop frequency of 4800 Hz. Furthermore, we use the CH 2 response over CH 1 as reference; CH 2 measures the response of the receiver in experiment [22].

The swept sine measurement consists of measuring each frequency alone at each point. The advantage of this consists of using the Auto Range to change the input range in each frequency to obtain a good SNR (signal-to-noise ratio).

The SR560 pre-amplifier is used as a buffer for observing the received signal on the oscilloscope. To measure the voltage it is necessary to set the equipment up, as shown in Figure 53. To measure the transmitting current of the reversible transducer we use the set of equipment shown in Figure 54. To get the current, we insert a resistor between the SR 785 CH2 and the Hp 476A Power Amplifier in order to measure the voltage drop across this current sensing resistor. This enables us to measure the current provided to the transmitter.

The raw data for the voltages and current are shown in Figure 55. We can see that there is good agreement between the blue and black curves. Since it is the same receiver with different sources, there is only a small difference between them. The red curve is the magnitude of reversible current. The current sensing resistor has an impedance of 1.0 ohms, which was not frequency dependent.

Figure 56 shows the reciprocity calibration of planar-magnetic transducer 1 and planar-magnetic transducer 2. We notice that they have different resonance frequencies. The reason for this difference is unknown.

67
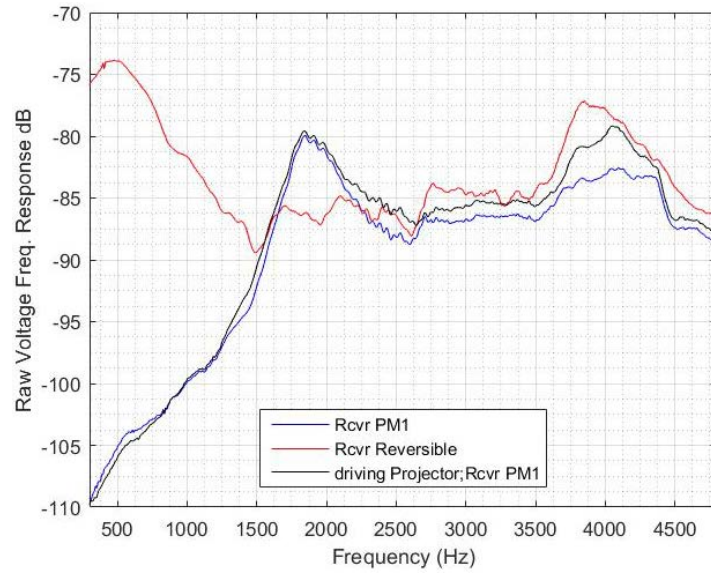
Figure 55. Raw Data of All Measurements of Reciprocity Calibration.
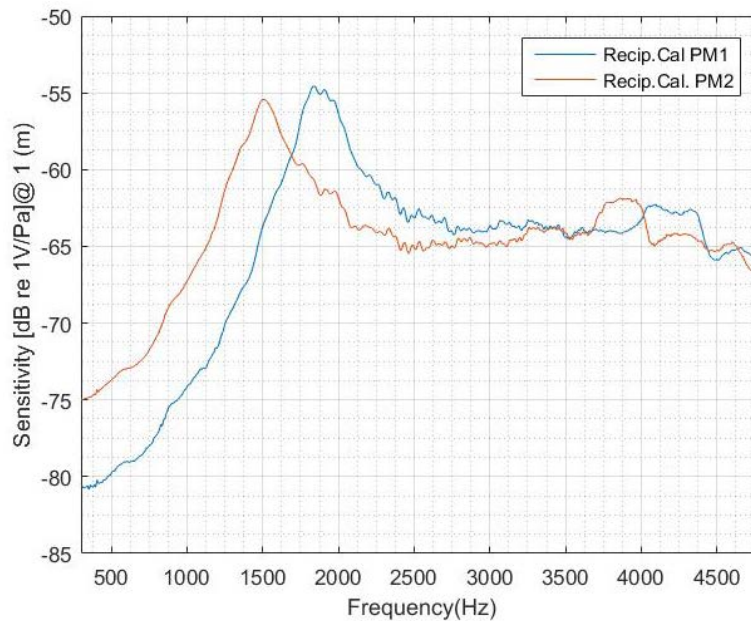
Figure 56. Reciprocity Calibration of Planar Magnetic Transducers 1 and 2.

Figure 57 shows the graph of the reciprocity calibration results compared to the comparison calibration results. We see fairly good agreement between the two results for frequencies above about 2.5kHz; however, we do not understand the discrepancy in the frequencies of peak sensitivity between the results.
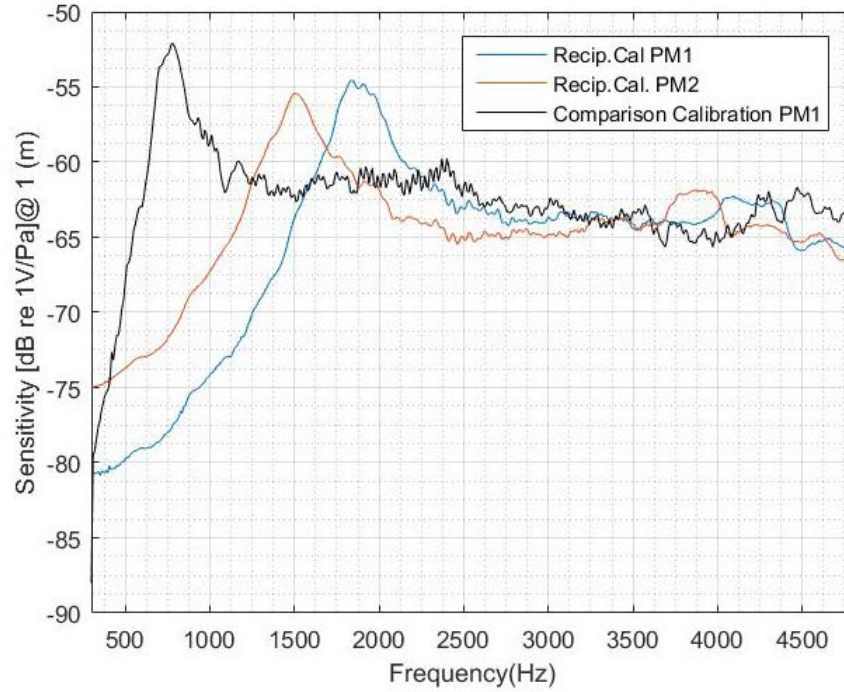
Figure 57.   Reciprocity Calibration Planar-Magnetic Transducers 1 and 2 Compared with Comparison Calibration of Planar-Magnetic Transducer 1.

G.   FREE-FIELD VELOCITY SENSITIVITY

Following the suggestion by Bobber (see Chapter II, Section D), we can estimate the free-field velocity sensitivity (magnitude) of a pressure-gradient transducer from its free-field pressure sensitivity (magnitude) by

$$
\begin{aligned}
free-field \text{ vel. sensitivity in } & \frac{\text{Volts}}{\left(\frac{m}{s}\right)} \\
= free-field \text{ pressure sensitivity in } & \frac{\text{Volts}}{Pa} \times \dots \\
& \frac{\rho c}{\sqrt{\left[1+\frac{1}{(kd)^2}\right]}},
\end{aligned}
\tag{3.11}
$$

where d is the separation distance employed during the pressure calibration, which is 2m in all our cases. In terms of decibels,

$$\textit{free} - \textit{field} \text{ vel. sensitivity level=free-field pressure sensitivity level+...}$$

$$20 \log_{10}(\rho c) - 20 \log_{10}\left(\sqrt{\left(1 + \frac{1}{(kd)^2}\right)}\right). \tag{3.12}$$

Were it not for the kd-dependent term above, the free-field velocity sensitivity level would equal the free-field pressure sensitivity level plus the constant $20 \log_{10}(\rho c) = 20 \log_{10}(415 \, \text{Pa} - \text{s}/\text{m}) = 52.4 \, dB$ at 1 atm pressure and room temperature.

The factor $20 \log_{10}\left(\sqrt{\left(1 + \frac{1}{(kd)^2}\right)}\right)$ as a function of frequency is negligible over the range of frequencies for which our free-field pressure calibrations are performed, 300-to-4800Hz. The worst case is to replace 300 Hz into the factor

$$20 \log_{10}\left(\sqrt{\left(1 + \frac{1}{(kd)^2}\right)}\right) = 0.036 \, dB. \tag{3.13}$$

Figure 58 shows the free-field velocity sensitivity of our planar-magnetic transducer 1 estimated from its comparison calibration results.
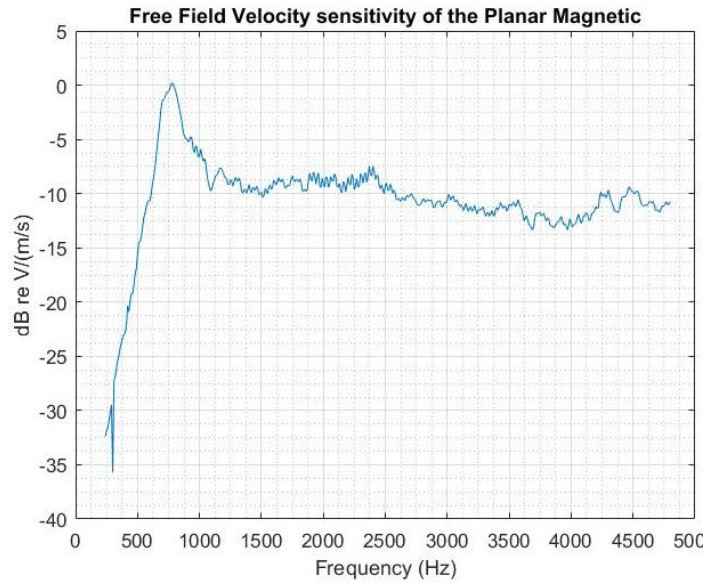
Figure 58.   Free-Field Velocity Sensitivity of the Planar-Magnetic Transducer.

70

IV.   IN WATER MEASUREMENTS

A.   TRANSDUCER HOUSING FOR UNDERWATER ACOUSTIC MEASUREMENTS

To investigate the performance of the planar-magnetic and true ribbon transducers in water, both are placed inside the plastic container shown in Figure 59, which is filled with distilled water.
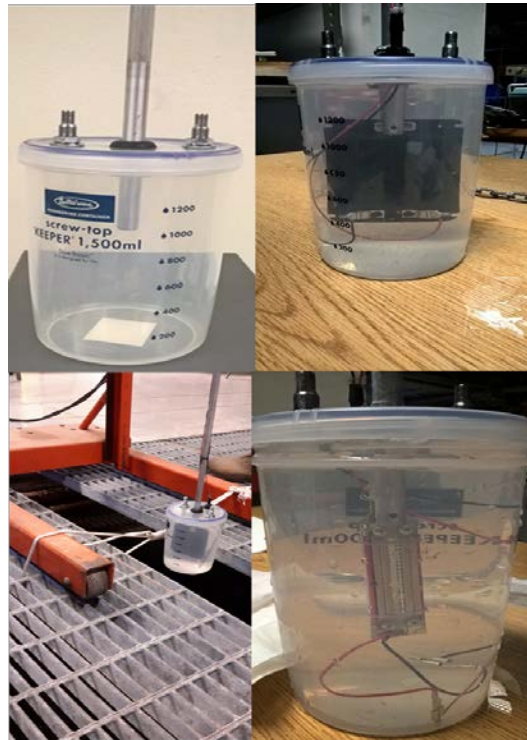
Figure 59.   True Ribbon and Planar-Magnetic Transducers inside the Plastic Container.

1.   Description

We selected a plastic (polyethylene) food storage container Lustro Wave Model B-2276, with a diameter of 11.0 cms, height of 16.3 cms, nominal volume of 1500 ml, and thickness of 1–1/4 mm. It has a screw top with an o-ring seal. We installed two automobile (Schrader) valves in the top for evacuating and filling it.

We also installed a rubber grommet through which passes the ½-inch diameter aluminum rod that holds the transducer as is depicted in Figure 60. The rod shown is secured above and below the grommet with hose clamps. There is also a homemade epoxy-filled feed-through for the wires. We used a vacuum to purge the container of air before filling as shown in Figure 61. It is important to mention that we practiced a lot on how to fill the plastic container with water—at least five times for two hours long. We became very proficient at filling the container with water and sealing it off with very little air trapped inside.
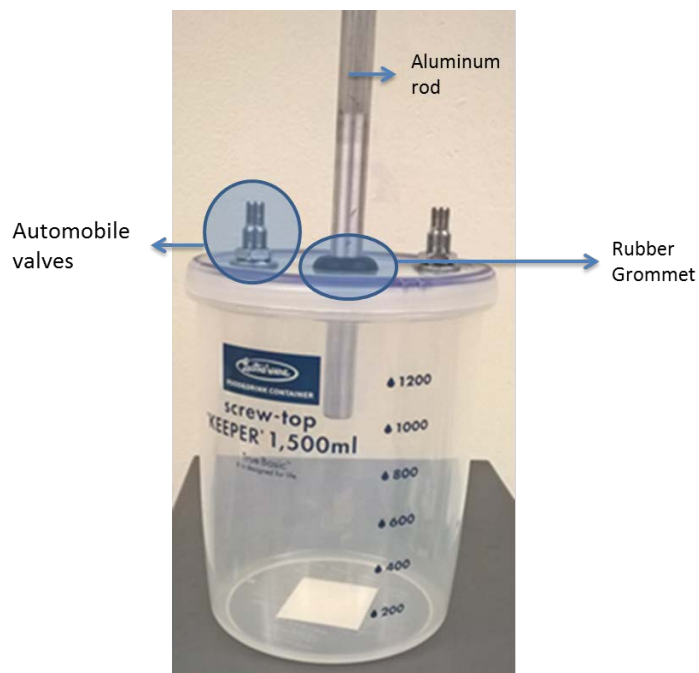
Figure 60.   Plastic Container Used as a Housing for the Underwater Experiments.

Figure 61.   Circuit to Purge and Fill with Water.

Normally, one would fill the underwater transducer housing with a standard so-called "sonar fill fluid," a fluid (such as castor oil) that has a characteristic impedance similar to that of water. For several reasons we decided to try distilled water first to see if that would work, and it did. Pure distilled water does not conduct electricity. We were hoping that the distilled water one can buy in plastic bottles at the grocery store was pure enough, and we were hoping that our transducers would not be short-circuited by immersing them in water. We measured this and found the distilled water does not conduct very well, and so it did not short-circuit our transducers. We estimated the effect of the water's conductivity on the signal voltage we measured. This analysis is presented later; the effect was very small.

2.   True Ribbon Transducer Damaged

True ribbon transducers are very fragile; the foil of ours is only 2.5 microns thick. One must avoid any motion of the transducer that would cause macroscopic fluid current to flow normally to the ribbon element, as this will permanently deform or destroy the ribbon. In fact, we unknowingly damaged one of our two transducers' ribbon elements during experiment construction, leaving us with only one. We were very careful to try not

to let the true ribbon transducer move side-to-side within its underwater housing. It could do this, because its mounting rod is not constrained against such motion by its rubber grommet seal where it passes through the lid of the housing. So we encapsulate the true ribbon transducer by a single-layer wrap of household plastic film to try to prevent any accidental macroscopic fluid flow from damaging the ribbon (the plastic film is assumed to be acoustically transparent in water). Even so, when we pulled the true ribbon transducer out of the underwater housing at the end of measurements, we saw that the ribbon was deformed, as depicted in Figure 62, and partially stuck to one side of the thin plastic film. We believe this occurred as a result of fluid capillary forces as the water drained from the plastic-film-wrapped ribbon transducer when it was removed from the underwater housing, but we cannot be sure. Figure 63 shows the true ribbon transducer sealed in the underwater housing prior to underwater testing. It appears to be undamaged.

Figure 62.   True Ribbon Transducer Damaged.
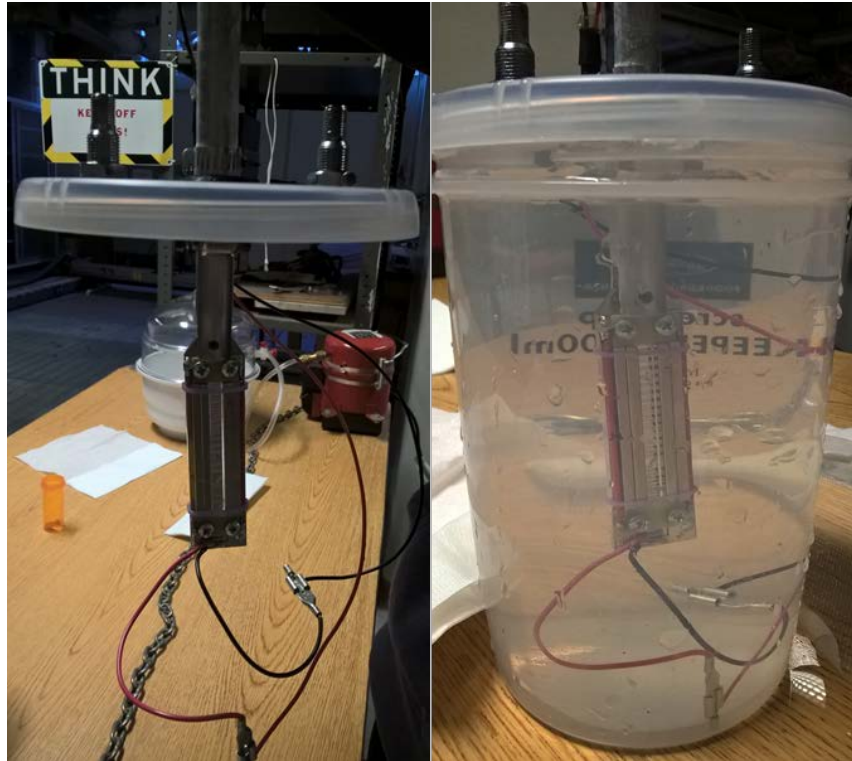
Figure 63.   True Ribbon Transducer before Testing in Water.

3.   Measured Underwater Transmission Loss of Transducer Housing

Before making measurements on the ribbon-type transducers, we first measure the insertion loss of the transducer housing. First, we place the hydrophone in the plastic container (see Figure 64) to collect data from the signal analyzer. Subsequently, we place the hydrophone directly into the water and obtain the data again. We compare both results (inside the container and outside). These results are shown in Figures 65 and 66. The idea is to prove how much affect the plastic container has on the measurements.

75

Figure 64.   Hydrophone inside the Container.
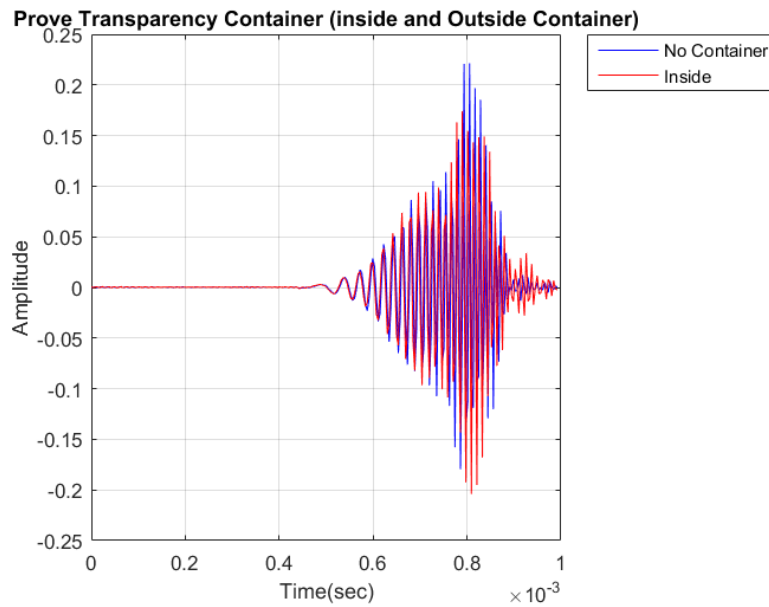
Compare both direct path signals inside the container and outside; the difference is minimal.

Figure 65.   Compare Both Direct Path Signals.
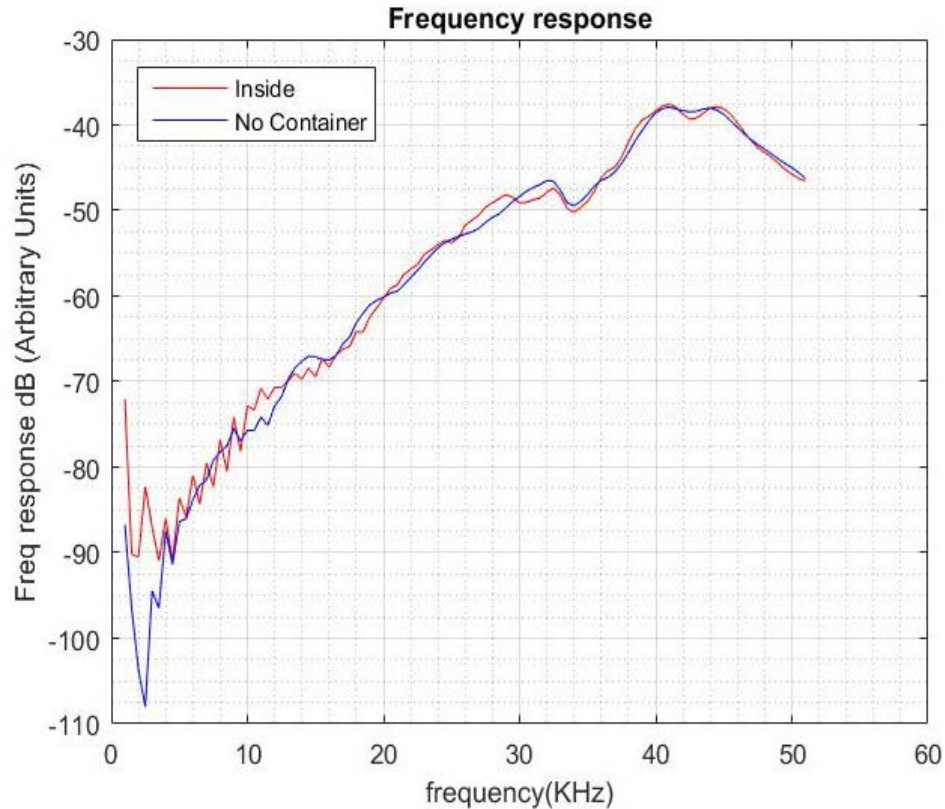
Figure 66. Frequency Response Comparing Two Cases.

As you can see in Figure 66, above 5 kHz the received hydrophones signals agree within 1 or 2 dB. Sometimes the red curve is above, and sometimes it is below the blue curve. One cannot really see a systematic insertion loss; therefore, the plastic container is considered ignorable. The data below 5 kHz are not reliable, and the sawtooth pattern sometimes seen in data below 10 kHz is a signal processing artifact.

4.   Procedure to Eliminate Reflections

All equipment is set up to eliminate reflections. Figure 67, the block diagram in Figure 68, and Table 17 describing the apparatus used explain the equipment setup. Figure 69 shows the typical ray paths in the water tank.

Figure 67.   Setting Up for the Measurement in Water.
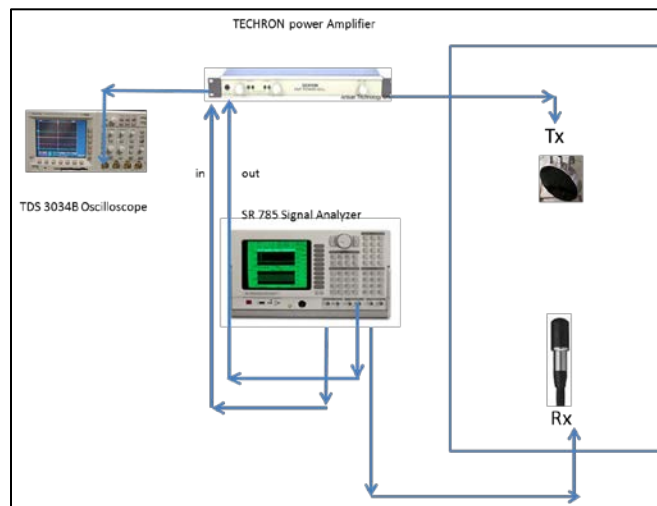
Figure 68.   Block Diagram for Measurement in Water.

Table 17.   Apparatus Used to Eliminate Reflections

Equipment	Brand
Hydrophone	Type 8103 (Receiver)
Transducer	Type F 33 (Source)
Power amplifier	TECHRON 5507 (set in order Input and Output are equal)
Oscilloscope	TDS 3034B
Signal Analyzer	Stanford Research Model SR785 (set 0 to 100 KHz)

1.- Surface reflection.
2.- Direct Path.
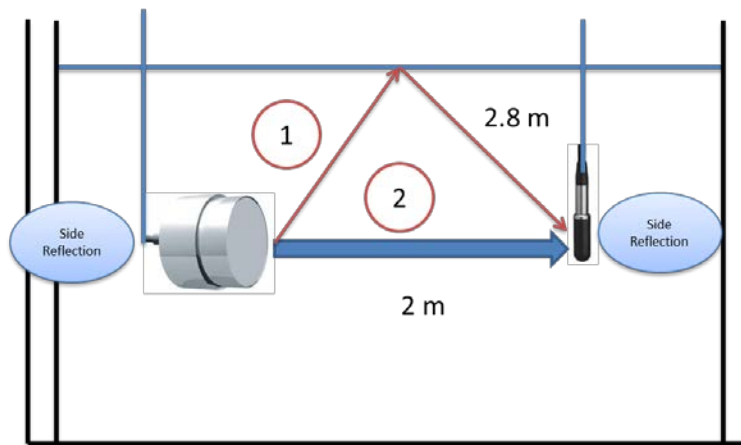
Figure 69.   Types of Reflection in the Water Tank. Adapted from [23].

A brief sine-wave chirp signal is transmitted by the F33 source. Figure 70 shows an example of a signal received by the hydrophone. Figure 70 shows an example of a reflection from the F33 transducer source received at the type 8103 hydrophone. The strong reflection appears at about 0.74 ms. We think this is a surface reflection. However, from the geometry of Figure 69, the surface reflection should occur at about 0.53 ms. Looking at Figure 70, there may be a reflection signal arriving about 0.53 ms after the direct signal, but, if so, it is very weak. To avoid the stronger reflection, we shorten the transmission pulse to 0.3 ms, and we set the delay of data collection to cut off 0.5 ms following the direct path arrival.
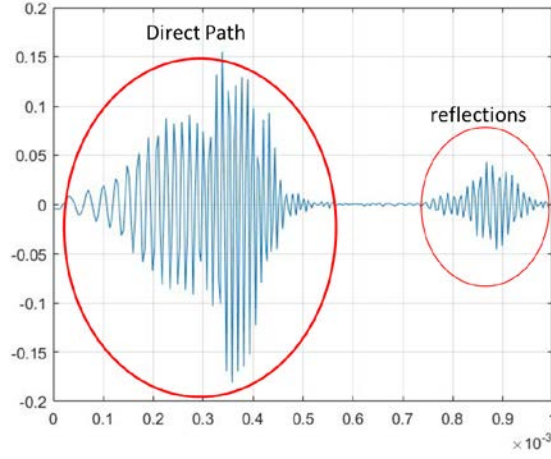
Figure 70.   The Direct Path Signal and Reflection.

5.   Correction for Water Conductivity to Measured Transducer Output Voltage

The output signal's raw data consists of the impedance, which is the ratio of the output voltage ($\tilde{V}_{out}$) and current ($\tilde{I}_{out}$). In order to get the source voltage ($\tilde{V}_{source}$) in this experiment, we could not obtain it directly, so the resistances need to be known. There are three different kinds of planar-magnetic transducer resistances in this experiment; the resistance of the planar–magnetic transducer in air ($R_{in\ air}$), the resistance of the connected wire (R_{wire}), and the resistance due to distilled water's conductivity (R_{shunt}). Figure 71 shows the resistances in the underwater experiment.
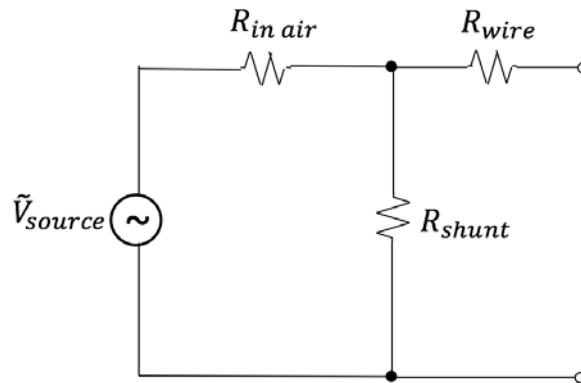
Figure 71.   Experiment Circuit in Water.

80

In each underwater measurement, we periodically measure the transducer's resistance at the cable junction at the top of the mounting rod for a frequency of 1 kHz, using an LCR meter. The results can be seen in Tables 18 and 19. Here is how we use this information to estimate the worst-case correction to the measured transducer output voltages for the conductivity of the distilled water in which they were immersed.

Table 18.   Resistances for the Planar-Magnetic Transducer

$N°$	Resistance in $\Omega @ 1KHz$	Comment
1	3.6	In air, time "0"
2	3.54	Housing Filling in water, at the bottom edge
3	3.523	Housing Filled with water
4	3.535	Housing Filled with water after 10 min of the measurements above
5	3.517	After 30 min
6	3.6	Housing lowered into the water
7	3.495	1:45 pm, before starting the beam pattern
8	3.483	2:35 pm
9	3.485	3:07 pm
10	3.487	5:07 pm
11	3.57	July 23 at 11:15 am

Table 19.   Resistances for the True Ribbon Transducer

$N°$	Time	Resistance in $\Omega @ 1KHz$	Comments
1	11:40 am	0.516	In Air
2	11:54 am	0.504	Housing filled Water
3	12:47 pm	0.501	Into tank
4	1:21 pm	0.499	Into tank
5	3:50 pm	0.498	Into tank

For the planar-magnetic transducer, R_{wire} was measured directly using a Universal LCR meter BK Precision 878, a handheld LCR meter. At the frequency of 1 kHz, R_{wire} is 0.317Ω and $R_{in\ air} + R_{wire}$ is 3.6Ω. Using substitution, we can calculate the value of $R_{in\ air}$, and it is 3.283Ω. When we measure the resistance of the planar-magnetic transducer in water, its (worst-case) minimum is 3.484Ω, and this value includes R_{wire}. Thus, $R_{in\ water}$ would be 3.166Ω.

By the voltage resistor relationship,

$$\frac{1}{R_{water}} = \frac{1}{R_{air}} + \frac{1}{R_{shunt}} \tag{4.1}$$

$$\frac{1}{3.166} = \frac{1}{3.283} + \frac{1}{R_{shunt}} \tag{4.2}$$

Thus, R_{shunt} is 88.756Ω at the frequency of 1kHz.

From the Thevenin Theorem, the ratio of $\tilde{V}_{source}$ and $\tilde{V}_{out}$ can be expressed in terms of the resistance in the open-circuit as:

$$\frac{\tilde{V}_{out}}{\tilde{V}_{source}} = \frac{R_{shunt}}{R_{air} + R_{shunt}} \tag{4.3}$$

For the planar-magnetic at the frequency of 1 KHz,

$$\frac{\tilde{V}_{source}}{\tilde{V}_{out}} = \frac{88.756}{3.283 + 88.756} = 0.964 \tag{4.4}$$

This means that, in the worst case, there is approximately a 4 percent difference between the measured voltage and the transducer's source voltage.

For the true ribbon transducer, R_{wire} is 0.317Ω, $R_{in\,air}$ is 0.516Ω, and the minimum $R_{in\,water}$ is 0.181Ω. From the same calculation with the planar-magnetic transducer, we obtain R_{shunt} as 2.001Ω, and the ratio of $\tilde{V}_{source}$ and $\tilde{V}_{out}$ is 0.910. In the worst case, there is a 9 percent difference between the measured and the transducer's source voltage signal. This is less than a 1dB difference. We take those differences (4 percent and 9 percent) to be negligible, and since this is the worst case, we ignore the conductivity of the water in the housing for all further analysis. We could always come back and make the correction, if warranted.

B. TRANSDUCERS AND HYDROPHONES USED IN THE INVESTIGATION.

Now we describe each transducer and hydrophone used in the water experiments.

a. *Hydrophone Type 8103*

The Type 8103 hydrophone is made from a piezoelectric cylinder, which is radially polarized and shown in Figure 72. The calibration chart is provided in Figure 73, and more details are provided in Appendix D.
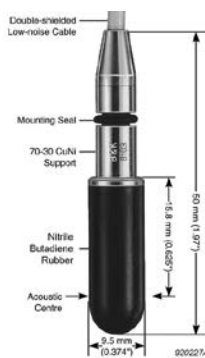
Figure 72.   Hydrophone Type 8103 Used as a Receiver.
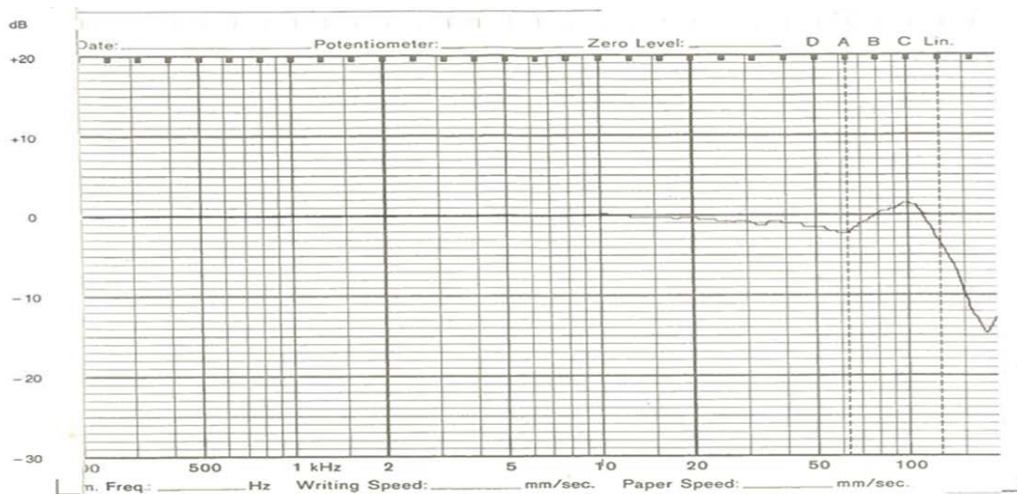
Figure 73.   Calibration Chart for the Hydrophone Type 8103.

In Figure 73, the response shown is very flat up to 20 KHz, dropping by only about 1.5 dB by 50 kHz. Its sensitivity is $26\mu V / Pa$ or $-211.7dB$ re $1V/\mu Pa$.

b. Transducer Type F 33 Equivalent

The F 33 Equivalent is an old style Navy transducer that is commercially manufactured by USRD, Inc. to be identical to U.S. Navy Type F33 (see Figure 74). It is a reversible transducer, which means it is capable of both transmitting and receiving.

It is made up of piezoelectric blocks and is filled with oil to match the impedance of water. It is used for calibration measurements in the frequency range of 1 to 150 kHz [12]. The specifications are shown in Table 20. More characteristics are available in Appendix D.

During the reciprocity experiment, two of them are used (one as a source and the other as a reversible transducer).

Table 20.   Specifications of Transducer F 33

SPECIFICATIONS	
Frequency	Inner 15 to 150 kHz. Both 1 to 50 kHz.
Transmitting Voltage Response	128 dB re 1 μPa/V. at 10 kHz (both) 133 dB re 1 μPa/V. at 50 kHz (inner)

Figure 74.   Transducer Type F 33 Equivalent Used as a Source and the Other
as a Reciprocal.

C.   GENERAL DESCRIPTION OF UNDERWATER EXPERIMENTAL SETUPS (IN COMMON)

In this section, we describe the basic procedure for the underwater measurements. These include placing the transducers two meters away from each other, measuring the effect of the plastic container containing the hydrophone, true ribbon, and planar-magnetic transducers, figuring out how to eliminate the fluctuations and reflections, and filling the plastic container with water to avoid bubbles.

1.   Set Up in Water (Range between Source and Receiver)

All experiments are performed with a range of two meters between the source and receiver, and the depth of each transducer is fixed at one meter (see Figure 75.)
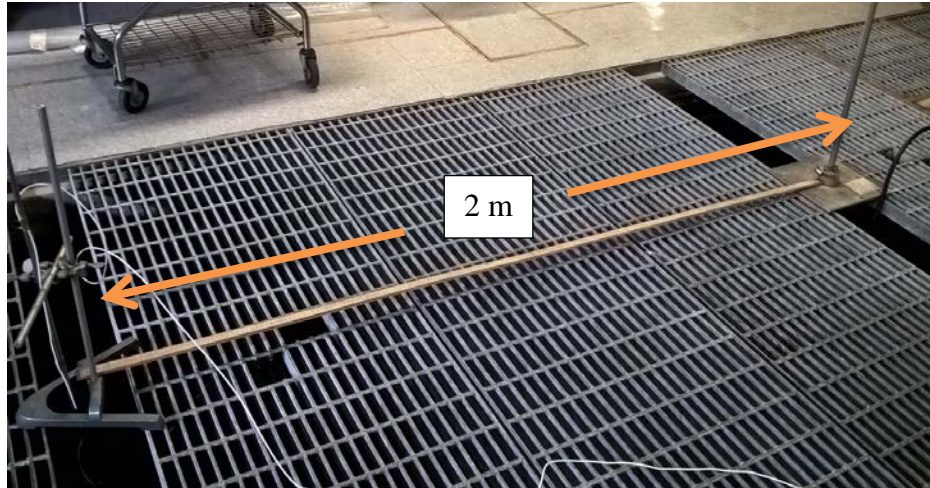
Figure 75.   Layout of Source and Receiver in the Experiments.

2.   Filling the Plastic Container with Water (Procedure)

This section discusses the procedure for filling the plastic container with water when the planar magnetic or true ribbon is inside. The main idea here is to fill the container without bubbles Figure 77, since the bubbles cause undesirable acoustic effects.

The setup for filling the container with water as shown in Figure 76 is performed with the following apparatus:

- Vacuum Pump
- Distilled water
- Hoses and clamps
- Two (2) plastic containers
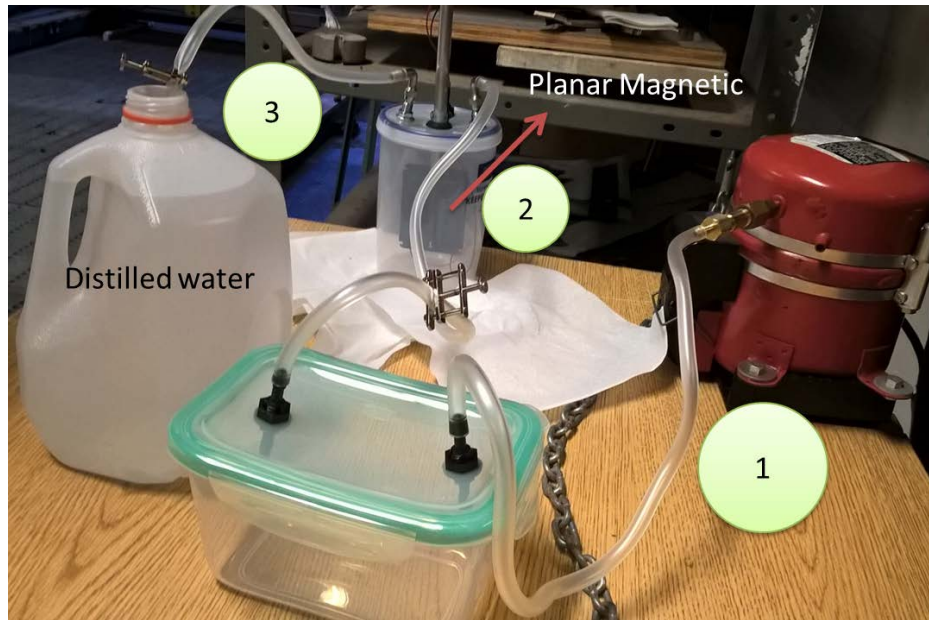
1. The vacuum pump evacuates air from the green topped plastic container. 2. Air is evacuated from the plastic container with the planar magnetic inside, and finally, 3. Distilled water is drawn into the sensor container.

Figure 76.   Diagram to Fill Water without Bubbles

Water drops are on outside.

Figure 77.   Fill with Water, No Bubbles.

The same procedure is used for the true ribbon transducer shown in Figure 78.

87

Figure 78.   Fill with Water, No Bubbles (True Ribbon).

D.   UNDERWATER BEAM PATTERNS

All equipment to set up the beam pattern measurement for both the planar-magnetic and true ribbon transducers is given in Table 21 and shown and set up as in Figures 79 and 80.

Table 21.   Beam Patterns Apparatus (Water)

Equipment	Brand
1 Planar Magnetic	NEO 3W (used Driving and Receiver)
1 True Ribbon	Model RE-254
Transducer	Type F 33
Oscilloscope	TDS 3034B
Rotary Control	HAAS Automation Inc.
Power Amplifier	TECHRON 5507 (set in order Input and Output are equal)
Signal Analyzer	Stanford Research Model SR785 (set 1KHz to 51 KHz)
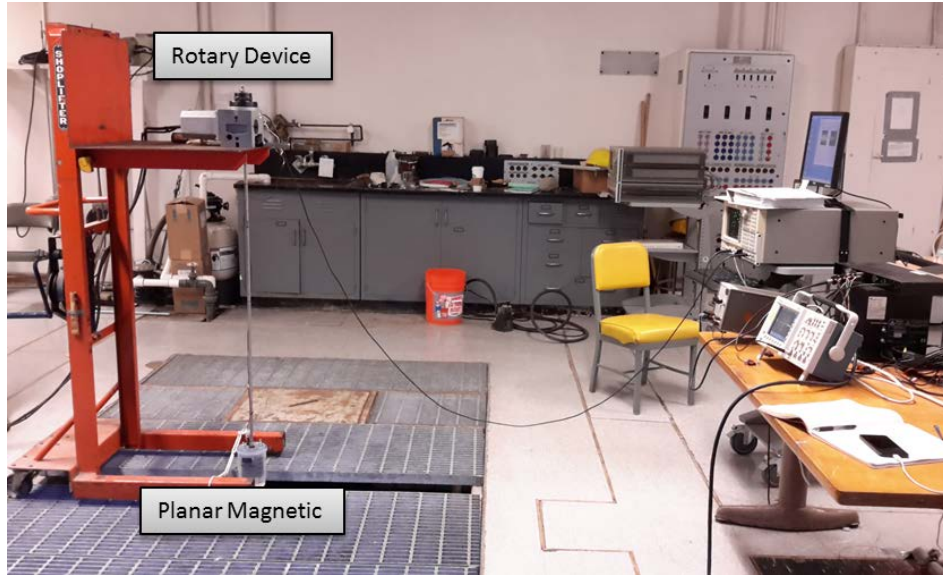
Figure 79.　Diagram to Perform Beam Patterns.
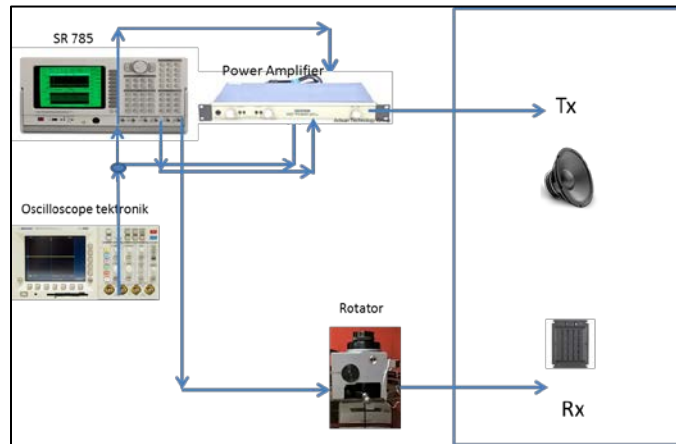
Figure 80.　Block Diagram for Beam Pattern in Water.

Experiments are conducted to measure the receiving beam patterns of the planar-magnetic and true ribbon transducers and to verify the shape and behavior of the lobes at different frequencies.

For all directional measurements of the beam pattern, we use chirp signals with bandwidths between 1 to 51 kHz. We start to measure from 0 to 360 degrees by 30 degrees increments. After that, we measure again from 0 to 360 degrees by 15 degree increments, except for the angles we have already measured. Finally, we measure the

beam patterns one more time from 0 to 360 degrees by 5-degree increment, except at angles we have measured before. Consequently, we obtain 72 points of amplitude data with 5-degree increments for all directions. The reason why we conduct the measurements this way is to protect ourselves against the possibility that the conductivity of the distilled water would increase over time to the point where the data becomes useless. However, this does not occur. Each data record represents the amplitude of the frequency range of 1 to 51 kHz in one orientation, and it has 101 data points.

The raw data represents the amplitude in terms of the chirp signal for a specific angle. Thus, all raw data are needed for the 360 degree beam pattern. We make one matrix of the data for each direction and extract the frequency we want to analyze. We find the data of 320 degrees over all frequencies are not useless because of experimental error. Therefore, all data from 320 degrees are removed in our beam pattern analyses.

1.   Receiving Planar Magnetic Transducer

Figure 81 shows the measured planar-magnetic transducer's beam patterns (linear scales) at selected frequencies from 1 to 51 kHz. We can see that the data up to a frequency of about 7 kHz are poor. We can also see generally at the lower frequencies the beam pattern is a dipole, but as the frequency increases the beam is more directional. This is expected since at the higher frequencies the wavelength becomes small compared to the width of the planar magnetic transducer.
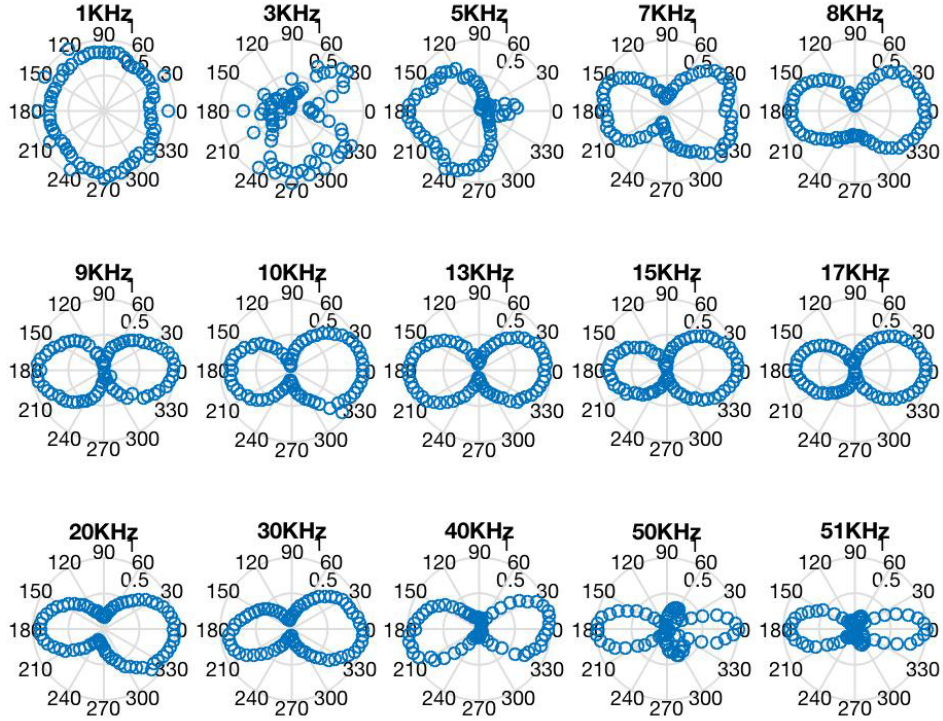
Figure 81.   Beam Pattern of Planar-Magnetic Transducer s/n 1 in Water.

2.   Receiving Magnetic Ribbon Transducer

Figure 82 shows the measured true ribbon transducer's beam patterns (linear scales) at selected frequencies between 1 and 51 kHz. Again, we see that the data are poor below about 7 kHz. Otherwise, we see that the beam patterns of the true ribbon transducer are more dipolar than the beam patterns of the planar-magnetic transducer. The difference of beam patterns is due to the fact that the width of the true ribbon transducer is smaller than the width of the planar-magnetic transducer. For this reason, it has a more ideal dipole beam pattern at higher frequencies, while the planar-magnetic transducer has more directionality at higher frequencies.

91
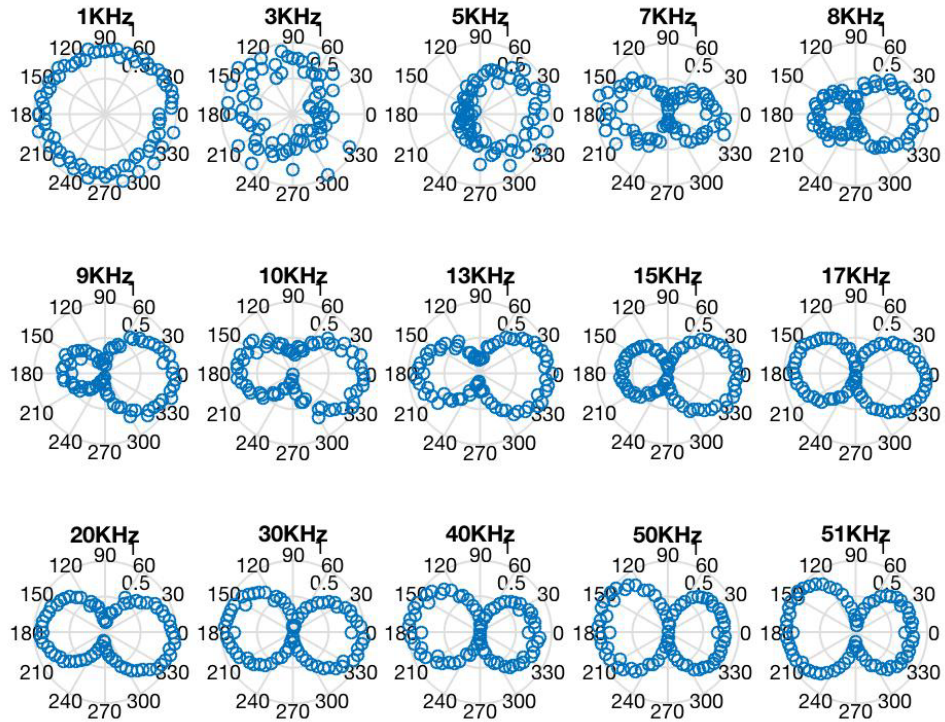
Figure 82.   Beam Pattern of True Ribbon Transducer in Water.

E.   COMPARISON CALIBRATIONS OF FREE-FIELD PRESSURE SENSITIVITY

This method consists of taking a hydrophone with the absolute calibration provided by calibration chart and comparing it with the unknown transducer. In case we do not have another calibrated transducer, we have to perform the reciprocity calibration method. Table 22 shows the equipment used in the experiment, and Figure 83 shows the block diagram.

Equipment	Brand
1 Planar Magnetic	NEO 3W (used as Receiver)
Hydrophone	Type 8103
1 true Ribbon	Model RE-254
Transducer	Type F 33 (used Projector)
Oscilloscope	TDS 3034B
Power Amplifier	TECHRON 5507 (set in order Input and Output are equal)
Signal Analyzer	Stanford Research Model SR785 (set 1KHz to 51 KHz)

Table 22.   Comparison Calibration Apparatus (Water)
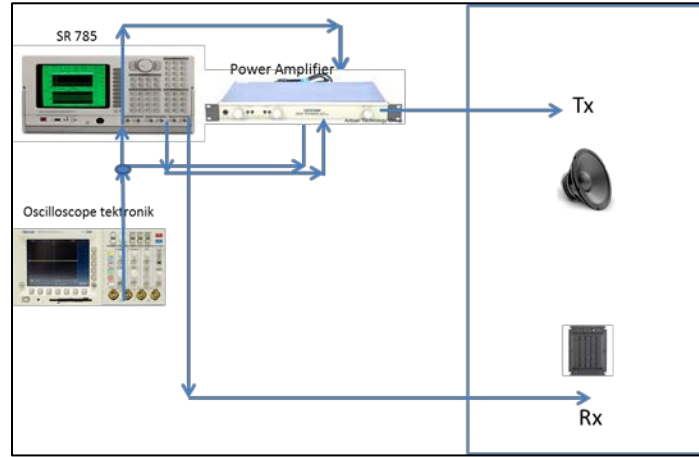
Figure 83.   Block Diagram Comparison Calibration in Water.

The common procedure to obtain the free-field receiving open circuit sensitivity calibration of either planar-magnetic transducer or true ribbon transducer is the following. First, it is necessary to obtain the sensitivity of the hydrophone Type 8103 to compare with the planar-magnetic and true ribbon transducer. In this case the sensitivity was -211.7 dB re $\dfrac{1V}{\mu Pa}$. After that, we convert units from $\dfrac{1V}{\mu Pa}$ to $\dfrac{1V}{Pa}$. Since all experiments performed had that unit of reference, it is necessary to add 120 dB, and the result is

$$-211.7 \text{ dB re } \frac{1V}{\mu Pa} \;\circ\; \left(20\log_{10}\left(\frac{10^6\,Pa}{1\mu Pa} \right) \right) =$$
$$-211.7 \text{ dB} + 120 \text{ dB} = -91.7 \text{ dB re } \frac{1V}{Pa}$$

(4.5)

93

Having the sensitivity of the hydrophone in the reference units utilized in the thesis, we carry out the procedure to obtain the sensitivity of either planar-magnetic or true ribbon transducer.

The first acoustic measurement in the water tank involves placing the transducer F 33 as a source and the hydrophone Type 8103 as a receiver. Subsequently, we replace the hydrophone Type 8103 with either the planar-magnetic transducer or the true ribbon, and we collect the data.

1.   Receiving Planar-Magnetic Transducer

The equation to obtain the sensitivity is the following:

$$M_{o_{planar}} = Planar \text{ Gain dB} - \text{Hyd. Gain dB} + \text{Hyd. sensitivity Level dB} . \qquad (4.6)$$

Figure 84 shows the result of the raw data from the planar-magnetic transducer and the hydrophone, and Figure 85 shows the free-field receiving open-circuit voltage sensitivity of the planar-magnetic transducer.
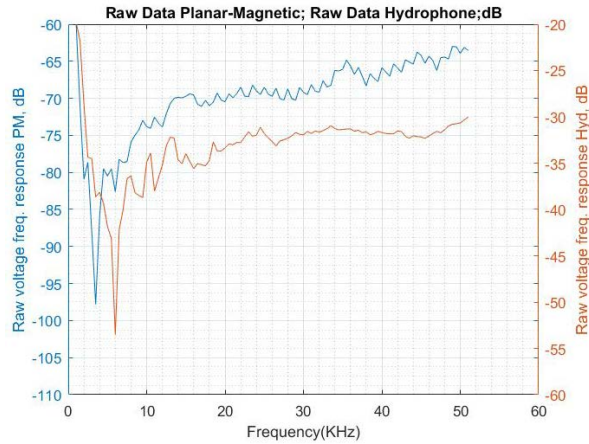
Figure 84.   Raw Data for Planar-Magnetic Transducer s/n 1 and Hydrophone.
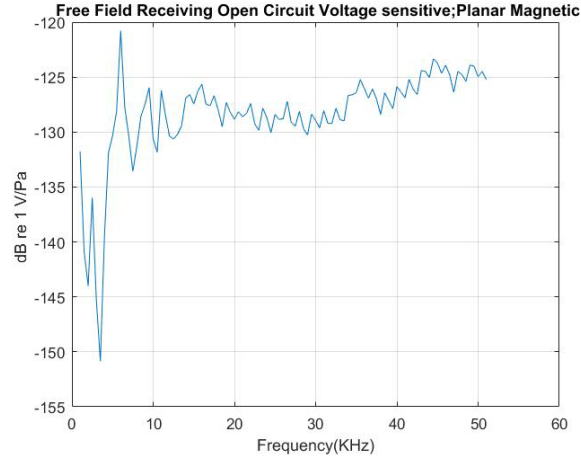
Figure 85.   Free Field Receiving Open Circuit Sensitivity Planar Magnetic Transducer s/n 1.

2.   Receiving True Ribbon Transducer

To obtain the free-field receiving open-circuit sensitivity calibration of the true ribbon transducer, a similar procedure is used. The equation used in this case is

$$M_{o_{ribbon}} = TrueRibbon \text{ Gain dB - Hyd. Gain dB + Hyd. sensitivity Level dB.} \qquad (4.7)$$

Figure 86 shows the result of the raw data from the true ribbon transducer and the hydrophone, and Figure 87 shows the free-field receiving open-circuit voltage sensitivity of the true ribbon transducer.
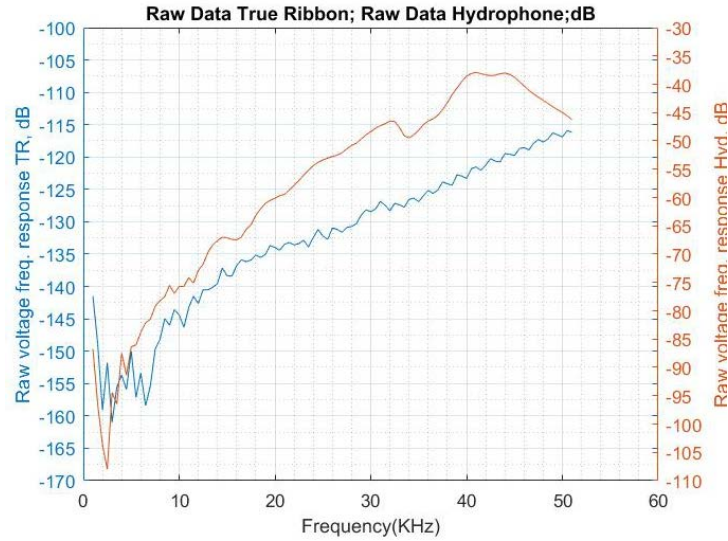
Figure 86.   Raw Data for True Ribbon Transducer and Hydrophone.
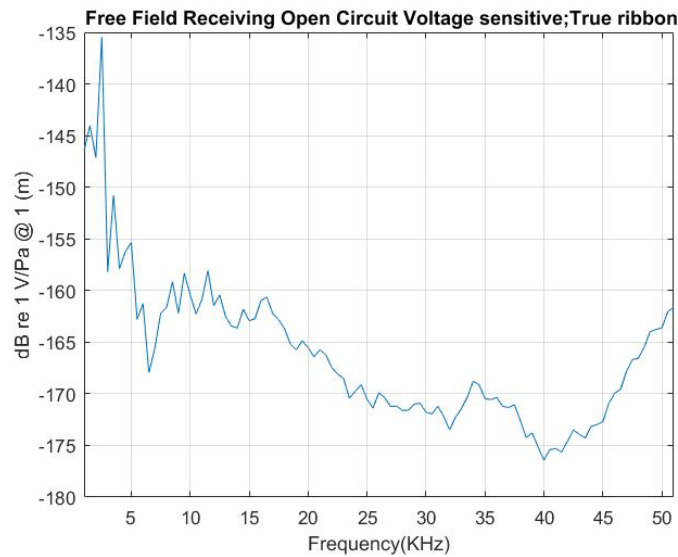
Figure 87.   Free-Field Receiving Open-Circuit Sensitivity True Ribbon Transducer.

F.   RECIPROCITY CALIBRATIONS OF FREE-FIELD PRESSURE SENSITIVITY

Reciprocity calibration is a powerful method to perform an absolute calibration, because it does not require another calibrated transducer. To set up this experiment we use the equipment shown in Table 23 and the block diagram and the layout of the equipment shown in Figures 88, 89, and 90.

Table 23.   Reciprocity Calibration Apparatus (Water)

| Equipment	Brand
1 Planar Magnetic	NEO 3W (used as Receiver)
Hydrophone	Type 8103
Transducer	Type F 33 (used as Projector)
Transducer	Type F 33 (used as Reversible)
Oscilloscope	TDS 3034B
Low Noise Amplifier	Model SR 560
Power Amplifier	TECHRON 5507 (set in order Input and Output are equal)
Signal Analyzer	Stanford Research Model SR785 (set 1KHz to 51 KHz)
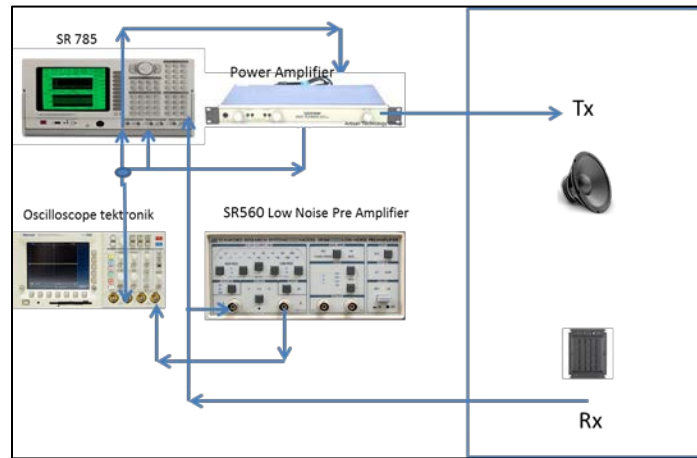
Figure 88.   Block Diagram Reciprocity Calibration in Water.

Figure 89.   Setup for Measure the Reciprocity Calibration in Water.

Figure 90.   Reciprocity Calibration of F 33 and Planar Magnetic Transducers.

This experiment is conducted only with the planar-magnetic transducer. To perform this experiment, we follow the procedure described in Figure 91.
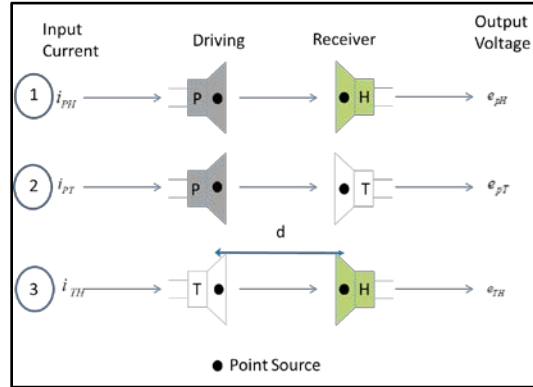
Figure 91.   Reciprocity Calibration Procedure. Adapted from [12].

The left hand side three numbers in Figure 91 correspond to the three types of measurements that are performed to obtain reciprocity calibration. Therefore, for measurement 1, we place the transducer F33 as the source and the planar-magnetic transducer as a receiver. And, for measurement 2, we place in the same point source of the planar-magnetic the reversible transducer F33 and then we collect the data. Finally,

for measurement 3, we placed the reversible transducer in the point source of the projector as a source and the planar-magnetic as a receiver.

To obtain the reciprocity calibration of the planar-magnetic transducer we use Equation (4.8) to obtain the open circuit receiving voltage sensitivity

$$M_{OH} = \left[\frac{e_{PH} i_{PT} e_{TH}}{i_{PH} e_{PT} i_{TH}} J_s \right]^{1/2},$$

(4.8)

where $J_s = 2d / \rho_0 f$ with d=2m.

Figure 92 shows the reciprocity calibration curve of the planar magnetic transducer. It shows a sensitivity between -135 to -130 dB 1V/Pa above 10 kHz, and the data below that frequency is not reliable.

Figure 93 shows both curves of the comparison and the reciprocity calibration to obtain the open-circuit receiving voltage sensitivity. There is good agreement between 8 and 13kHz, with a sensitivity of about -5 dB 1V/Pa, +/- 2 dB.
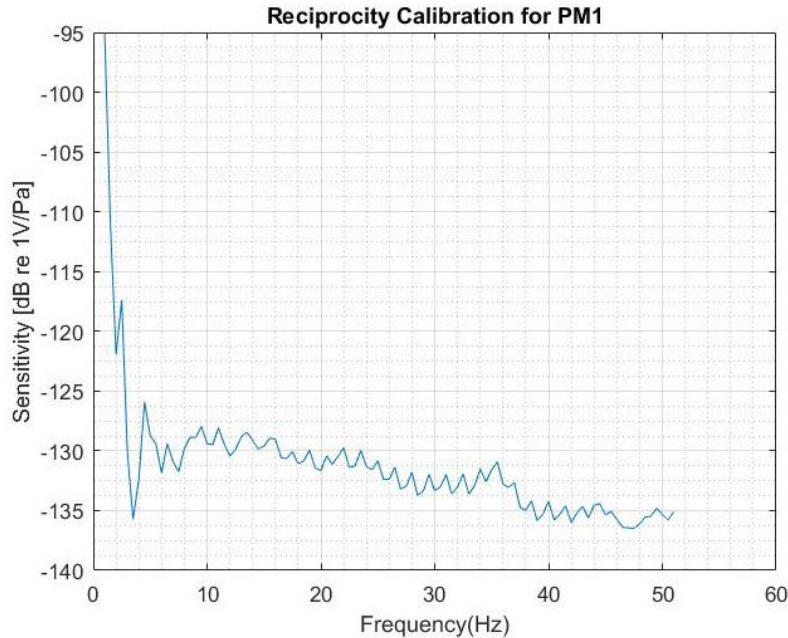
Figure 92.   Reciprocity Calibration Planar-Magnetic Transducer in Water.

99
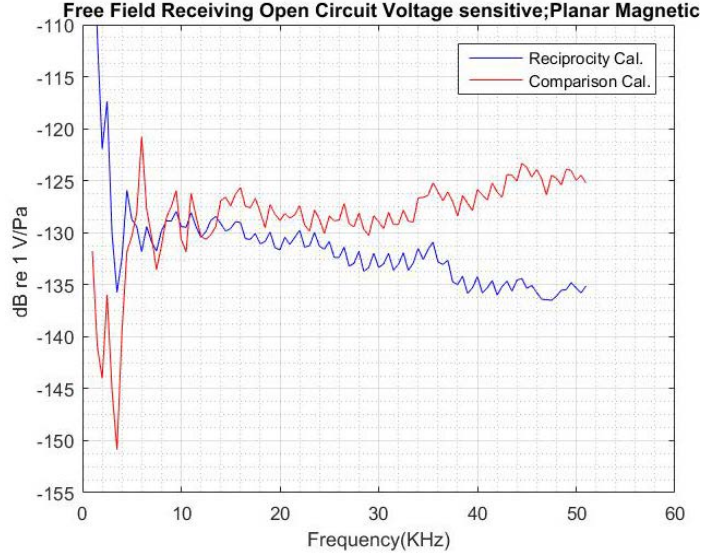
Figure 93.   Reciprocity Calibration and Comparison Calibration Curves of the Planar-Magnetic Transducer.

G.   FREE-FIELD VELOCITY SENSITIVITY

In order to obtain the free-field velocity sensitivity, we follow the same Bobber procedure to obtain the velocity sensitivity from the pressure sensitivity as we did in air (see Chapter II, Section D.2).

The free-field velocity sensitivity level would equal the free-field pressure sensitivity level plus the constant $20\log_{10}(\rho c) = 20\log_{10}(1.54 \times 10^6 \text{ Pa} - \text{s/m}) = 123.8 \ dB$.

The factor $20\log_{10}\left(\sqrt{(1+\dfrac{1}{(kd)^2})}\right)$ (factor comes from Chapter II, Section D.2) as a function of frequency is negligible, over the range of frequencies for which our free-field pressure calibrations are performed, 300 to 4800 Hz. The worst case results in a factor of

$$20\log_{10}\left(\sqrt{(1+\dfrac{1}{(kd)^2})}\right) = 0.06 \ dB. \tag{4.9}$$

100

Figure 94 shows the free-field velocity sensitivity in water using the comparison calibration pressure sensitivity, and Figure 95 shows the results using the reciprocity calibration.
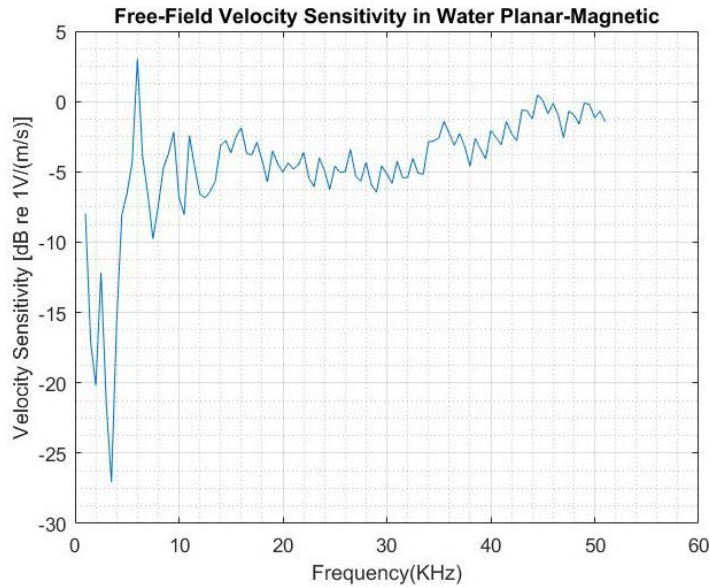
Figure 94.   Free-Field Velocity Sensitivity of the Planar-Magnetic Transducer in Water; from Comparison Calibration.
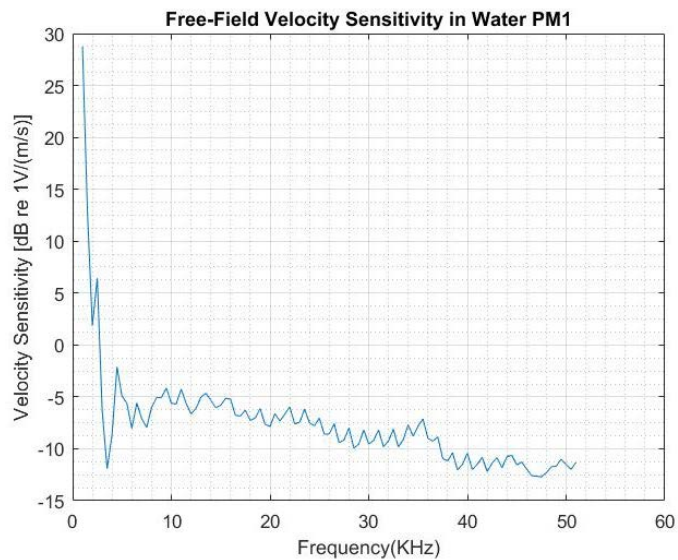
Figure 95.   Free-Field Velocity Sensitivity of the Planar-Magnetic Transducer in Water; from Reciprocity Calibration.

Figure 96 shows both velocity sensitivities. There is good agreement between 8 and 13 kHz, with a velocity sensitivity of about -5 dB 1V/(m/s) +/- 2 dB.
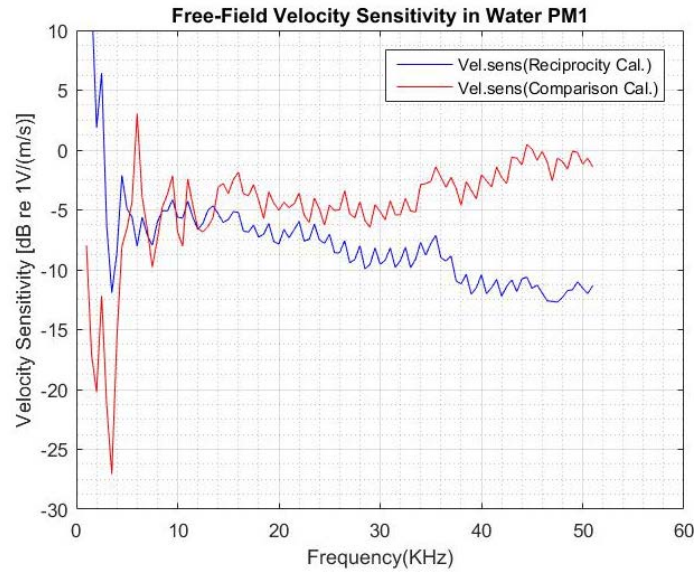
Figure 96.   Velocities Sensitivities of Planar-Magnetic.

V.   SUMMARY AND CONCLUSIONS

As far as we know, our research is the first to investigate the use of magnetic ribbon-type transducers for use underwater. These are pressure-gradient (velocity) transducers. By their magnetic induction sensor design, they produce an output voltage that is directly proportional to acoustic velocity. This is a benefit for a vector sensor.

To prove this kind of technology works well in water, we carried out beam pattern and receiving sensitivity measurements for a planar-magnetic transducer and a true ribbon transducer both in air and in water. As expected, we observed directional characteristics approaching those of an ideal dipole, for long wavelengths, with two principal lobes, each becoming narrower with increasing frequency.

With a focus on the more practical planar-magnetic transducer, Figure 97 shows the free-field, open-circuit velocity sensitivity of our planar-magnetic transducer 1 in air and in water. It is remarkable that the sensitivities are not a lot different, though we do observe the sensitivity in water to be significantly greater than in air. To take the average sensitivities for both measurements, we used the frequency range from 1.5 to 2 kHz in air, and a range from 7.5 to 10 kHz in water. At these frequency ranges, the planar-magnetic transducer had a good dipole characteristic due to the relatively large wavelength compared to the width of the transducer. Also, the range of wavelengths in air and in water are about same using these frequencies. The velocity sensitivity in air is about -10 dB re 1V/(m/s) and the velocity sensitivity in water is -6 dB re 1V/(m/s); the difference is -4 dB.
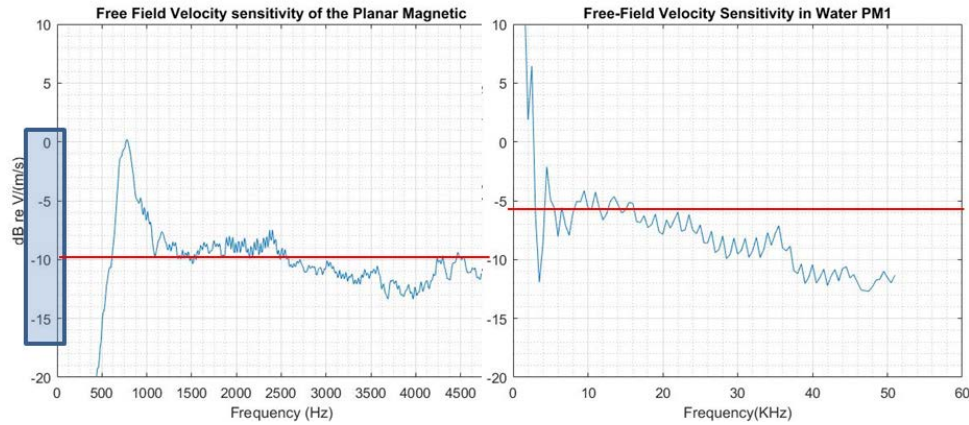
Figure 97.   Comparison of Both Velocity Sensitivities in Air and Water.

The observation that we make is the free-field, open-circuit velocity sensitivity of our planar-magnetic sensor seems to be significantly greater in water than in air. This observation raises the questions: should it be, and, if so, by how much? To answer these questions, we undertook a simplified Newton's Second Law analysis of the performance of magnetic ribbon-type sensors, valid for long wavelengths, and applied the result to our planar-magnetic sensor. This analysis is presented in Appendix A. The result is that we estimate the velocity sensitivity of our planar-magnetic sensor should be about 11 dB greater in water than in air. An observed sensitivity level difference of about 4 dB versus an estimated 11 dB corresponds to a bit more than a factor of two discrepancies in sensitivity ratio, water-to-air.

APPENDIX A. LONG-WAVELENGTH, NEWTON'S SECOND LAW ESTIMATE OF MAGNETIC RIBBON-TYPE TRANSDUCER VELOCITY SENSITIVITY IN WATER VERSUS AIR

1.   Simplified Newton's Second Law Analysis of Motion for Magnetic Ribbon-Type Sensors

In the long-wavelength limit, the local velocity field of an acoustic wave in the vicinity of an object (obstacle) is very nearly the same as that for inviscid, incompressible potential (curl-free) flow. The distributed reaction force by the fluid on the object, due to their relative motion, is inertial in character and can be phenomenologically represented by ascribing an effective mass to the relative flow. (Note, this mass also goes by many other names, e.g., induced mass, hydrodynamic mass, (dipole) radiation mass, entrained mass, virtual mass.) This force is in addition to the force that would exist if the object and the fluid moved together, which equals the force required to accelerate the mass of fluid displaced by the object. Applied to a magnetic ribbon-type transducer, the object (obstacle) is the transducer's diaphragm. Then, in the long-wavelength limit, we can approximate Newton's Second Law for the motion of the diaphragm of a magnetic ribbon-type transducer irradiated by an incident acoustic wave (assume on-axis incidence) by

$$m_{eff}(a_f - a_d) + m_{displ}a_f = m_d a_d \text{,} \tag{A.1}$$

where m_{eff} is the effective mass ascribed to the relative velocity field, m_d is the mass of the diaphragm, m_{displ} is the mass of fluid displaced by the diaphragm, and a_f and a_d are, respectively, the acceleration of the fluid and of the diaphragm. Equation (A.1) assumes the motion of the diaphragm is mass-controlled, which is the usual situation. More generally, the right side of Equation (A.1) could be replaced by $Z_d u_d = Z_d a_d/j\omega$, where Z_d is the diaphragm's mechanical impedance and u_d is its velocity. Importantly, the fluid acceleration and velocity here are their values away from the object, and so these are identified as *free-field values*.

The effective mass equals the fluid mass density ρ_f multiplied by a factor with the dimensions of volume; call it an effective volume V_{eff}:

$$m_{eff} = \rho_f V_{eff} \, .$$

(A.2)

This effective volume depends only upon the "shape" of the relative velocity field, and not upon the fluid density or the fluid velocity itself, or upon any motion variable; it is a purely geometry-dependent factor. In the present context of a moving (very thin) diaphragm, it is convenient to parameterize V_{eff} as the product of the object's projected area perpendicular to the free-field velocity field A_∞ and an effective thickness in the direction of flow; call it τ_{eff}:

$$V_{eff} = A_\perp \tau_{eff} \, .$$

(A.3)

Then,

$$m_{eff} = \rho_f A_\perp \tau_{eff} \, .$$

(A.4)

For a sphere of radius a, for example [24],

$$V_{eff} = \frac{2}{3}\pi a^3 = \frac{1}{2}\left(\frac{4}{3}\pi a^3\right) = \frac{1}{2}V_{sph} = A_\perp \tau_{eff} = \left(\pi a^2\right)\frac{2a}{3},$$

(A.5)

that is, the effective mass of a sphere moving through a fluid equals 1/2 the mass of fluid it displaces, and its effective thickness is 2/3 of its radius. For a flat circular disc (which has no volume) moving perpendicular to its normal [24],

$$V_{eff} = \frac{8}{3}a^3 = \left(\pi a^2\right)\frac{8a}{3\pi} = A_\perp \tau_{eff}$$

(A.6)

that is, the effective thickness associated with the effective mass in this case is $(8/3\pi) = 0.85$ times its radius.

In making an estimate of the effective mass of the planar-magnetic transducer we investigated, whose lateral dimensions are almost but are not the same, we use the previous formula for the effective thickness, $\tau_{eff} = (8a/3\pi)$, and we estimate the radius a as 1/2 the estimated average lateral dimension of the diaphragm; call it W_{avg}: $a_{planar-magnetic} \approx 1/2\ W_{avg}$, so that

$$(\tau_{eff})_{\text{planar-magnetic}} \approx (4W_{avg}/3\pi) \approx 0.4\ W_{avg}. \tag{A.7}$$

2.   Estimated Free-Field, Open-Circuit Velocity Sensitivity of a Magnetic Ribbon-Type Sensor, Valid for Long Wavelengths

The open-circuit voltage e_o generated by a magnetic induction sensor is proportional to the perpendicular velocity of the length of its conductor, which is immersed in its magnetic field. The transduction coefficient φ is the sensor's "Bl product." Optimally, the directions of the velocity u_d, of the magnetic field B and of the length of conductor in the magnetic field l are all mutually orthogonal, so we may simply write

$$e_o = \varphi u_d = Blu_d. \tag{A.8}$$

(Alternatively, we can replace l above by an effective perpendicular length l_{eff}.) The free-field, open-circuit *velocity* sensitivity of a magnetic ribbon-type sensor, call it M_{uo}, would be defined by

$$M_{uo} = \frac{e_o}{u_f}. \tag{A.9}$$

Then,

$$M_{uo} = Bl\frac{u_d}{u_f}, \tag{A.10}$$

That is, the velocity sensitivity is proportional to the ratio of the sensor's diaphragm velocity to the free-field acoustic velocity.

From Newton's Second Law previously given, we have

$$\frac{u_d}{u_f} = \frac{a_d}{a_f} = \frac{m_{disp} + m_{eff}}{m_d + m_{eff}},$$ (A.11)

and so we have

$$M_{uo} = Bl\left(\frac{m_{disp} + m_{eff}}{m_d + m_{eff}}\right).$$ (A.12)

As all quantities on the right hand side are constants for a given fluid, we see that, at frequencies for which the diaphragm motion is mass-controlled and for long acoustic wavelengths, the prediction of a Newton's Second Law analysis is that the free-field, open-circuit velocity sensitivity of a magnetic ribbon-type sensor is a constant. Furthermore, we see that its velocity sensitivity would be fluid-independent if the effective mass is much greater than the diaphragm mass (which is already at least several times greater than the displaced fluid mass, for any magnetic ribbon-type transducer, in air or in water). The question remains, is it?

3. Estimated Velocity Sensitivity in Water Relative to Air

For a given sensor, the *Bl* product and diaphragm mass are constant. The displaced fluid mass m_{displ} and the effective mass m_{eff} are both proportional to fluid density ρ_f, which is the only place where any fluid property enters.

The displaced fluid mass m_{displ} and the diaphragm mass m_d may be parameterized as

$$m_{disp} = \rho_f A_\perp \tau_d, \ \ m_d = \rho_d A_\perp \tau_d,$$ (A.13)

where ρ_f is the fluid mass density, and ρ_d and τ_d are the mass density and thickness of the diaphragm. Recall, the effective mass may be parameterized similarly: $m_{eff} = \rho_f A_\perp \tau_{eff}$, with $\tau_{eff} \approx 0.4 \, W_{avg}$ for our planar-magnetic sensor. Thus, we may write

$$M_{uo} = Bl\left(\frac{m_{disp}+m_{eff}}{m_d+m_{eff}}\right) = Bl\left(\frac{\rho_f A_\perp \tau_d + \rho_f A_\perp \tau_{eff}}{\rho_d A_\perp \tau_d + \rho_f A_\perp \tau_{eff}}\right) = Bl\left(\frac{\rho_f \tau_d + \rho_f \tau_{eff}}{\rho_d \tau_d + \rho_f \tau_{eff}}\right) \quad \text{(A.14)}$$

Note that the only fluid property in the expression for velocity sensitivity is the fluid's mass density ρ_f.

The thickness and length parameters required in Equation (A.14) for our planar-magnetic transducer are not readily obtainable or are proprietary. The manufacturer has published that the diaphragm of our transducer is made of DuPont Kaladex, but its thickness is not published; neither are the dimensions of the diaphragm published. We estimated these from inspection of our transducer together with what information we could find from a web search for our particular planar-magnetic transducer as well as for other planar-magnetic transducers. The following parameters were adopted to estimate M_{uo}/Bl for our planar-magnetic sensor in air and in water (2-digit precision).

Mass density of air: $\quad\quad\quad\quad \rho_{air} = 1.2 \text{ kg/m}^3$

Mass density of water: $\quad\quad\quad \rho_{water} = 1000 \text{ kg/m}^3$

Mass density of Kaladex: $\quad\quad \rho_{Kaladex} = 1400 \text{ kg/m}^3$

Mass density of aluminum: $\quad \rho_{Al} = 2700 \text{ kg/m}^3$

(taken as the conductor)

Effective diaphragm thickness: $\quad\quad \tau_d = 25 \text{ microns}$

(taking 1/2-mil-thick Kaladex + effectively 1/2-mil-thick aluminum conductor)

Effective diaphragm mass density: $\quad \rho_d = 2000 \text{ kg/m}^3$

(avg of Kaladex and aluminum)

Estimated avg diaphragm width: $\quad\quad W_{avg} = 42 \text{ mm}$

(from mfgr's exterior dimensions; avg of 35 mm & 49 mm; see thesis Fig. 19)

With these parameters, the following are estimated (all mks units):

In air:

$$\frac{M_{uo}}{Bl} \approx \left(\frac{(1.2)(25 \times 10^{-6}) + (1.2)(0.4)(0.042)}{(2000)(25 \times 10^{-6}) + (1.2)(0.4)(0.042)} \right) = \left(\frac{3.0 \times 10^{-5} + 0.020}{0.050 + 0.020} \right) = 0.29 \ (-10.9 \ dB)$$

In water:

$$\frac{M_{uo}}{Bl} \approx \left(\frac{(1000)(25 \times 10^{-6}) + (1000)(0.4)(0.042)}{(2000)(25 \times 10^{-6}) + (1000)(0.4)(0.042)} \right) = \left(\frac{0.025 + 17}{0.050 + 17} \right) = 1.00 \ (0.0 \ dB)$$

Then, our estimate is that the long-wavelength, free-field, open-circuit velocity sensitivity of our planar-magnetic sensor should be $10.9 \approx 11$ dB greater in water than in air. This estimate is about 5 dB greater than we observe. However, this is within a factor of 2 of what is observed.

APPENDIX B. SPHERICAL WAVES RECIPROCITY PARAMETER

This section is to prove that $\dfrac{M_{off}}{S_I} = J_S$, where M_{off} the free field receiving voltage sensitivity for a reversible (reciprocal or anti-reciprocal) transducer, S_I is the speaker strength or free-field pressure at a point or transmitting response of a reciprocal transducer.

$$M = \frac{\text{electrical output (I or E)}}{\text{avg acoustic pressure over Am (real or free-field)}} \quad \text{(B.1)}$$

$$S = \frac{\text{avg acoustic pressure over As or at P(real or free-field)}}{\text{electrical input (I or E)}} \quad \text{(B.2)}$$

Reciprocity calibration is based on for reversible transducer as is shown in Figures 98 and 99.
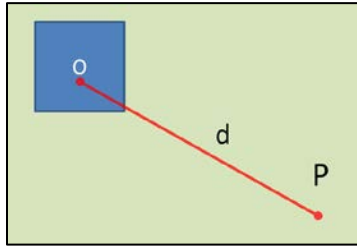
Figure 98.   Reversible Transducer and a Field Point P.
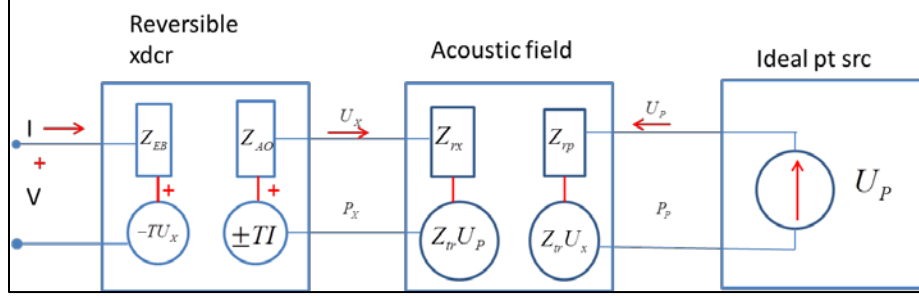
For convention, if the current is flowing into the transducer it is positive, it is the Volume Velocity of the transducer, when the red arrow is out, the sign is negative.

Figure 99. The Network Representation for an Ideal Reversible Transducer.

Acoustic matrix for reversible xcdr: canonical equation.

$$\begin{bmatrix} V \\ P_X \end{bmatrix} = \begin{bmatrix} Z_{EB} & T \\ \pm T & Z_{ao} \end{bmatrix} \times \begin{bmatrix} I \\ (-U_X) \end{bmatrix} = \begin{bmatrix} Z_{EB}I + T(-U_X) \\ \pm TI + Z_{ao}(-U_X) \end{bmatrix} \tag{B.3}$$

Acoustic field: Acoustic radiation impedance matrix.

$$\begin{bmatrix} P_x \\ P_p \end{bmatrix} = \begin{bmatrix} Z_{rx} & Z_{tr} \\ Z_{tr} & Z_{rp} \end{bmatrix} \times \begin{bmatrix} U_x \\ U_p \end{bmatrix} = \begin{bmatrix} Z_{rx}U_x + Z_{tr}U_p \\ Z_{tr}U_x + Z_{rp}U_p \end{bmatrix} \tag{B.4}$$

where U_p is the volume velocity at point source (pt src), U_x volume velocity of the transducer's radiating face out to the transducer for negative U_x. P_x is the acoustic pressure averaged over the transducer's radiating face, and P_p is the pressure at P point Figure 99.

Situation 1: a current I is supplied into the xdcr, producing U_x and a P_p at P.

The ideal pt src is infinity stiff; therefore, $U_P = 0$, then:

$$U_x = \frac{\pm TI}{\left(Z_{ao} + Z_{rx}\right)} \tag{B.5}$$

It is possible to calculate P_p knowing $U_p = 0$, therefore from Equation (B.5):

$$P_p = Z_{tr}U_x = \frac{Z_{tr} \times \pm TI}{\left(Z_{ao} + Z_{rx}\right)} \tag{B.6}$$

112

by definition, $S_I = \dfrac{P_P}{I}$, turns out:

$$S_I = \pm \frac{Z_{tr}T}{\left(Z_{ao} + Z_{rx}\right)}$$ (B.7)

Z_{ao} Transducer open circuit I=0 acoustical impedance, Z_{rx} Self-radiation impedance, Z_{tr} Acoustic radiation transfer impedance between A_m and A_s as is shown in Figure 74, so reciprocity parameter $J = \pm \dfrac{1}{Z_{tr}}$ is the transfer admittance.

Situation 2: U_p produces open circuit voltage output V_0 ; therefore, the condition is $V_0 = -TU_x$ and given U_p

$$U_x = -\frac{Z_{tr}U_p}{\left(Z_{ao} + Z_{rx}\right)}$$ (B.8)

Replacing Equation (B.8) on V_o,

$$V_0 = \frac{Z_{tr}TU_p}{\left(Z_{ao} + Z_{rx}\right)}$$ (B.9)

From Equation (B.1),

$$M_o = \frac{V_0}{P_{ff}}$$ (B.10)

where P_{ff} is the pressure reference point at origin, the transducer is not in the network,

$P_{ff} = U_P Z_{trff} = \dfrac{U_p}{J_S}$, and where the free field acoustic transfer impedance is the following calculation:

Acoustic radiated pressure must look like

$$\delta \tilde{p}(r,t) = \frac{\tilde{A}}{r} e^{j(\omega t - kr)} = \left(\frac{\tilde{A}}{r} e^{-jkr} \right) e^{j\omega t} = \delta \tilde{p}(r) e^{j\omega t}$$ (B.11)

And from

$$\delta \vec{V} = -\frac{1}{j\omega \rho_0} \times \vec{\nabla} \delta \tilde{p}$$ (B.12)

There is only a radial component of $\delta \vec{V}$, call it $\tilde{u}$ or $\tilde{V}_r$, and the spherical acoustic impedance:

$$\tilde{Z}(r) = \frac{\delta \tilde{p}(r)}{\tilde{V}_r(r)} = \rho_0 c \times \frac{jkr}{(1+jkr)} \tag{B.13}$$

Then, on the surface of a radially pulsating sphere of radius "a":

$$\delta \tilde{p}(a) = \rho_0 c \times \frac{jka}{(1+jka)} \times \tilde{u}(a) = \frac{\tilde{A}}{a} e^{-jka} \tag{B.14}$$

$$\tilde{Z}(a) = \rho_0 c \times \frac{jka}{(1+jka)} \tag{B.15}$$

Acoustical radiation impedance for a sphere:

$$\tilde{Z}_{ar}(a) = \frac{\delta \tilde{p}(a)}{\tilde{u}(a) \times S} = \frac{\delta \tilde{p}(a)}{\tilde{u}(a) \times 4\pi a^2} \tag{B.16}$$

$$\tilde{A} = \rho_0 c \frac{jka^2 e^{jka}}{(1+jka)} \tag{B.17}$$

At an arbitrary radius "r" from:

$$\delta \tilde{p}(r) = \frac{\tilde{A}}{r} e^{-jkr} \tag{B.18}$$

Replace "r" by a radius "a"

$$\delta \tilde{p}(\text{a}) = \frac{\tilde{A}}{a} e^{-jka} \tag{B.19}$$

It must be that

$$\delta \tilde{p}(r) = \frac{\delta \tilde{p}(r)}{\delta \tilde{p}(\text{a})} \delta \tilde{p}(\text{a}) = \left(\frac{a}{r}\right) e^{-jk(r-a)} \tilde{Z}(a)\tilde{u}(a) \tag{B.20}$$

Replace $\tilde{Z}(a)$ from Equation (B.15) and multiply the whole equation by $\dfrac{S}{S}$

114

$$\delta \tilde{p}(r) = \left(\frac{a}{r}\right) e^{-jk(r-a)} \rho_0 c \frac{jka}{(1+jka)} \tilde{u}(a)\frac{S}{S}$$

(B.21)

Volume velocity for spherical waves:

$$\tilde{U}_{spherical} = \tilde{u}(a)S$$

(B.22)

From Equations (A.21) and (A.22) and $S = 4\pi a^2$,

$$\delta \tilde{p}(r) = \left(\frac{a}{r}\right) e^{-jk(r-a)} \frac{\rho_0 c}{4\pi a^2} \frac{jka}{(1+jka)} \tilde{U}_{spherical}$$

(B.23)

So, between the surface at radius "a," and a field point, at radius "r," we have between a finite size pulsating sphere and a point source (pulsating sphere of radius $a \to 0$):

$$\tilde{Z}_{rx} = \left(\frac{\delta \tilde{p}(a)}{\tilde{U}(a)}\right) = \frac{\rho_0 c}{4\pi a^2} \frac{jka}{(1+jka)},$$

(B.24)

Multiply in the numerator and denominator $\left(\frac{1-jka}{1-jka}\right)$,

$$\tilde{Z}_{rx} = \frac{\rho_0 c}{4\pi a^2} \frac{\left[jka + (ka)^2\right]}{\left[1 + (ka)^2\right]}$$

(B.25)

Now to calculate the transfer impedance, and from Equation (B.24), where $\tilde{Z}_{rx} = \left(\frac{\delta \tilde{p}(a)}{\tilde{U}(a)}\right),$

$$\tilde{Z}_{trff} = \frac{\delta \tilde{p}(r)}{\tilde{U}(a)} = \frac{\delta \tilde{p}(r)}{\delta \tilde{p}(a)} \times \frac{\delta \tilde{p}(a)}{\tilde{U}(a)} = \frac{\delta \tilde{p}(r)}{\delta \tilde{p}(a)} \times \tilde{Z}_{rx}$$

(B.26)

From Equations (A.18) and (A.19)

$$\tilde{Z}_{trff} = \left(\frac{a}{r}\right) e^{-jk(r-a)} \times \tilde{Z}_{rx}$$

(B.27)

Replace $\tilde{Z}_{rx}$ from Equation (B.25),

$$\tilde{Z}_{trff} = \left(\frac{a}{r}\right)e^{-jk(r-a)} \times \frac{\rho_0 c}{4\pi a^2} \times \frac{\left[jka+(ka)^2\right]}{\left[1+(ka)^2\right]} \tag{B.28}$$

If r = d and $a \to 0$ (small transducer)

$$\tilde{Z}_{trff} = j\frac{\rho_0 f}{2d} \times e^{-jkd} \tag{B.29}$$

From Equation (2.12), $J_S = \dfrac{2d}{\rho f}$, the transfer Impedance yields

$$\tilde{Z}_{trff} = \frac{1}{J_S} \tag{B.30}$$

The transfer impedance between a pair of ideal transducers separated by a distance "d," and from Equations (B.9) and (B.10), and knowing that $P_{ff} = U_P Z_{trff} = \dfrac{U_p}{J_S}$:

$$M_o = \frac{V_0}{P_{ff}} = \frac{Z_{tr}TU_P}{(Z_{ao}+Z_{rx})} \times \frac{J_S}{U_P} \tag{B.31}$$

And, from Equations (A.7) and (A.31)

$$\frac{M_o}{S_I} = \pm\frac{Z_{tr}TJ_S}{(Z_{ao}+Z_{rx})} \times \frac{(Z_{ao}+Z_{rx})}{Z_{tr}T} = \pm J_S \tag{B.32}$$

The reciprocal parameter has no difference in magnitude, only a difference in the polarities, that means in the case of the reciprocal transducer, the parameter $+J_S$ its polarity is positive; however, in the case of the anti-reciprocal, the polarity is negative.

APPENDIX C. THE PRINCIPLE OF RECIPROCITY FOR THE TIME-HARMONIC ACOUSTIC FIELD CREATED BY COLLECTION OF DISCRETE, FINITE-SIZE SOURCES IN AN UNBOUNDED, STATIONARY FLUID

Before we consider specific cases relating to acoustic transducer calibration, we first consider the more general case of time harmonic acoustic fields generated by a collection of finite size, discrete sources in an otherwise infinite, stationary, homogeneous and isotropic fluid, and what we can conclude from the Principle of Reciprocity applied to such acoustic fields.

Consider a collection of sources as just described, for two different "source activation" situations. Let a particular source be denoted by subscript, and let situations 1 and 2 be denoted by the superscripts (1) and (2), respectively. Then, for example, $\tilde{p}_i^{(1)}$ and $\tilde{u}_{\perp i}^{(1)}$ are the (phasor) surface acoustic pressure and surface normal velocity on source I for situation i. Then, the Principle of Reciprocity applied to situations as described here can be cast as [11]

$$\sum_{source\ i} \int \tilde{p}_i^{(1)} \tilde{u}_{\perp i}^{(2)} \, dS_i = \sum_{source\ i} \int \tilde{p}_i^{(2)} \tilde{u}_{\perp i}^{(1)} \, dS_i \tag{C.1}$$

Consider now the following two situations: (1) in situation 1, only radiator *"m"* is active, that is, $\tilde{u}_{\perp i}^{(1)} \neq 0$ only for *i=m,* otherwise $\tilde{u}_{\perp i}^{(1)} = 0$; (2) in situation 2, only radiator *"n"* is active, that is, $\tilde{u}_{\perp i}^{(2)} \neq 0$ only for i=n, otherwise $\tilde{u}_{\perp i}^{(2)} = 0$. Then each sum has only one contribution, and we have

$$\int \tilde{p}_n^{(1)} \tilde{u}_{\perp n}^{(2)} \, dS_n = \int \tilde{p}_m^{(2)} \tilde{u}_{\perp m}^{(1)} \, dS_m. \tag{C.2}$$

This relation is the basis for the reciprocity calibration technique, a first principle procedure that has been applied for decades to the primary calibration of pressure transducers; however, this relation applies to all types of acoustic transducers, including velocity (pressure gradient) transducers.

THIS PAGE INTENTIONALLY LEFT BLANK

APPENDIX D. CHARACTERISTIC OF MICROPHONE TYPE 40 AF, HYDROPHONE 8103, TRANSDUCER F33, ROTATOR AND PLANAR-MAGNETIC, USED IN THE THESIS

Calibration Chart
Type 40AF
½" Free Field Microphone

Serial No. 31881

Sensitivity :   45.30 mV/Pa
                       -26.88 dB re. 1V/Pa

Cal. Date :   13-mar-03
Operator :   CA

Reference conditions:
Temperature : 23 Celcius
Relative humidity : 50%
Barometric pressure : 101.3 kPa

The calibration is performed by comparison with a Calibration Reference Microphone Cartridge Type 40AG and is traceable to the National Physical Laboratory, UK.

The stated sensitivity for the microphone cartridge is the Open Circuit Sensitivity. When used with a typical preamplifier, like the G.R A.S. Type 26AH, the sensitivity will be 0.2 dB lower.

The frequency response is recorded by electrostatic actuator. The lower curve is the pressure response and the upper curve is the free field response for 0° incidence with the protection grid mounted on the microphone. (See back for more information)

Calibration Chart for Hydrophone Type 8103   Serial No.:2241680

Date: _____ Potentiometer: _____ Zero Level: _____ D A B C Lin.

dB
+20
+10
0
−10
−20
−30

200   500   1 kHz   2   5   10   20   50   100

Lm. Freq.: _____ Hz   Writing Speed: _____ mm/sec.   Paper Speed: _____ mm/sec.

Calibration Chart for Hydrophone Type 8103

Serial No.: 2241680

Reference Sensitivity at 250 Hz* ± 2% at 23 °C
Including integral cable   6 m

Voltage Sensitivity (Open Circuit Sensitivity):
−211.3 dB ± 0.25 dB re 1 V/µPa** or 26.0 µV/Pa

Charge Sensitivity: 95 · 10⁻³ pC/Pa

Capacitance (including integral cable): 3440 pF

Cable Capacitance: 95 pF/m

Leakage Resistance: 28000 MΩ at 23 °C

Frequency Response (at ref. pos.):
Individual Free Field Frequency Response Curve attached

Measurement Uncertainty (re 10kHz):
10 to 80 kHz ± 1.5 dB
80 to 100 kHz ± 1.8 dB
100 to 200 kHz + 3.5 dB, − 1.5 dB

Summarized Specifications (re 250 Hz)

Frequency Response (tolerance field excluding measurement uncertainty):
0.1 Hz to 20 kHz + 1 dB, − 1.5 dB
0.1 Hz to 100 kHz + 1 dB, − 6 dB
0.1 Hz to 180 kHz + 2.5 dB, − 12.5 dB

Horizontal Directivity 100 kHz:
(XY – plane) ± 2 dB

Vertical Directivity 100 kHz:
(XZ – plane) ± 4 dB

Date 30 Jun. 00 Signature L. H.

Physical (mm)

Ref. Point
Acoustic Centre
z x y
ø 4.4
ø 7
2
10.5
50
15.8±0.3
25
5.6 ø

Cable: Double shielded low noise

Weight (including 6 m cable): 170g

Environmental

Operating Temperature Range:
Short term − 40°C to + 120°C
Continuous − 40°C to + 80°C

Change of Sensitivity with Temperature:
Charge 0 to 0.03 dB/°C
Voltage 0 to − 0.03 dB/°C

Change of Sensitivity with Static Pressure:
0 to − 3x10⁻⁴ dB/Pa
(0 to − 0.03 dB/atm)

Temperature Transient Sensitivity: < 50 Pa/°C
(ANSI S2.11–1969); measured with Brüel & Kjær Charge
Preamplifier Type 2626, LLF 3 Hz

Allowable Total Radiation Dose: 5 x 10⁷ Rad

Acceleration Sensitivity   < 130 dB re 1 µPa/ms⁻²

Maximum Operating Static Pressure:
4 x 10⁶ Pa (40 atm)

Note: All values are typical at 25°C (77°F), unless
measurement uncertainty or tolerance limit is specified.
All uncertainty values are specified at 2 σ (i.e. ex-
panded uncertainty using a coverage factor of 2).

For further information see User Manual

* Sensitivity Traceable to:
DPLA: Danish Primary Laboratory of Acoustics
NIST: National Institute of Standards and Technology, USA
** 1 Pascal = 1N/m² = 10 µbar

TYPE F33 TRANSDUCER

Fig. F33-1 - Type F33 transducer.

FUNCTION: A general-purpose directional transducer with two coaxial arrays that provide a bandwidth of over two decades. Reversible but deigned and used primarily as a projector.

DESIGN: A small inner array consists of 12 PZT disks. The larger concentric array consists of 64 PZT squares (older units may contain barium titanate squares). The inner array is used at high frequencies and both are used simultaneously at low frequencies.

FREQUENCY RANGE: Both arrays: 1-50 kHz; Inner array: 15-150 kHz

TVR: See Fig. F33-2

MAXIMUM DEPTH: 340 m

TEMPERATURE RANGE: 0 to 35°C

MAXIMUM DRIVING SIGNAL: 200 V rms

ELECTRICAL IMPEDANCE: See Fig. F33-3

DIRECTIVITY: Patterns in the horizontal (XY) plane for both arrays are shown in Fig. F33-5, and for the inner array only in Fig. F33-6. Vertical (XZ) plane patterns are similar.

WEIGHT: 17.3 kg (38 lbs)

SHIPPING WEIGHT: 25 kg (55 lbs)

NORMAL CABLE LENGTH: 30 m

121

CABLE CODE: Blue   outer array, high signal
                Red   outer array, low signal
                Black   inner array, low signal
                White   inner array, high signal
                Shield   ground

INSTRUCTIONS FOR THE USER: See Appendix D for preparation for use
                              A hanger is a permanent part of the transducer
                              The acoustic center is the mid-point of the acoustic window
                              (see Fig. F33-4)
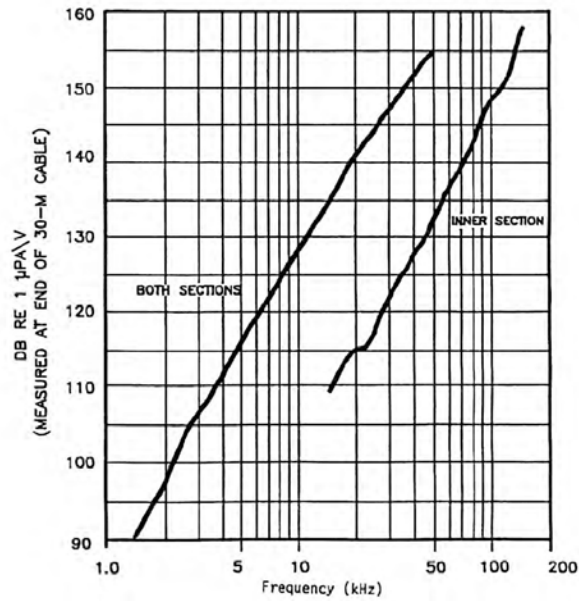
Fig. F33-2 - Typical TVR for Type F33 transducer.
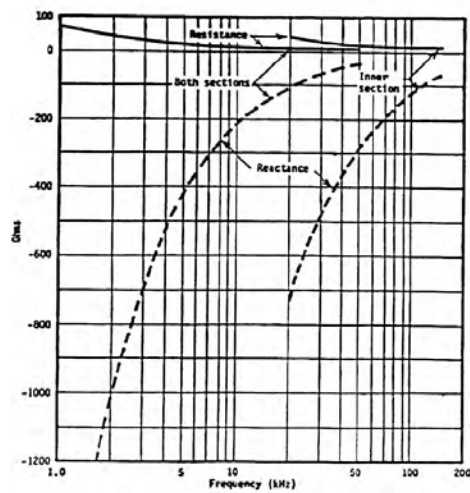
Fig. F33-3 - Typical equivalent series impedance for Type F33 transducer.

122
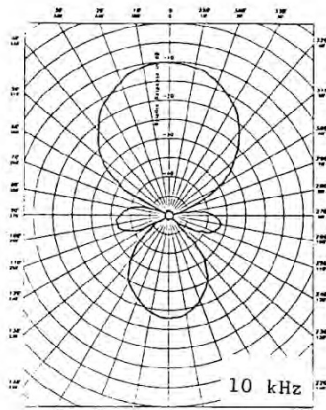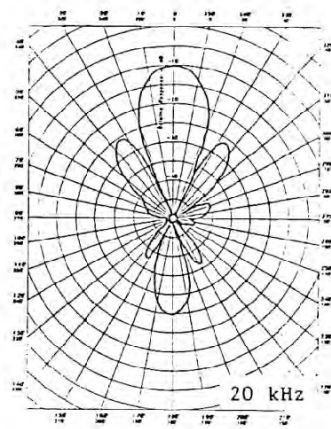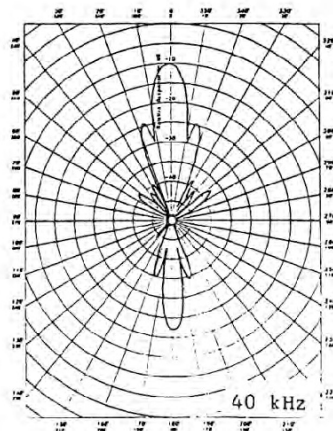
Fig. F33-4 – Typical directivity patterns in the horizontal (XY) plane for Type F33 transducer, both sections in parallel. Scale: center to top of grid in each pattern is 50 dB

123
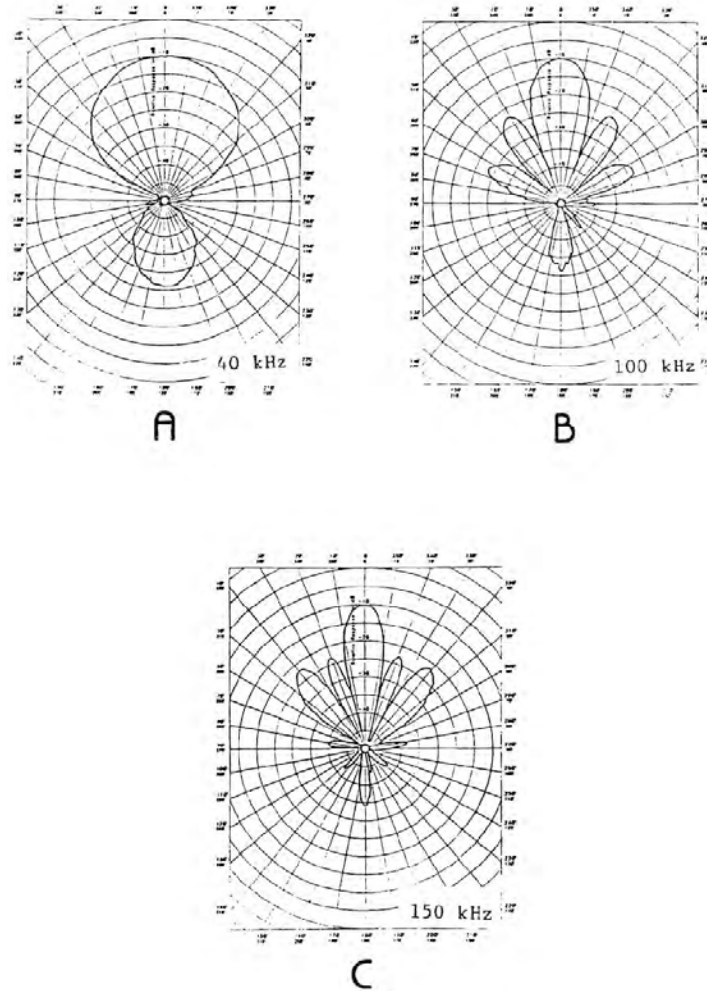
Fig. F33-5 - Typical directivity patterns in the horizontal (XY) plane for Type F33 transducer, inner section only. Scale: center to top of grid in each pattern is 50 dB.

Fig. F33-6 - Dimensions (in cm) and orientation of Type F33 transducer.
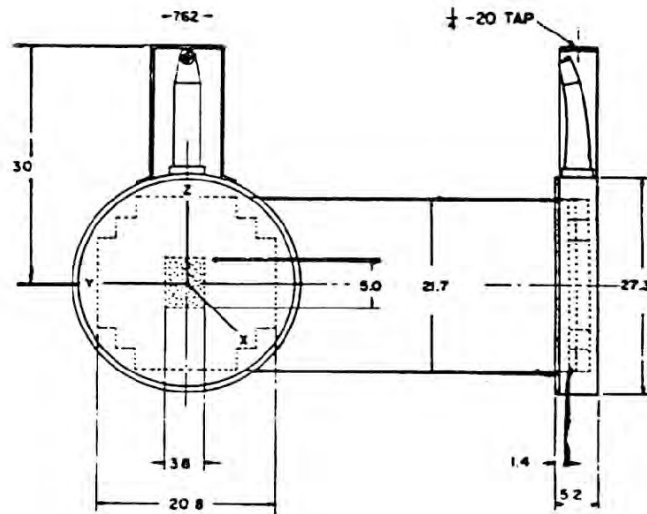
ACTIVE ELEMENT

OUTER ARRAY	64 PZT-4 PLATES
	(1. 0 in. X 0.75 in. X 0.250 in. THICK)
INNER ARRAY	12 PZT-4 DISKS
	(0.50 DIA X 0.10 THICK)

*NOTE: 1.   Starting with S/N 132, the steel backing blocks are embedded in polyurethane.
2.   Transducers beginning with S/N 140 have stainless-steel housings rather than high copper alloy.
3.   Older units may contain barium titanate squares in outer array.

125

PRODUCT DATA

Turntable System — Type 9640

Turntable System Type 9640 consists of Controllable Turntable Type 5960, Turntable Controller Type 5997 and Remote Control WB 1254. The Turntable System is designed to rotate a test object, such as a loudspeaker, microphone, or hydrophone, for measurement of directional response. Used in combination with a personal computer, Type 9640 becomes part of a system capable of automatically recording the directional characteristics of many different test objects.

960035/1

USES
- Controlling test-object (e.g., loudspeaker, microphone, hydrophone) orientation during:
  - Directional response measurements
  - Sound power measurements
  - Directional noise radiation measurements

FEATURES
- Rotation of up to 100 kg load, supported or suspended
- Continuous, relative or absolute rotation
- Controlled from turntable controller, remote control unit or PC over IEEE–488 interface
- Adjustable turntable speed and acceleration
- Connection of test object power supply and signal through slip ring
- Front panel read-out of mode and current test-object position

Applications
Type 9640 can be used to measure directivity by means of frequency-response test methods. The test object can be accurately rotated using the Turntable System so that it is located at the desired angle to a measurement microphone. The response of the test object can then be obtained for any direction using PULSE Directivity and Polar Plot BZ 5551.

Controlling the Turntable
Turntable Controller Type 5997 offers three modes of operation (Turn_Rel, Turn_Abs and Cont.) and three commands Set 0°, Acc. and Max_360. Turn_Rel and Turn_Abs allow a relative or absolute turn (specified in degrees) to be made. When a polar plot of a single frequency is required, the CONT mode is to be selected as it rotates the turntable continuously at a constant speed.

As test objects have different inertia, the acceleration and deceleration in the start and stop phases can be controlled

by using the command ACC. The acceleration of the turntable can be adjusted to accommodate different test object masses, up to 100 kg.

The Set 0° command is used to set the zero degree mark that will be the reference for a given test. In order to prevent cable wrapping, the MAX_360 command limits the turns between 0° and 360°. Alternatively, the cable can be fed through the slip ring on the turntable, allowing an unlimited number of rotations.

Remote Control WB 1254 offers 5 commands for controlling Turntable Type 5960 via a 15 m cable. The "<" and ">" keys are used to turn the test object clockwise and anticlockwise, respectively. When the test object has been positioned at the starting point, the zero degree mark can be set by pressing Set 0°. The mode of operation can be chosen at the front panel of Turntable Controller Type 5997. The turntable can then be started or stopped by using the Start and Stop keys.

Brüel & Kjær

Connections to the Test Object

Two types of connection can be made from the base plate of the turntable, through slip rings, to the test object on the table plate. One supplies power to the test object while the other, a screened coaxial connection, carries signals to and from the test object. The connections are heavily screened from each other, making spurious signals negligible under normal conditions.

Compliance with Standards

CE, C	CE-mark indicates compliance with: EMC Directive, Low Voltage Directive and Machinery Directive. C-Tick mark indicates compliance with the EMC requirements of Australia and New Zealand.
Safety	EN/IEC/UL 61010–1: Safety requirements for electrical equipment for measurement, control and laboratory use.
EMC Emission	EN/IEC 61000–6–3: Generic emission standard for residential, commercial and light industrial environments. CISPR 22: Radio disturbance characteristics of information technology equipment. Class B Limits. FCC Rules, Part 15: Complies with the limits for a Class B digital device.
EMC Immunity	EN/IEC 61000–6–1: Generic standards – Immunity for residential, commercial and light industrial environments. EN/IEC 61326: Electrical equipment for measurement, control and laboratory use – EMC requirements. **Note:** The above is only guaranteed using accessories listed in this Product Data Sheet.
Temperature	IEC 60068–2–1 & IEC 60068–2–2: Environmental Testing. Cold and Dry Heat. Operating Temperature: 5°C to 40°C (41°F to 104°F) Storage Temperature: −25°C to +70°C (−13°F to +158°F)
Humidity	IEC 60068–2–78: Damp Heat 0 to 90% RH (5°C to 40°C), non-condensing at 40°C
Enclosure	IEC 529: IP 20

Specifications – Turntable System Type 9640

Controllable Turntable Type 5960

Load: Max 100 kg (220 lb.) on centre, 30 kg (66 lb.) on periphery, when table plate is lined up perfectly in horizontal plane. Same loads apply with turntable hung upside down
Thread of Mounting Holes: UNF 10−32 and M5
Resolution: 1°
Speed of Rotation:
· **Cont. Mode:** 22.7 to 720 seconds per revolution
· **Turn_abs and Turn_rel Modes:** 10 seconds per revolution (max.)
Cable Length: 15 m (48.5 ft)
Table Plate Diameter: 354 mm (13.9″)
Weight: 12 kg (26 lb.)

Turntable Controller Type 5997

OPERATING MODES
Turn_rel: Sets the relative turn in degrees

Turn_abs: Sets the absolute turn in degrees
Cont.: Sets the continuous speed in seconds per revolution

COMMANDS
Set 0 Deg: Sets the reference angle
Acc.: Sets the acceleration
Max_360 On/Off: Turns max. 360° on or off. On prevents cable wrapping

IEEE INTERFACE
Conforms with IEEE–488.1 and compatible with IEC 625-1. Provides remote control of all front-panel functions

FUNCTIONS IMPLEMENTED
SH1 – Source Handshake
AH1 – Acceptor Handshake
L3 – Listener
SR1 – Service Request
DC1 – Device Clear
RL1 – Remote/Local

COMMAND SET
Standard engineering English reflecting the front panel and screen names
Device Address: Set to 10 (decimal) on delivery

POWER SUPPLY
Voltage: 100, 115, 127, 200, 220 and 240 V AC ±5%
Power Rating: approx. 15 VA

GENERAL
Cabinet: Supplied as model A (metal cabinet)
Dimensions:
Height: 143 mm (5.6″)
Width: 188 mm (7.4″)
Depth: 235 mm (9.3″)
Weight: approximately 3 kg (6.6 lb.)

Ordering Information

Type 9640	Turntable System	AN 0019 Power Cable (country specific)	WQ 1270 IEEE–488 Interface Card, PCI-GPIB
Includes the following accessories:		AN 0020 Power Cable	
Type 5960	Controllable Turntable	2 × JP 0101 Screened Plug	or
Type 5997	Turntable Controller		WQ 1290 IEEE–488 Interface Card, PCMCIA
WB 1254	Remote Control	**REQUIRED ACCESSORIES**	
AO 0422	Turntable Cable	AO 0265 Interface Cable (2 m), IEEE–488	

Brüel & Kjær

127

The Neo3 PDR – a high performance wideband, wide dispersion planar-magnetic transducer

1	Effective frequency range (recommended LF crossover point): Standard version Dipole or with a tuned rear chamber or in an array	2000 Hz – 28000 Hz 1200 Hz – 26000 Hz
2	Sensitivity (2.83V/1m) Averaged in 2kHz – 20 kHz range Standard version Dipole	93.5 dB 90.5 dB
3	Impedance (resistive) DCR	4 ohm 3.5 ohm
4	Power handling: RMS Program Peak	10 W 20 W 50 W
6	Weight	300 g

APPENDIX E. MATLAB CODE

MATLAB code for the beam pattern in air.

```matlab
% Author: Steve Baker
% Rev 30 Aug 2016
% Estimates the front lobe acoustic axis as bisecting the angles to the
% minima at nominally ±90 degrees. Corrects raw angle data to place 0 deg
% on the estimated acoustic axis.
% Does not re-scale angles to place nulls at exactly ±90 deg; assumes
% rotation rate set on B&K rotator is accurate, e.g., 3 deg/s.
% Script to process beam pattern data taken on True Ribbon
 % this script was modified from version 4 to process students' time, magnitude data

% Note -- before executing this script, recorded time & mag beam pattern
% data must be stored in columns 1 and 2 of an array with the same name as
% a MATLAB data file (.mat) that follows the naming convention below.

% Example MATLAB data file name for 300 Hz-----------------------------------------------

% Clear data space & close all open figure windows------------------------------------------

clear all
close all

% Must set nominal rotation rate for data collected-----------------------------------------------

NomRotRate = 1;              % 360sec/rev = 1 deg/s  Must set number of oscope
                            samples/sec


OscopeFs = 25;                % oscope sample rate was 25/s
SamplesPerDeg = OscopeFs/NomRotRate;

% get frequency--------------------------------------------------------------------------------

freq = input('Enter frequency for this data: ');

% open data file---------------------------------------------------------------------------------

fnam=['BeamPatternTR_',num2str(freq),'Hz'];
display(['Loading file ',fnam,'.mat']);
load([fnam,'.mat']);

% Set default figure window size on computer screen. Units are pixels.---------------------
```

```matlab
oldunits = get(0,'DefaultFigureUnits');
oldposn = get(0,'DefaultFigurePosition');
set(0,'DefaultFigureUnits','pixels')
set(0,'DefaultFigurePosition',[72*1 72*3 72*8 72*10])

% Load data vectors into convenient variables------------------------------------------------------

eval(['TimDat=',fnam,'(:,1);']);
eval(['MagDat=',fnam,'(:,2);']);

% Make sure there are no negative magnitudes------------------------------------------------------

MagDat(find(MagDat<0))=0;

% MagDat=MagDat(241:end);  TimDat=TimDat(241:end);  create nom rot deg data vec

RotDegDat=NomRotRate*TimDat;         % approx rot angle in deg, from scope
                                     times:   120sec/rev = 3 deg/s; zero not
                                     significant.



% Plot unprocessed data--------------------------------------------------------------------------

figure(1)
subplot(2,1,1)
plot(RotDegDat,MagDat)
legend('Mag','Location','southeast')
title(['Mag mic rec''d sig ampl vs uncorrected est az angle; ',...
    'B-G Neo3W s/n 1; ',num2str(freq),' Hz'])
xlabel('Nominal azimuth angle (arbitrary zero) [deg]')
ylabel('Mic rec''d sig ampl [arb units]')
print([num2str(freq),'HzBP_Fig1_Unprocessed.pdf'],'-dpdfwrite')

% Estimate ±90-deg nulls First clip out the data from -DegLim deg to +DegLim deg------

DegLim=90;
nClip=find(RotDegDat>-DegLim & RotDegDat<DegLim);
ClipOffset=nClip(1)-1;
ClippedRotDegDat=RotDegDat(nClip);
ClippedMagDat=MagDat(nClip);

% plot unprocessed clipped data---------------------------------------------------------------------

figure(2)
```

```matlab
subplot(2,1,1)
plot(RotDegDat,MagDat,ClippedRotDegDat,ClippedMagDat)
title(['Unprocessed mag data showing ±',num2str(DegLim),...
    '-deg region used to estimate ±90-deg nulls; B-G Neo3W s/n 1; ',...
    num2str(freq),' Hz'])
xlabel('Nominal azimuth angle (arbitrary zero) [deg]')
ylabel('Mic rec''d sig mag [arb units]')

% perform a n-point avg of magnitude data-----------------------------------------------------------

n=257;                              % ±128 pts = (128pts/50pts/s)3deg/s = ±7.68 deg
SmoothMagDat=smooth(MagDat,n);
ClippedSmoothMagDat=SmoothMagDat(nClip);

% plot smoothed clipped data-------------------------------------------------------------------

subplot(2,1,2)
plot(RotDegDat,SmoothMagDat,ClippedRotDegDat,ClippedSmoothMagDat)
title1=([num2str(n),'-pt (',num2str(n/SamplesPerDeg,'%4.1f'),'-deg) ',...
    'smoothed mag data showing ±',num2str(DegLim),'-deg region used to ',...
    'estimate ±90-deg nulls; B-G Neo3W s/n 1; ',num2str(freq),' Hz'])
xlabel('Nominal azimuth angle (arbitrary zero) [deg]')
ylabel('Mic rec''d sig mag [arb units]')
hold on;

% Find max magnitude point of clipped smoothed data----------------------------------------

[MaxSmoothMag,nMax]=max(ClippedSmoothMagDat);
RotDegSmoothedMax=ClippedRotDegDat(nMax);

% Find first and last >-3dB pts in clipped smoothed data This will locate the -3dB pts of
% the frontside lobe index numbers from find function applied to clipped data are corrected
% to unclipped data by adding ClipOffset--------------------------------------------------------
%-----------------------------------------------------------------------------------------------------

tgtMagVal=MaxSmoothMag/sqrt(2);
nlower3dBfront=find(ClippedSmoothMagDat>tgtMagVal,1,'first')+ClipOffset;
nupper3dBfront=find(ClippedSmoothMagDat>tgtMagVal,1,'last')+ClipOffset;

% Find first and last <-3dB pts in entire smoothed data this will locate the -3dB pts of the
% backside lobe--------------------------------------------------------------------------------
%-----------------------------------------------------------------------------------------------------

nupper3dBback=find(SmoothMagDat<tgtMagVal,1,'first');
```

131

```
nlower3dBback=find(SmoothMagDat<tgtMagVal,1,'last');

% Est acoust axis angle offset based on -3dB pts of front lobe--------------------------------

RotDegOffset3dB=(RotDegDat(nlower3dBfront)+RotDegDat(nupper3dBfront))/2

% Locate the estimated nulls find first and last >-12dB) pts in clipped smoothed data this
% will locate the -12dB pts. of the frontside lobe--------------------------------------------------
%-----------------------------------------------------------------------------------------------------


tgtMagVal12dB=MaxSmoothMag/4;
nlower12dBfront=find(ClippedSmoothMagDat>tgtMagVal12dB,1,...
    'first')+ClipOffset;
nupper12dBfront=find(ClippedSmoothMagDat>tgtMagVal12dB,1,...
    'last')+ClipOffset;

% Find first and last <-12dB pts in entire smoothed data, this will locate the -12dB pts. of
% the backside lobe------------------------------------------------------------------------------


nupper12dBback=find(SmoothMagDat<tgtMagVal12dB,1,'first');
nlower12dBback=find(SmoothMagDat<tgtMagVal12dB,1,'last');

% Estimate locations of nulls as bisecting -12dB pts. -------------------------------------------

nlowernull=round((nupper12dBback+nlower12dBfront)/2);
estlowernull = RotDegDat(nlowernull)
nuppernull=round((nupper12dBfront+nlower12dBback)/2);
estuppernull = RotDegDat(nuppernull)
null_diff_angle = estuppernull - estlowernull
ctr_angle_of_nulls = (estuppernull + estlowernull)/2

% Est central max angle based on -12dB pts is avg of these est -12dB angles----------------

RotDegOffset=ctr_angle_of_nulls

% Add estimated acoustic axis pt & -3dB pts to smoothed data plot acoustic axis & -3dB
% pts. for front lobe-------------------------------------------------------------------------------


plot(RotDegOffset,MaxSmoothMag,'+g',RotDegDat(nlower3dBfront),...
tgtMagVal,'+g',RotDegDat(nupper3dBfront),tgtMagVal,'+g')

% -3dB pts for back lobe--------------------------------------------------------------------------
```

```matlab
dltan = round((nupper3dBfront-nlower3dBfront)/2);
plot(RotDegDat(nupper3dBback-dltan),MaxSmoothMag,'+g',...
RotDegDat(nupper3dBback),tgtMagVal,'+g',...
RotDegDat(nlower3dBback),tgtMagVal,'+g',...
RotDegDat(nlower3dBback+dltan),MaxSmoothMag,'+g')

% -12dB pts---------------------------------------------------------------------------------

plot(RotDegDat(nupper12dBback),tgtMagVal12dB,'+g',...
RotDegDat(nlower12dBfront),tgtMagVal12dB,'+g',...
    RotDegDat(nupper12dBfront),tgtMagVal12dB,'+g',...
    RotDegDat(nlower12dBback),tgtMagVal12dB,'+g')

title2=(['CCW est acoust axis angle diff, -3dB vs minima = ',num2str(RotDegOffset3dB-
RotDegOffset,'%4.1f'),...
    ' deg; Est angle btwn nom ±90-deg minima = ',num2str(null_diff_angle,'%5.1f'),...
    ' deg']);
title({title1;title2})
hold off
print([num2str(freq),'HzBP_Fig2_ClippedAvgd.pdf'],'-dpdfwrite')

% Adjusted rotation angle w.r.t. estimated central max angle----------------------------------

AdjRotDegDat=RotDegDat-RotDegOffset;

% Perform nom 1-deg avg of Mag data------------------------------------------------------------

n=ceil(SamplesPerDeg);
SmoothMagDat=smooth(MagDat,n);

% Find front lobe max magnitude of 1-deg smoothed data, take avg over ±2.5 degrees;
% use this to normalize 1-deg smoothed data---------------------------------------------------


nClip=find(RotDegDat>-2.5 & RotDegDat<2.5);
MaxSmoothMagFront = mean(SmoothMagDat(nClip));

% apply normalization-------------------------------------------------------------------------

NormSmoothMagDat=SmoothMagDat/MaxSmoothMagFront;

% Clip out data from -90 deg to +90 deg and find the -6 dB points----------------------------

nClip=find(AdjRotDegDat>-90 & AdjRotDegDat<90);
```

```
ClippedAdjRotDegDat=AdjRotDegDat(nClip);
ClippedSmoothMagDat=NormSmoothMagDat(nClip);

% Target -6dB magnitude----------------------------------------------------------------

tgtMagVal=1/2;
nlower6dBfront=find(ClippedSmoothMagDat>tgtMagVal,1,'first');
nupper6dBfront=find(ClippedSmoothMagDat>tgtMagVal,1,'last');

% Est acoust axis angle offset based on -3dB pts of front lobe--------------------------------

Front6dBWidth=ClippedAdjRotDegDat(nupper6dBfront)...
        -ClippedAdjRotDegDat(nlower6dBfront)

% Clip out data from -180 deg to +180 deg re est acoustic axis-----------------------------

nClip=find(AdjRotDegDat>-180 & AdjRotDegDat<180);
ClippedAdjRotDegDat=AdjRotDegDat(nClip);
ClippedSmoothMagDat=NormSmoothMagDat(nClip);

% Write out clipped, adj rot angle and norm mag data to file--------------------------------

save(['ClippedSmoothMagDat_',num2str(freq),'Hz.mat'],'ClippedAdjRotDegDat','Clip
pedSmoothMagDat')

figure(3)
subplot(2,1,1)
plot(ClippedAdjRotDegDat,ClippedSmoothMagDat)
xlim([-180,180])
legend('Mag','Location','southeast')
title1=(['Normalized Mag mic rec''d sig ampl vs est angle from ',...
    'acoustic axis; B-G Neo3W s/n 1; ',num2str(freq),' Hz']);
title2=(['Data processed for est offset angle of acoustic axis & ',...
    num2str(n),'-point (1-deg) avgd; -6dB beamwidth = ',...
    num2str(Front6dBWidth,'%4.1f'),' deg']);
title({title1;title2})
xlabel('Estimated azimuth angle re estimated acoustic axis [deg]')
ylabel('Mic rec''d sig ampl [arb units]')
print([num2str(freq),'HzBP_Fig3_Processed.pdf'],'-dpdfwrite')

figure(4)
pax=polaraxes;
anglerad=ClippedAdjRotDegDat*pi/180;
polarplot(anglerad,abs(cos(anglerad)),'m',anglerad,ClippedSmoothMagDat,'b')
pax.RLim=[0 1.1];
```

```
pax.RTick=[0:0.2:1];
pax.ThetaTick=[0:10:360];
title([num2str(n),'-point (1-deg) avgd normalized mic rec''d sig mag; ',...
    'B-G Neo3W s/n 1; ',num2str(freq),' Hz'])
print([num2str(freq),'HzBP_Fig4_PolarPlot.pdf'],'-dpdfwrite')

figure(5)
pax=polaraxes;
anglerad=ClippedAdjRotDegDat*pi/180;
b=max(20*log10(ClippedSmoothMagDat),-40);
bideal=max(20*log10(abs(cos(anglerad))),-40);
polarplot(anglerad,bideal,'m',anglerad,b,'b')
pax.RLim=[-40 3];
pax.RTick=[-40:10:0];
pax.ThetaTick=[0:10:360];
title([num2str(n),'-point (1-deg) avgd normalized mic rec''d beam pattern; ',...
    'B-G Neo3W s/n 1; ',num2str(freq),' Hz'])
print([num2str(freq),'HzBP_Fig5_PolarPlot.pdf'],'-dpdfwrite')

% Restore original default figure window size---------------------------------------------------

set(0,'DefaultFigureUnits',oldunits)
set(0,'DefaultFigurePosition',oldposn)
```

THIS PAGE INTENTIONALLY LEFT BLANK

LIST OF REFERENCES

[1]   Acoustic vector sensors: Principles, applications, and practical experience (n.d.). Acoustical Society of America. [Online]. Available: http://scitation.aip.org/content/asa/journal/jasa/138/3/10.1121/1.4933588. Accessed Aug. 21, 2016.

[2]   D. Tassia, "Receiver operating characteristic curves for linear arrays of vector sensors using nonlinear cardynull processing," M.S. thesis, Dept. USW, Naval Postgraduate School, Monterey, CA, 2011.

[3]   G. Arfken, *Mathematical Methods for Physics*, New York, NY: Academic Press Inc., 1973.

[4]   Acoustic vector sensor array processing. (n.d.); Dept. of Electrical and Systems Engineering, Washington Univ., St. Louis. [Online]. Available: http://www.ese.wustl.edu/~nehorai/research/avs/avssensor.htm. Accessed Aug. 7, 2016.

[5]   Measurement principles of LDA. (n.d.); Dantec Dynamics. [Online]. Available: http://www.dantecdynamics.com/measurement-principles-of-lda. Accessed Aug. 7, 2016.

[6]   "Underwater Acoustics for Naval Applications," class notes for Engineering Acoustics, USW, Naval Postgraduate School, Monterey, CA, winter 2016.

[7]   Tradition Innovation Advanced Technology. (n.d.); Magnepan Inc. [Online]. Available: http://www.magneplanar.com/magneplanar_technology. Accessed Aug. 7, 2016.

[8]   RE-254 ribbon microphone motor for DIY mic project. (n.d.); DiY Audio Components. [Online]. Available: http://www.diyaudiocomponents.com/diy-ribbon-mic/re-254-ribbon-motor. Accessed July 27, 2016.

[9]   The Movil Coil Transducer (n.d.). Electronics Tutorial. [Online]. Available: http://www.electronics-tutorials.ws/io/io_8.html. Accessed Aug. 20, 2016.

[10]   How maggies work, Part II (n.d.) Maggie Users Group. [Online]. Available: http://www.integracoustics.com/MUG/MUG/articles/planar/. Accessed Aug. 7, 2016.

[11]   L.E. Kinsler, A. R. Frey, A. B. Coppens, and J. V. Sanders, *Fundamentals of Acoustics*, 4th ed., Hoboken, NJ: John Wiley & Sons, Inc., 1999.

[12]   R.J. Bobber, *Underwater Electroacoustic Measurement*. Los Altos, CA: Peninsula Publishing, 1990.

[13]   Pistonphone type 4228(n.d.) Bruel & Kjaer.[Online]. Available: http://www.bksv.com/Products/transducers/acoustic/calibrators/4228. Accessed Aug. 17, 2016

[14]   R. J. Bobber, "General reciprocity parameter," *The Journal of the Acoustical Society of America*, vol. 39, no. 4, pp. 680–687, Nov. 1965 .

[15]   T. Hertsens. (2011, May 11). Audio science guide: How planar magnetic headphones work. [Online]. Available: http://www.innerfidelity.com/content/how-planar-magnetic-headphones-work#BPBcYgAxMkdGH6wT.97.

[16]   Neo 3 A High-Performance Wideband, Planar-Magnetic transducer, B&G Corporation, Carson City, 2000, page 4

[17]   Bohlender- Graebner Neo 3W Planar Tweeter (n.d.) Parts Express. [Online].Available: http.//www.parts-express.com/bohlender-graebener-neo3w-planar-tweeter-w-back-cup--264-730. Accessed July 27, 2016

[18]   Caption hangs outside Anechoic Chamber located in Spanagel, Room 17.

[19]   GRAS 40 AF ½" Polarized Free Field Microphone (n.d.) GRAS Sound & Vibrations . [Online]. Available: http://www.gras.dk/40af.html. Accessed Aug. 23, 2016

[20]   Index to Speaker Systems and Components (n.d.) Radio Shack. [Online]. Available: http://support.radioshack.com/support_audio/27069.htm. Accessed Aug.14, 2016

[21]   Turntable system Type 9640, Bruel & Kjaer, Naerum, Denmark.

[22]   *Stanford Research System Operating Manual and Programming Reference 1290-D*, Stanford Research System, Sunnyvale, CA. Dec. 2006 pages 546.

[23]   Acoustic measurements for sonar transducer test personnel (1990, March). Naval Underwater System Center, New London, CT. [Online]. Available: http://www.docfoc.com/acoustic-measurements-for-sonar-transducer-test-personnel-q8h9.

[24]   E.J. Skudrzyk, *The Foundations of Acoustics*, NY; Vienna: Springer-Verlag, 1971.

INITIAL DISTRIBUTION LIST

1.   Defense Technical Information Center
        Ft. Belvoir, Virginia

2.   Dudley Knox Library
        Naval Postgraduate School
        Monterey, California